MAGNETIC MOMENTS, E3 TRANSITIONS AND PARTICLE-VIBRATION COUPLING IN THE Rn REGION

by

Stephen Poletti

A thesis submitted for the degree of
Master of Science
at the Australian National University
Canberra

May 1985

ACKNOWLEDGEMENTS

Science is always a co-operative venture. "No person is an island entire unto themself ...", to paraphrase John Donne. So to all the friends and colleagues who generously gave their time (and patience) over the last year I would like to say thank you.

I would particularly like to thank George Dracoulis. To quote just one example (of many) of the invaluable help I received from George, I draw the reader's attention to the tables A4.1-A4.5 (which it must be observed are very fine tables!), George, realising that I was having trouble with the tables, generously suggested the stylistic formalism which the reader can admire in due course!! Speaking of tables, I would like to thank Norma for help with the typing.

A special mention should go to those people who helped with the diagrams over the final few frenzied days (not a bad sentence eh!); Gavin, George, Gerald, Anne and Aiden. I would like to thank Gavin and Aiden (who came in on a weekend!) for the photography. To all my co-workers Aiden, Alan P., Jurgen, George and Andrew, who were always ready to help "Thanks Guys". I appreciate also the help Alan Baxter gave.

I would like to thank Fee (if she hadn't left it would have taken a month longer). To the comrades I say thanks on behalf of the people! And to all the regulars in the darkroom Trevor, Gordon, Jack, etc., etc. "Cheers". Finally I would like to thank all the people at the lab who have made my stay here so enjoyable.

Well it's been hard work writing this section, and the bottle of

Cabernet is nearly empty, so its time for a toast "To all the people who helped".

L'chaim

CONTENTS

ABSTRACT

The g-factors of high-spin yrast states in ^{210}Rn have been measured. The results are: $g(25^+) = 0.733(9)$, $g(22^+) = 0.702(7)$, $g(20^+) = 1.115(5)$, $g(17^-) = 1.052(5)$, $g(14^+) = 1.064(7)$ and $g(8^+) = 0.898(7)$.

The structure of these states and related ones is calculated within the framework of the shell model, using empirical residual interactions and including particle-vibration configurations explicitly.

This Thesis is based on work carried out in the Department of Nuclear Physics, the Research School of Physical Sciences, Australian National University, Australia.

All results and conclusions are those of the author unless otherwise stated.

Stephen Poletti

CHAPTER 1

INTRODUCTION

A striking feature of the high-spin level schemes of nuclei with several valence particles outside the ^{208}Pb shell is the enhanced E3 transitions. To try to understand the structure of such states the g-factors of the isomeric states in ^{210}Rn were measured.

The E3 transition strengths and the g-factor information can be explained simultaneously by invoking substantial configuration mixing. In Chapter 4 the properties of related high spin states in $^{210-212}Rn$ are calculated by explicitly including the particle-octupole states responsible for the fast E3s; this leads naturally to the required mixing.

CHAPTER 2

WHAT IS THE STRUCTURE OF THE HIGH SPIN STATES IN THE RN NUCLEI?

2.1 INTRODUCTION

Since ^{208}Pb is a "doubly magic" nucleus the neighbouring nuclei can be described in spherical shell model terms. Another approach is the deformed field method where the single particle energies are summed in a deformed potential. In the following chapter we will be looking at the structure of the radon nuclei near the closed neutron shell, such as ^{211}Rn, which can be thought of as a ^{208}Pb core with four valence protons and one neutron hole. In particular the problem which is considered here is the following: how well do we understand the structure of the high-spin states in the "radon region"? To this end we will look at the available experimental information and its suggested interpretation.

2.2 EXPERIMENTAL INFORMATION

The yrast spectroscopy of ^{212}Rn up to spin 30 $\hbar$ was established in 1977 (Ho77). Recently the yrast states of ^{211}Rn (Pol81, Dra81, Pol85) and ^{210}Rn (Pol82) have been investigated to spins higher than 30 $\hbar$. A simplified level scheme of each nucleus is reproduced in fig. 2.1.

A significant feature of these level schemes, as emphasised in the diagram, is the number of states which decay via enhanced E3 transitions. We shall see later that these enhanced transitions place

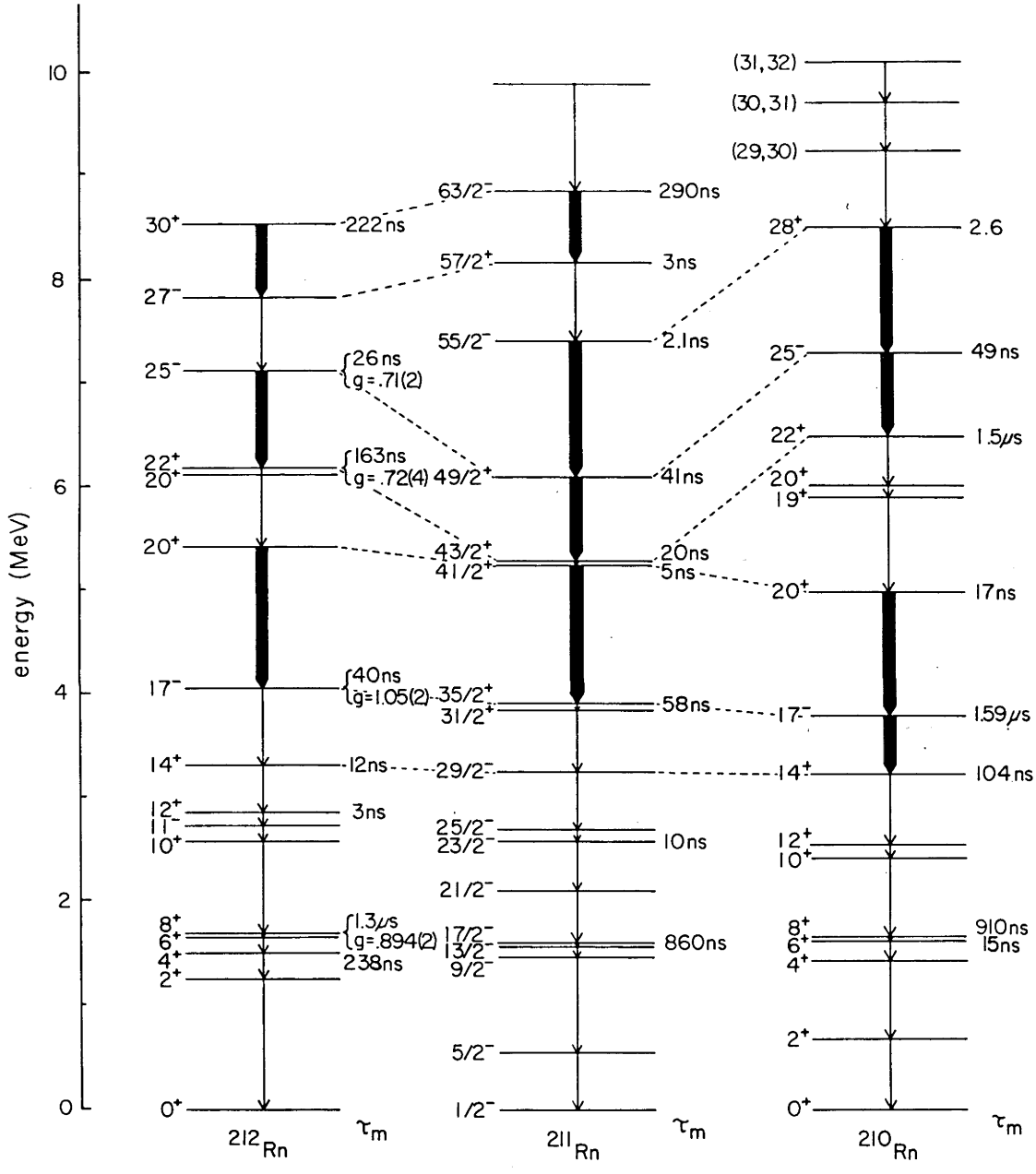

Figure 2.1: Selected yrast states in the radon isotopes discussed in text. Enhanced E3 transitions are denoted by bold arrows.

severe restrictions on the possible structure of the two states involved, and that they are associated with particular single particle transitions. In the diagram, related states in neighbouring nuclei are connected by lines. The relationship between the states will be explained in later chapters, but for now it should be noted that their decay properties are consistent with the proposed relationships. Another (sometimes related) feature of the yrast schemes of the three nuclei is the number of isomeric states. These so-called yrast traps are convenient experimentally as the lifetimes of the states are often long enough to enable accurate g-factor measurements using the time dependent perturbed angular distribution (TDPAD) method. (More will be said about the TDPAD technique in chapter 3.) Accurate lifetime measurements of the long lived isomers are possible using direct timing methods. Since states that decay via E 3 transitions are often isomeric the lifetimes of these states (and hence the B(E3) values) can be determined easily. Thus a "complete" set of information can be obtained for many of the high spin states, enabling detailed comparisons to be made with theory.

2.3 REVIEW OF CALCULATIONS

The yrast and near yrast spectra of ^{210}Rn and ^{211}Rn have been calculated up to spin 20 $\hbar$ by Morrison (Pol81, Pol82) using a full shell model approach, however basis space limitations make such calculations infeasible for states with spin higher than 20 $\hbar$. A simpler but very accurate shell model approach, pioneered by Blomqvist et al. (Blo77, Blo79) is to reduce the configuration space and use empirical residual interactions, which to some extent includes implicitly the effect that configuration mixing has on the energy. Since experimental residual interactions are used, energies can be calculated in some cases to an astonishing accuracy (Blo77). The high

spin yrast spectra of the radon nuclei have been analysed using a related shell model approach (Lon80, Byr82), and further calculations will be presented in chapter 4.

An alternative approach is to use the deformed independent particle model (DIPM) (Dud80, Mat78, And78, Cer79, Dud80) which is based on the summation of single particle energies in a distorted potential. For small deformations the deformation energy is given by:

$$E(\delta) = \sum_i [e_i + \Delta e_i(\delta)] + E_c(\delta)$$

where e_i is the single particle energy at zero deformation, $e_i(\delta)$ is the change in the single particle energy as a function of the deformation and $E_c(\delta)$ is the [liquid drop + shell correction] energy which is quadratic in the deformation for small δ. (As the deformation changes the shell structure changes, hence the shell correction term.) The energy as a function of the deformation parameter is minimised to give the excitation energy at the preferred deformation. To illustrate the method we will look at a simple example involving three valence particles.

From Myers and Swiatecki (Mye65) the change in energy of the ^{208}Pb core for small deformations is:

$$E_c \sim \frac{2}{5} c_2 A^{2/3} a^2 - \frac{1}{5} \frac{c_3 Z^2}{A^{1/3}} - S(N,Z) \frac{a^2}{a_0^2} ,$$

where the terms represent in turn the surface energy, the Coulomb energy and the shell correction energy and a is related to δ. Using parameters suggested by Myers and Swiatecki the expression reduces to:

$$E_c(\delta) = (95 - 65 + 305)\ \delta^2 \text{ MeV} = 335\ \delta^2 \text{ MeV} .$$

Note that the largest contribution to the deformation energy of the core is the shell correction term.

The change in energy of the particles as the quadrupole deformation is switched on is (from e.g. (Ham76)):

$$\frac{K(3m^2 - j(j+1))}{j(j+1)} ,$$

where

$$K \simeq \frac{25}{3} \delta \text{ MeV} .$$

For the maximally aligned $(\pi(i_{13/2}h_{9/2})\nu g_{9/2})_{31/2^-}$ state in ^{211}Po the energy sum $E(\delta)$ above is $335\ \delta^2 + 38\ \delta$ MeV. Setting $dE/d\delta = 0$ gives the preferred deformation as $\delta = -.06$ and the energy gain as -1.1 MeV.

For larger deformations the ground state energy is renormalised using the Strutinsky method (see for instance (Rin80)). Essentially, the ground state energies of nuclei show an oscillatory behaviour superimposed on the smooth liquid drop energy with the minima of the oscillations occurring at closed shells. When the shell structure changes, the energy of the core changes. The Strutinsky method enables one to calculate the shell dependent part of the energy which is added on to the liquid drop energy. Pairing effects can also be included in the calculations.

The deformed field model assumes that each particle experiences the same potential and a good choice of potential includes the polarisation contributions of the shell model residual interaction directly. Since for high-spin maximally-aligned states, a large fraction of the shell model residual interaction is due to polarisation effects, the model may be a significant improvement over the extreme weak coupling shell model. However failure of the model to describe repulsive interactions such as the proton-(neutron hole) shell model residual interaction (Mat78) can have important consequences. Also most potentials have difficulty reproducing the single particle energies for zero deformation and often arbitrary changes have to be made to the model to correct this. The shell model

approach with empirical residual interactions avoids the above problems, although other problems are introduced.

The shell model calculations (Byr82, Lon80) assume that the Hamiltonian can be written as:

$$\sum_i [(H_0(i) + H_{pol}(i)] + \sum_{i<j} [H_0(i,j) + H_{pol}(i,j)] + \ldots \equiv \sum_i H(i) + \sum_{i<j} H(i,j) + \ldots$$

The energy is approximated by:

$$\sum_i \langle\psi|H(i)|\psi\rangle + \sum_{i<j} \langle\psi| H(i,j)|\psi\rangle ,$$

where the sums are over the valence particles and/or holes. The matrix elements are recoupled in terms of two-body matrix elements taken directly from experiment. Note that the effective two-body matrix elements include configuration mixing effects, and the deformation of the core away from equilibrium is included via the polarisation contribution $H_{pol}(i) + H_{pol}(i,j)$. For illustrative purposes consider the (idealised) case where N valence particles align to give a deformation of $N\delta$ (i.e. assuming the deformation changes linearly with the number of valence particles). If the deformation energy of the core is proportional to the square of the deformation we have a contribution of say $C(N\delta)^2$ from the core. However there are $N(N-1)/2$ pairs, each contributing $2C\delta^2$ to the calculated energy. (Remembering that the single particle energies already include implicitly a polarisation term $C\delta^2$.) The error involved is then $C(N\delta)^2 - (CN(N-1)2\delta^2/2) = NC\delta^2$. In the example above C was taken to be $\sim$ 300 MeV, so for the case where six valence particles are aligned with a total deformation of 6δ equals -.06 (a typical deformation for this number of particles) the energy would be underestimated by ~200 keV, which is indicative of the accuracy to be expected from the shell model calculations. In practice of course the deformation will not change linearly with the number of particles as assumed here.

The question now is how do the various calculations compare with experiment? Up to spin 20 $\hbar$ in ^{212}Rn the different methods all assign the same configurations to the yrast states. The state properties expected from these assignments are in reasonable agreement with experiment. However, as pointed out by Dracoulis (Dra81), for the high-spin core excited configurations, many of the suggested configurations are not consistent with experiment. In table 2.1 below we compare the expected g-factors of the suggested configurations with experiment. The g-factors were calculated using experimental single particle g-factors and additivity. For the single particle g-factors which have not been measured experimentally the theoretical values of Bauer et al. (Bau73) were used. As we saw in fig. 2.1 many of the high spin states decay via very fast E3 transitions. If a calculation is to be consistent with experiment it must also predict these enhanced transition rates, so in table 2.1 the predicted transition rates are compared with the observed ones.

The transition rates are determined by recoupling the matrix elements in terms of "single particle" transitions, which are taken from experiment if possible. It is well known that the enhanced E3s are caused by admixtures of particle-(octupole vibration) states in the wavefunction (Boh75). For example consider the "$j_{15/2}$" state in ^{209}Pb; the $\nu j_{15/2}$ particle will mix with the particle vibration state $(\nu g_{9/2} \otimes 3^-)_{15/2}$ (where the 3^- state is the 2.6 MeV octupole vibration state in ^{208}Pb). The wavefunction of the "$j_{15/2}$" state can therefore be written as:

$$|"j_{15/2}"\rangle = \alpha\,|\nu j_{15/2}\rangle + \beta\,|(\nu g_{9/2} \otimes 3^-)_{15/2}\rangle$$

while the wavefunction of the "$g_{9/2}$" ground state is:

$$|"g_{9/2}"\rangle = \gamma\,|\nu g_{9/2}\rangle + \delta\,|(\nu j_{15/2} \otimes 3^-)_{9/2}\rangle \ .$$

TABLE 2.1: HIGH SPIN STATES IN ^{212}Rn

		Configurations[b]				
	Experiment[a]	And78	Mat78	Dud78	Der79	Byr82
$I^{\pi} = 22^{+}$		$\pi(h^3i)_{17^-}$ $\nu(p^{-1}g)_{5^-}$	$\pi(h^3i)_{17^-}$ $\pi(p^{-1}g)_{5^-}$	$\pi(h^3i)_{17^-}$ $\nu(p^{-1}g)_{5^-}$	$\pi(h^3i)_{17^-}$ $\nu(p^{-1}g)_{5-}$	$\pi(h^3i)_{17^-}$ $\nu(p^{-1}g)_{5-}$
g-factor	.72(1)	.76	.76	.76	.76	.76
$I^{\pi} = 25^{-}$		$\pi(h^2i^2)_{20^+}$ $\nu(p^{-1}g)_{5^-}$	$\pi(h^2i^2)_{20^+}$ $\nu(p^{-1}g)_{5^-}$	$\pi(h^2i^2)_{20^+}$ $\nu(p^{-1}g)_{5^-}$	$\pi(h^3i)_{17^-}$ $\nu(p^{-1}j)_{8^+}$	$\pi(h^3i)_{17^-}$ $\nu(p^{-1}j)_{8^+}$ $+\pi(h^2i^2)_{20^+}$ $\nu(p^{-1}g)_{5^-}$
g-factor	.71(2)	.86	.86	.86	.70	$>.78$
$B(E3)^{c}_{25^- \to 22^+}$	83(8)	8	8	8	65	<107
$I^{\pi} = 27^{-}$		$\pi(h^3i)_{17^-}$ $\nu(p^{-2})_{0^+}(gi)_{10^+}$	$\pi(h^3i)_{17^-}$ $\nu(p^{-2})_{0^+}(gi)_{10^+}$	$\pi(h^2i^2)_{20^+}$[d] $\nu(p^{-1}j)_{8^+}$	$\pi(h^3i)_{17^-}$ $\nu(gi^{-1})_{11^+}$	$\pi(h^2i^2)_{20^+}$ $\nu(f^{-1}g)_{7^-}$
g-factor	.63(3)	.63	.63	-	.56	.80
$I^{\pi} = 30^{+}$		$\pi(h^2fi)_{18^-}$ $\nu(p^{-2})_{0^+}(gj)_{12^-}$	$\pi(h^2fi)_{18^-}$ $\nu(p^{-2})_{0^+}(gj)_{12^-}$	$\pi(h^2fi)_{18^-}$ $\nu(p^{-2})_{0^+}(gj)_{12^-}$	$\pi(h^2fi)_{18^-}$ $\nu(p^{-2})_{0^+}(gj)_{12^-}$	$\pi(h^2i^2)_{20^+}$ $\nu(f^{-1}j)_{10^+}$
g-factor	.657(3)	.62	.62	.62	.62	.74
$B(E3)_{30^+ \to 27^-}$	91(13)	0	0	-	0	65

[a] (Hor77).

[b] The proton configurations i, f, h stand for $\pi i_{13/2}$, $\pi f_{7/2}$ and $\pi h_{9/2}$ and the neutron configurations i, i^{-1}, p^{-1}, f^{-1}, g, j stand for $\nu i_{11/2}$, $\nu i^{-1}_{13/2}$, $\nu p^{-1}_{1/2}$, $\nu f^{-1}_{5/2}$, $\nu j_{15/2}$ and $\nu g_{9/2}$.

[c] B(E3) values are in units of $e^2\ fm^6 \times 10^3$.

[d] The parity here is positive so the configuration can be ruled out immediately.

The different components contribute coherently to the total transition strength as shown below:

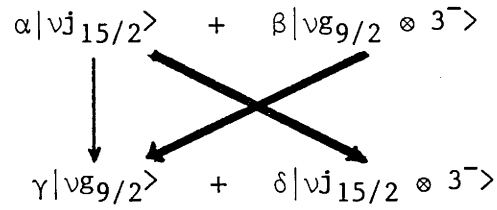

When the calculated component amplitudes are used (Ham73) the resultant transition rate is in excellent agreement with the experimental value of $65(14) \times 10^3$ e^2fm^6 (Mar77). By using experimental "single particle" B(E3)s the octupole contribution is included implicitly, and in the remainder of this thesis, quotation marks will be used to indicate configurations which contain implicitly such couplings.

We see from the table that many of the calculated configurations are inconsistent with experiment. The large difference between the experimental and calculated g-factors for many of the suggested configurations is evident. Perhaps a more serious problem is the difference between the expected transition rates and the observed ones for many of the states. Of course it is an obvious simplification to assume that the given configurations are pure. However where the transition is forbidden, even allowing for reasonable admixtures of other configurations into the given state, the B(E3) value would still be several orders of magnitude too low. Since the measured lifetime of the 30^+ state corresponds to a very enhanced B(E3) ~30 W.u., major structural changes between the 30^+ and 27^- states are ruled out. This restriction would eliminate, for example, the $\pi(h^2fi)_{18}{}^-\nu p_0^{-2}{}^+ (gj)_{12}{}^-$, 30^+ configuration if any of the suggested 27^- configurations are correct. In fact, independent of the 27^- configuration, there are no possible enhanced stretched E3 transitions from a 30^+ state with the

configuration $\pi(h^2fi)_{18^-}$ $\nu p_{0^+}^{-2}$ $(gj)_{12^-}$ to a 27^- state. (The "single particle" transitions which would give rise to enhanced E3s are $\pi i_{13/2} \rightarrow \pi f_{7/2}$, $\pi i_{13/2} \rightarrow \pi h_{9/2}$ and $\nu j_{15/2} \rightarrow \nu g_{9/2}$ transitions. However the above configuration is maximally aligned so if we replace the $\pi i_{13/2}$ proton by a $\pi f_{7/2}$ proton the maximum coupling possible is spin 26 $\hbar$ which would eliminate the first "single particle" transition. Similar geometric considerations eliminate the other transitions.)

Configurations suggested by Byrne and Dracoulis (Byr82) for these states reproduce the B(E3) well but energetically are not favoured (the calculated energies are about 1.5 MeV too high) and the g-factor evidence is not consistent with the proposal.

Matsuyanagi, Dossing and Neergard (Mat78) have also calculated the high spin yrast states (using the DIPM) in ^{210}Rn. These calculations predict that core excited states will not enter the yrast line until spin 33 $\hbar$. However there is strong evidence (Pol82) that the states above and including 22 $\hbar$ are core excited. Although certainly inconsistent with the predictions of Matsuyanagi et al., the assignments of Poletti et al. are consistent with the shell model calculations (Byr82) which predict core excited states to be yrast near spin 22 $\hbar$.

In chapter 4 we will try to formulate a consistent picture of the structure of the high spin states in the radon nuclei discussed above, by explicitly including the particle-vibration coupled states responsible for the fast E3 transitions.

It should be apparent that it is important to have a "complete set" of experimental information to test the suggested structure of these high-spin states. To obtain definitive evidence of the spin at which core excited states enter the yrast line and to cast further light on the nature of the high spin states in the radon region we

measured the g-factors and lifetimes of several of the high spin states in ^{210}Rn. In the next chapter the experimental techniques and the results of the measurements are discussed. (A companion study of g-factors and lifetimes in ^{211}Rn has also been carried out (Pol85), and some of the those results will be discussed in the theoretical comparisons in chapter 4.)

CHAPTER 3

G-FACTOR MEASUREMENTS

3.1 INTRODUCTION

The g-factors of the high-spin isomeric states in ^{210}Rn were measured using the time differential perturbed angular distribution technique [TDPAD] (Rec74, Mor76). The experimental setup is shown in fig. 3.1.

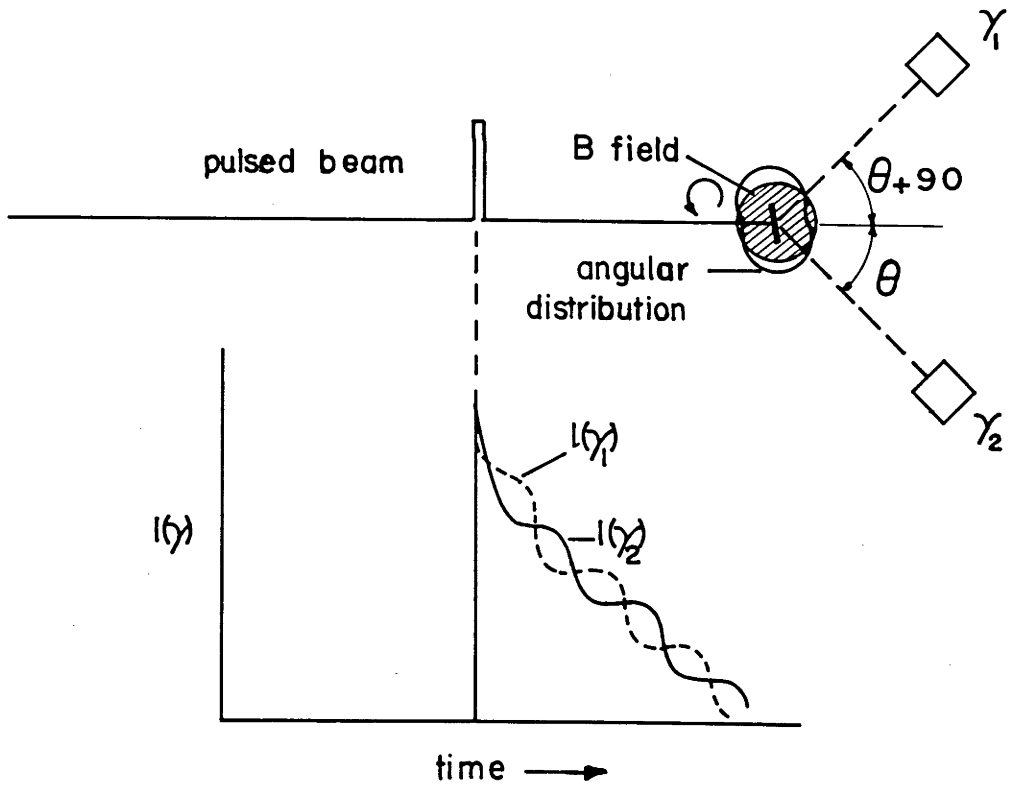

Fig. 3.1: Experimental setup for a TDPAD measurement.

The idea is that a heavy ion fusion reaction will produce excited states in the nuclei of interest with the nuclear spins of the states oriented in the plane perpendicular to the beam. If this spin alignment can be maintained a magnetic field with an axis perpendicular to the beam will cause the nuclear spins to precess in phase. The γ-radiation is emitted anisotropically with an angular distribution characteristic of its multipolarity and electromagnetic character. Hence if the beam is pulsed with a repetition time $T > \tau$, where τ is the lifetime of the state of interest, detectors located in the plane of rotation will see a radiation pattern such as that depicted in fig. 3.1.

Classically (and quantum mechanically) the nuclei will precess with the Larmor frequency

$$\omega_L = \frac{\mu g B}{\hbar}$$

The usual way that the Larmor frequency (and hence the g-factor) is determined is to form the ratio function:

$$R(t,\theta,B) = \frac{I(t,\theta,B)-I(t,\theta+90,B)}{I(t,\theta,B)+I(t,\theta+90,B)}$$

where $I(t,\theta,B)$ is the radiation intensity seen by a detector at the angle θ as a function of time.

In the simple case where there is only one isomer and where the A_4 coefficient can be neglected, the radiation intensity is:

$$I(t,\theta,B) = I \exp(-t/\tau)(1+A_2P_2(\cos(\theta-\omega_L t)) .$$

Consequently the ratio function becomes:

$$R(t,\theta,B) = \frac{3A_2}{4+A_2}\cos[2(\theta-\omega_L t)] .$$

The extension to cases where there are multiple isomers in a cascade feeding the state of interest is straightforward (Hau76).

In this chapter the techniques required to form the nuclei of

interest in an environment suitable for retaining the alignment of the nuclear spins will be examined. Also, the experimental methods used to measure the Larmor frequency will be described and the results will be presented.

It was seen in chapter 2 that an enhanced E3 transition between two states puts certain constraints on the configurations of the states. To accurately test the configurations of the high-spin states proposed in chapter 4 a timing experiment was carried out to determine the B(E3) for the 1245 keV ($28^+ \rightarrow 25^-$) transition. In section 3.5 the results of this experiment will be presented.

3.2 TECHNIQUES

3.2.1 The (HI,xn) Reaction

The heavy ion fusion reaction, where a nuclear projectile (with sufficient energy) and the target nucleus fuse, can be used to produce excited states of nuclei at high spin and excitation energy. For reviews on heavy ion reactions see for example (New74, Dia80, Bas80, Pel82).

The "hot" compound nucleus produced by the reaction can fission or decay by particle emission. As the angular momentum of the compound system increases the fission barrier is lowered and fission becomes the dominant process. However the states in ^{210}Rn considered in this thesis can be formed by making compound nuclei which decay initially by neutron evaporation. (The Coulomb barrier inhibits charged particle emission and is not a competing process except when the compound nucleus is very neutron deficient.) In the reaction ^{202}Hg(^{12}C,4n), used to produce the excited states in ^{210}Rn for the g-factor measurements, the initial compound system would have an excitation energy of approximately 60 MeV. Typically 4 neutrons would be boiled off taking away a total 6 MeV in kinetic energy and 36 MeV

in binding energy. Since the evaporation of neutrons is a statistical process, and the centrifugal barrier inhibits neutrons with a large amount of angular momentum from escaping, the evaporated neutrons will carry off only a small fraction of the total angular momentum. When the excitation energy is a few MeV above the yrast line the system generally decays by emitting γ-rays (which are thought to be mainly stretched) until the yrast line is reached, where the intensity is collected in a series of discrete γ-transitions which proceed down the yrast line.

Since the angular momentum of the incoming projectile relative to the centre of the target nucleus is large and perpendicular to its line of flight the spin of the compound nucleus is initially oriented in the plane perpendicular to the beam direction. Experimentally it is seen that the spin alignment is retained during the de-excitation process. The reason is that the neutrons take away only a small fraction of the total angular momentum aligned in a roughly random manner, while the subsequent continuum γ-rays, and indeed the yrast γ-rays, are mainly stretched. To measure the g-factors of the longer lived isomers in ^{210}Rn the initial spin-alignment needs to be retained for several μs.

3.2.2 Relaxation Effects

There are several factors which can cause relaxation of the nuclear spins.

In the presence of an electric field gradient ∇E a nucleus with a quadrupole moment Q will experience a torque $T = \nabla E \times Q$ (see fig. 3.2). Unlike the magnetic case the precession frequency depends on the z component of the spin. The basic frequency is:

$$\omega = \begin{cases} -\frac{3}{4I(2I-1)}\frac{eqQ}{\hbar} & \text{if I is an integer} \\ -\frac{3}{2I(2I-1)}\frac{eqQ}{\hbar} & \text{if I is half integer} \end{cases}$$

For a typical interstitial field gradient of 10^{17} V_{cm}^{-1} the factor $eqQ/h \sim 10^8$ rad s^{-1} so that the precession frequency is of the same order as the Larmor frequency for a typical external field of 2T ($\sim 10^8$ rad s^{-1}). Consequently, unless the host material has zero electric field gradient at the lattice sites the initial nuclear spin alignment will be washed out, the relaxation time being determined by the magnitude of the quadrupole field. Even for targets with a cubic crystal structure (and hence zero electric field at the lattice sites) radiation damage, which results from lattice defects caused by the stopping of the recoil ions, can cause spin relaxation (Daf78). This local distortion of the lattice structure results in randomly orientated electric field gradients and hence spin relaxation. As cubic crystals are heated to near melting point the radiation damage can be annealed out much faster. However many metals, such as platinum, cannot be heated easily to the required temperatures. Thus a good reaction for populating the high spin states in ^{210}Rn such as ^{198}Pt(^{17}O,5n) which was used previously (Pol82) is unsuitable for g-factor measurements, as evidenced by the small anisotropies observed in that reaction.

Other ways that spin orientation is lost are via magnetic coupling of the nuclear spins with the spins of the conduction electrons (Ack83 and refs cited therein), and by the nuclear spins interacting with the atomic hyperfine field. The atomic spin of an ion changes direction in a random manner which causes a fluctuating magnetic field, which in turn leads to alignment loss. Since the

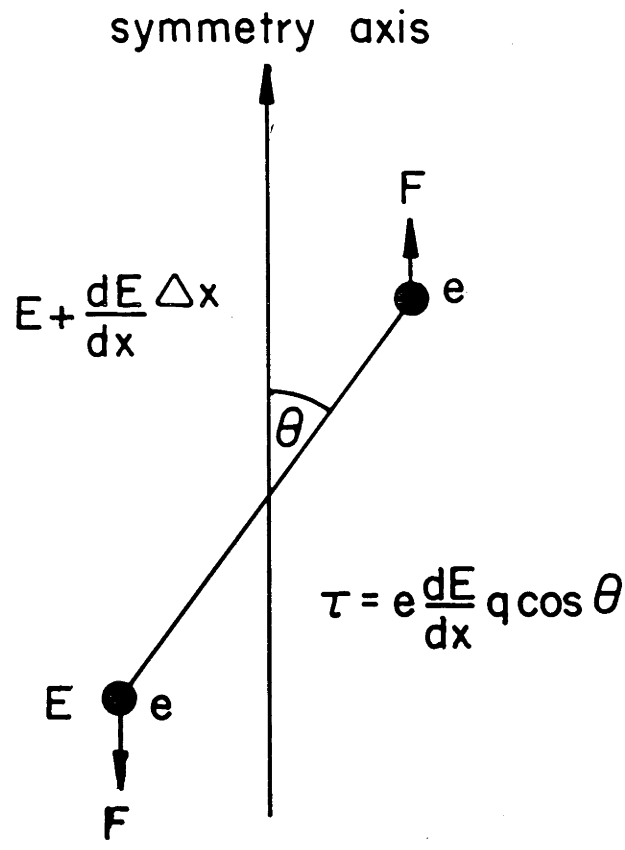

Fig. 3.2: Schematic of the quadrupole interaction.

magnetic field at the nuclear site due to the atomic electrons is much larger for paramagnetic ions than for diamagnetic ones the effect is most important for the former, where the relaxation time can be as small as 1 ns (Nor70). However for diamagnetic substances the effect is negligible.

Since the average electric field gradient in a liquid is zero a standard technique for retaining the initial spin alignment is to use a diamagnetic liquid as the target. In fig. 3.3 the decay curves for the 564 keV γ-ray, which decays from the yrast 17^- state in ^{210}Rn, are plotted out. It can be seen that the amplitude of the oscillations are initially large, and persist for several μs with little damping

which demonstrates that the liquid mercury target used to produce the high-spin states in ^{210}Rn is indeed a suitable environment for the radon nuclei to decay in.

Because of atomic effects the field experienced by the nuclei is not necessarily the same as the applied magnetic field. In general the orbital motion of the electrons produces a field antiparallel to that of the applied field. For Rn in Hg the diamagnetic correction factor is 1.91% (Hau78). Another much smaller correction that needs to be made to the external field is the Knight shift correction, which is due to the fact that in a metal the s-like conduction electrons are polarised along the external field. For Rn in Hg this effect has been measured by Hausser et al. (Hau78) and was found to be small (-0.05%).

3.3 EXPERIMENTAL TECHNIQUES

The reaction used to populate the high-spin isomers in ^{210}Rn was ^{202}Hg(^{12}C,4n) at 78 MeV with a 160 mg cm^{-2} ^{202}Hg liquid target (96% pure) mounted on a copper block. To minimise evaporation of the mercury the target was covered by a thin mylar sheet and maintained at a temperature near 0 °C. Since γ-rays that populate a state directly from the continuum do not in general follow a path which proceeds through isomers, it is an advantage to increase the sidefeeding intensities populating the yrast isomers of interest. As the beam penetrates into the mercury it loses energy, hence decreasing the average initial spin. Consequently, if a thick target is used, which was the case in this experiment, the amount of sidefeeding is increased (see fig. 3.4b). The ^{12}C,4n reaction was chosen rather than the ^{13}C,5n reaction (which would bring in more angular momentum) for the same reason.

Two hyperpure germanium detectors were placed at ±135° to the beam axis (see fig. 3.4). For each detector the energy and time

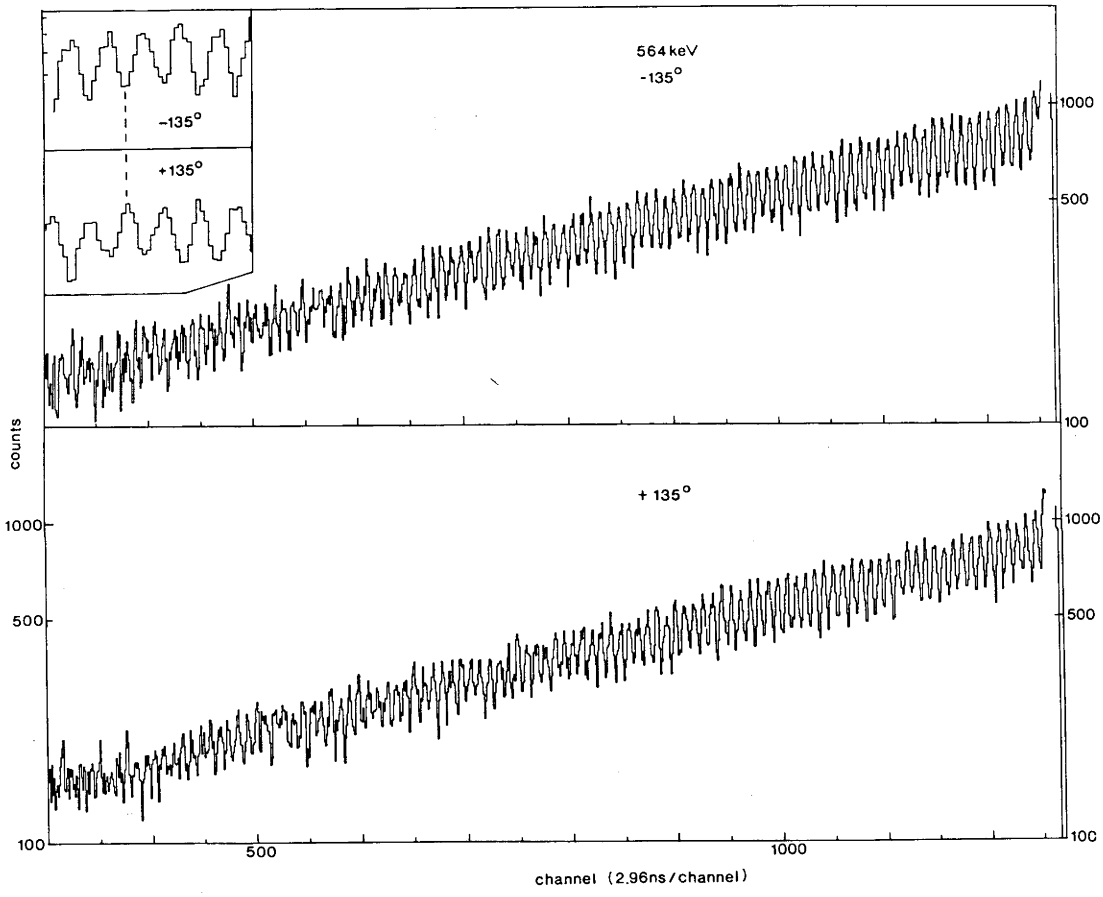

Fig. 3.3: Decay curves for the 564 keV γ-ray.

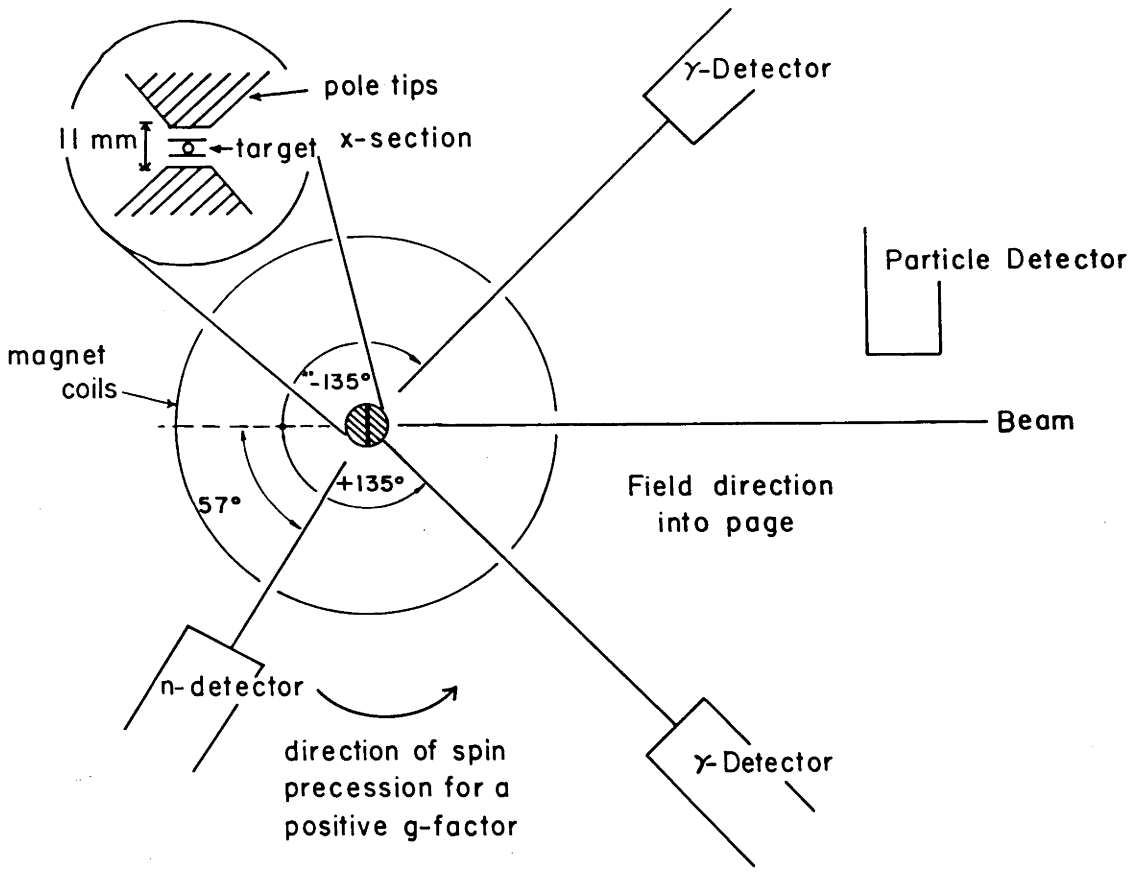

Fig. 3.4: Schematic of experimental setup used to measure the g-factors of states in ^{210}Rn.

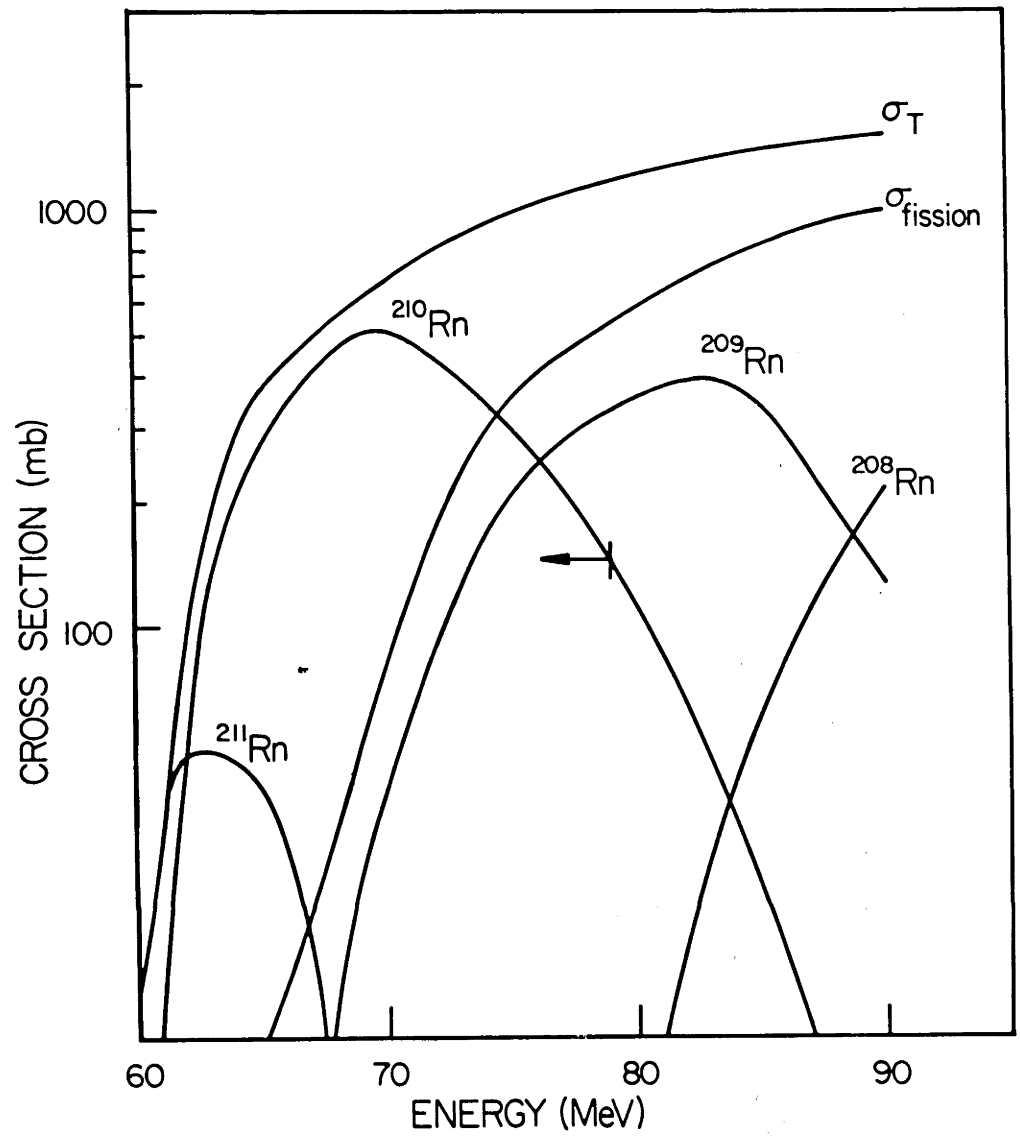

Fig. 3.4b: Cross sections for the reaction used in the g-factor experiment (as calculated using the computer code ZPACE). The total cross section is integrated from 0-78 MeV.

signals were stored in event-by-event mode on magnetic tape, however a fast veto system of width 30 ns filtered out 99% of the prompt γ-rays to avoid collecting unnecessary data. One-percent of the prompt γ-rays were allowed through to enable the time zero to be determined. The magnetic field was maintained at 2.42(2) with a homogeneity of 99.95%, and during the experiment the magnetic field was monitored using a Hall probe.

A pulsed beam from the ANU 14UD pelletron accelerator of width ~ 1 ns and 4320 ns separation was used. The pulsing system was initially tuned using a particle detector (with intrinsically better time resolution than the germanium detectors used for detecting γ-rays) viewing directly a tantalum foil placed in the beam path. During the run the pulsing was monitored by the neutron detector (see fig. 3.4) and corrected for time zero drifts.

Figure 3.5 shows a block diagram of the electronics used for the experiment. An important aspect of the electronic arrangement was that the time signals from both detectors were combined to feed the same time to amplitude convertor "(TAC)". (If a separate TAC was used for each detector there could have been systematic errors introduced in calibrating their dispersions.) The stop pulse for the TAC was derived directly from the master oscillator controlling the pulsing. The time range used was 4 μs while its dispersion was determined to be 1.482(2) ns/chan using an Ortec 462 TAC calibrator which has a nominal accuracy of 1 part in 1000. Slow rise time rejection was used to improve the timing resolution. The use of slow rise time rejection has the side effect of reducing the detector efficiency below ~ 250 keV. Only γ-rays in the energy interval 300-1600 keV were collected, again to save storage space. Associated energy and time signals were "strobed" to ensure that they arrived at the ADCs at the same time.

During the experiment approximately 2×10^8 events were recorded on magnetic tape. From the delayed γ-ray spectra shown in fig. 3.7 it is apparent that the reaction produced the ^{210}Rn nuclei cleanly. Most of the contaminant lines could be identified as being from the neighbouring radon isotopes or from ^{208}Po or ^{206}Po. However there were other contaminants such as the 937 keV line from ^{18}F and the

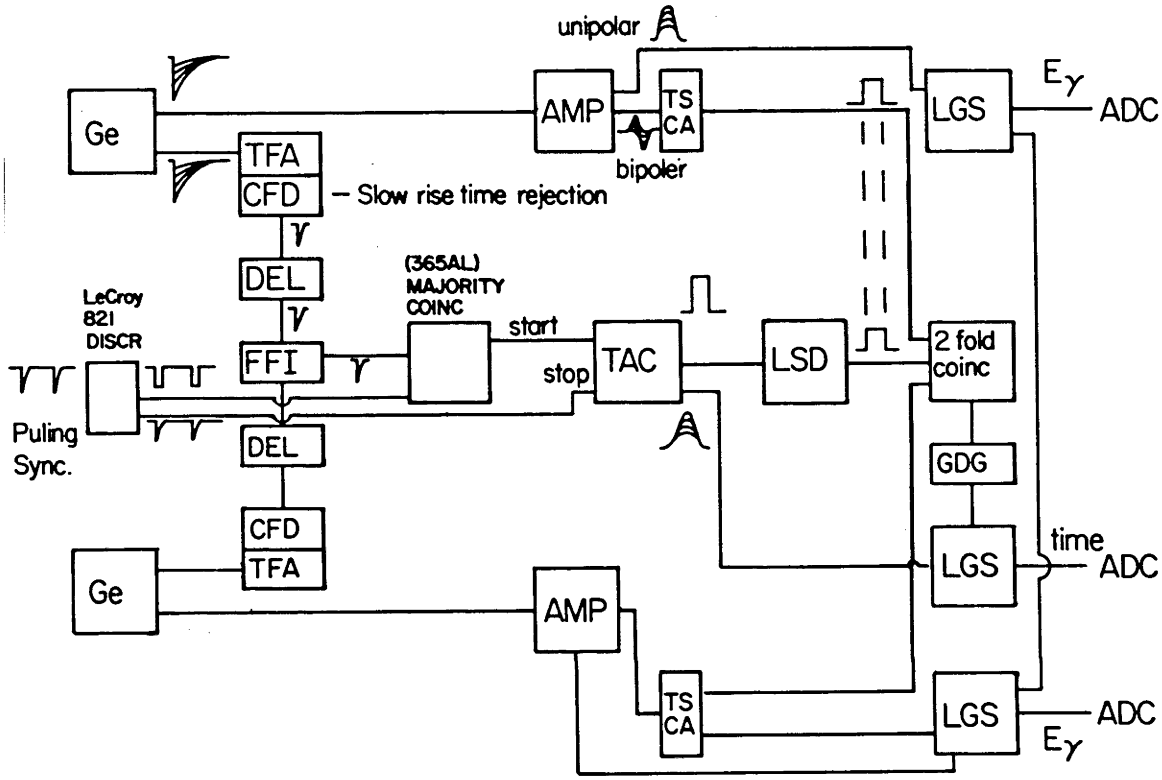

Fig. 3.5: Circuit diagram of electronics used for the g-factor experiment. The boxes represent standard electronic modules. Abbreviations: SCA = single channel analyser, TFA = timing filter amplifier, LGS = linear gate and stretcher, TSCA = timing single channel analyser, FFI = fast fan-in, GDG = gate and delay generator, LSD = logic shaper and delay, CFD = constant fraction discriminator, ADC = analogue to digital converter and TAC = time to amplitude converter.

1000 keV line from ^{71}As. The ^{18}F was produced by a reaction on the mylar film covering the mercury, the recoils subsequently decaying in the mercury, while the ^{71}As was produced by a reaction on the copper target holder. Although the ^{202}Hg target thickness of 160 mg cm^{-2} was sufficient to stop the beam, the small size of the target (radius - 0.3 cm) enabled a small amount of beam to strike the copper directly.

3.4 ANALYSIS AND RESULTS

The time spectrum for each γ-ray was formed by sorting the data to select events which fell within a particular digital energy window. Their associated times were accumulated in a time spectrum. Time spectra for all the discrete γ-ray lines of interest together with background windows nearby in energy were generated in this way. The background time spectra were subtracted from the discrete γ-line time spectra, after appropriate scaling, to form the background subtracted time distributions.

Care had to be taken in choosing background windows to ensure their characteristics were as close as possible to the true background under the peak of interest. As an example of the precautions necessary, consider the 842 keVγ-ray which decays directly from the 25^- state in ^{210}Rn (fig. 3.7). By comparing the different time slices in fig. 3.6 it can be seen that the background under the 842 keV line changes with time. The time varying background associated with the 842 keV line results from both the nearby 847 keV $^{56}Fe(n,n')$ line and the "neutron edge" at 834 keV.

The "neutron edge" results from neutrons created during the reaction which inelastically scatter from the ^{72}Ge nuclei in the detector exciting the 2^+ state at 834 keV. To conserve momentum the scattered nucleus gains kinetic energy, hence the energy absorbed in the detector is usually greater than 834 keV. It can be seen from

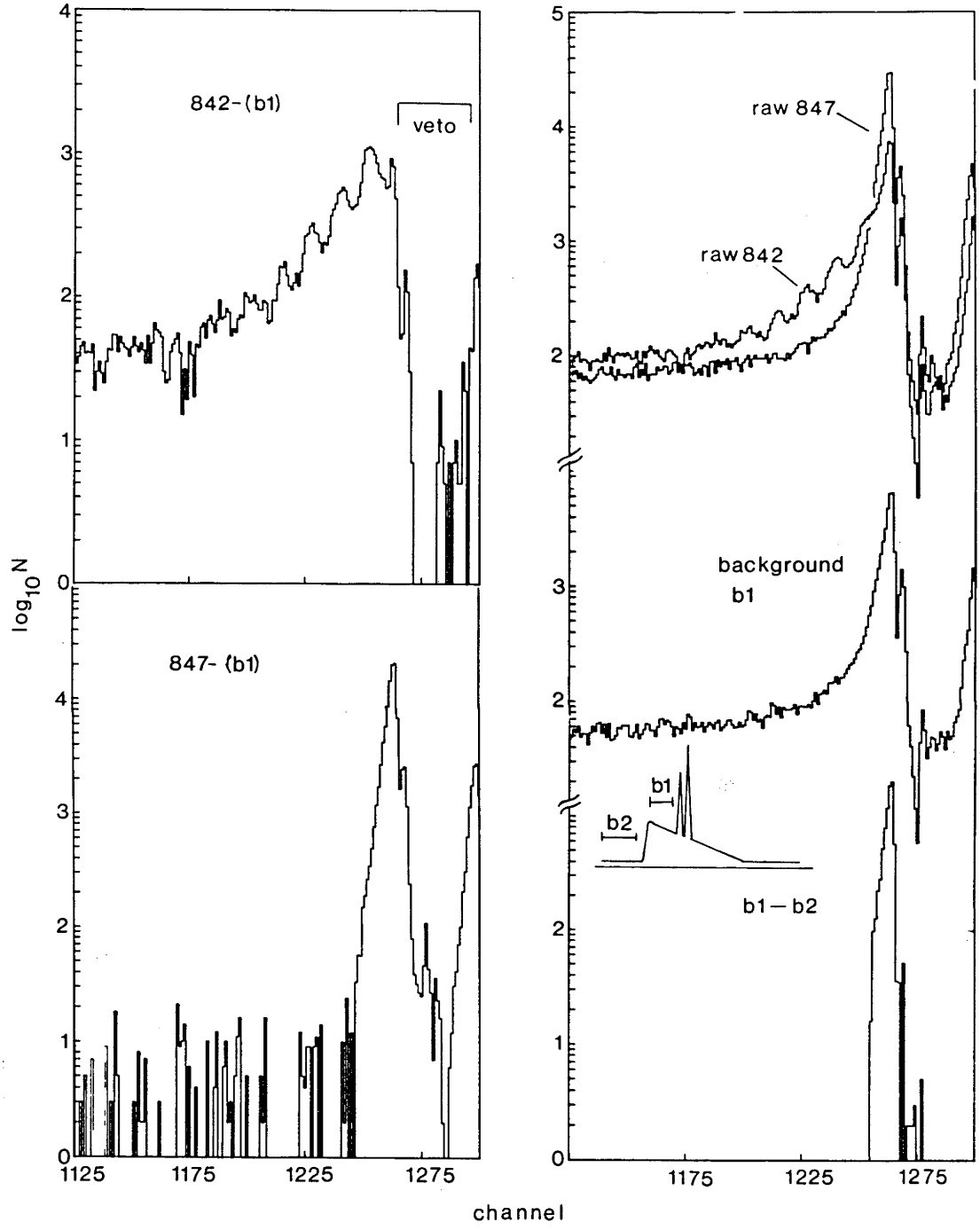

Fig. 3.6: Time slices of regions near the 842 keV line illustrating background subtraction procedures.

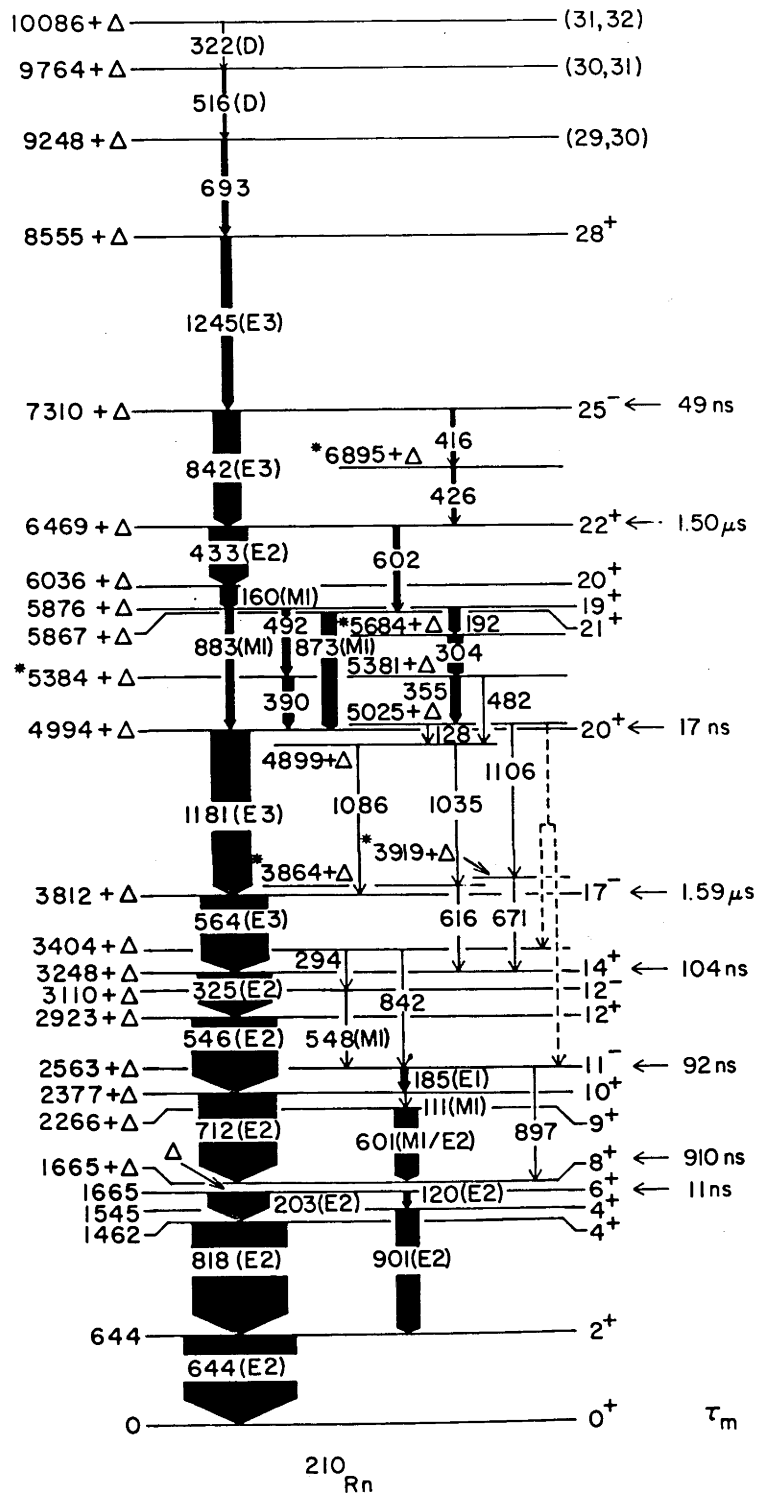

Fig. 3.7: ^{210}Rn level scheme (Pol82) where the width of the lines represent the γ-ray intensities.

fig. 3.9 that there are other neutron edges at 596 keV and 691 keV. Many of the neutrons involved in the process are not directly from the reaction in the target, but have lost energy by scattering from nuclei in the surrounding environment (e.g. the pole pieces). The lower right panel of fig. 3.6 shows the background window set on the "neutron edge" after the time spectrum of a background window set away from the "neutron edge" has been subtracted. The time distribution of the resulting spectrum is clearly consistent with the above explanation (remembering that the 834 keV level in ^{72}Ge is not isomeric). In the top right panel of fig. 3.6 the 842 keV and 847 keV γ-ray lines are illustrated. As expected that for the 847 keV line is free from the oscillations which are evident in the time spectrum of the 842 keV line.

Using the background subtracted windows and correcting for the differing detector efficiencies, the ratio functions can be formed.

The detector efficiencies as a function of energy were obtained from the totalised yields of the major peaks in the ^{210}Rn energy spectrum. It was found that the relative efficiencies of the two detectors differed by only a few percent in the energy range of interest.

In fig. 3.8 theoretical ratio functions for the 325 keV γ-ray which decays from the 14^+ state and is strongly fed by the 17^- state, are plotted. The g-factors for the 14^+ and 17^- states are expected to be close in value. From the figure it can be seen that in this case the g-factor of the 14^+ state will be determined mainly from a phase shift. To determine such a phase shift the effective time zero needs to be known accurately. As well as uncertainty in the absolute time zero, due to "time walk" it will be a function of γ-ray energy. Time zero was initially determined using the prompt γ-ray peaks in the

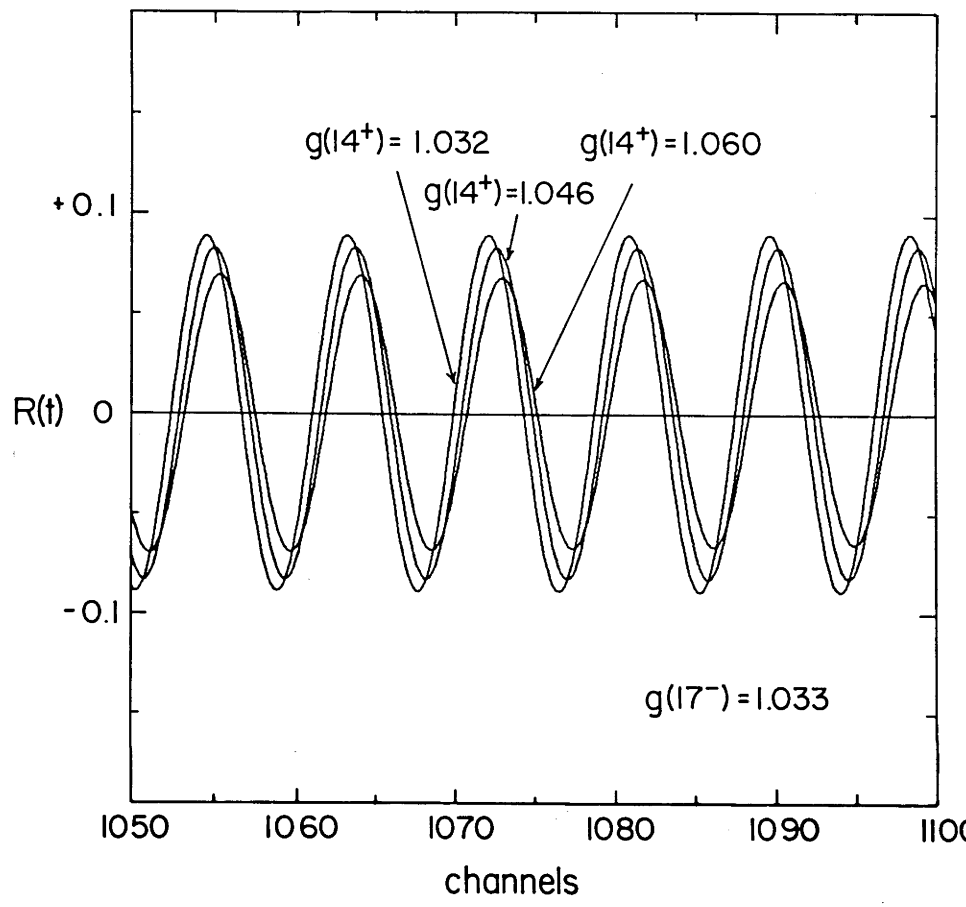

Fig. 3.8: Theoretical curves for the ratio function of the 325 keV γ-ray which decays form the 14^+ state. The three curves illustrate the expected phase shift in the long time region for values of the 14^+ g-factor which are close to the value of the 17^- g-factor.

spectrum. Since there were only a few of these, the time zero of the background windows as a function of energy were plotted, through which a smooth curve was drawn (fig. 3.10). Only part of the background at time zero is due to prompt γ-rays from the continuum. Hence the curve will not be a true indication of effective time zero. In fact much of

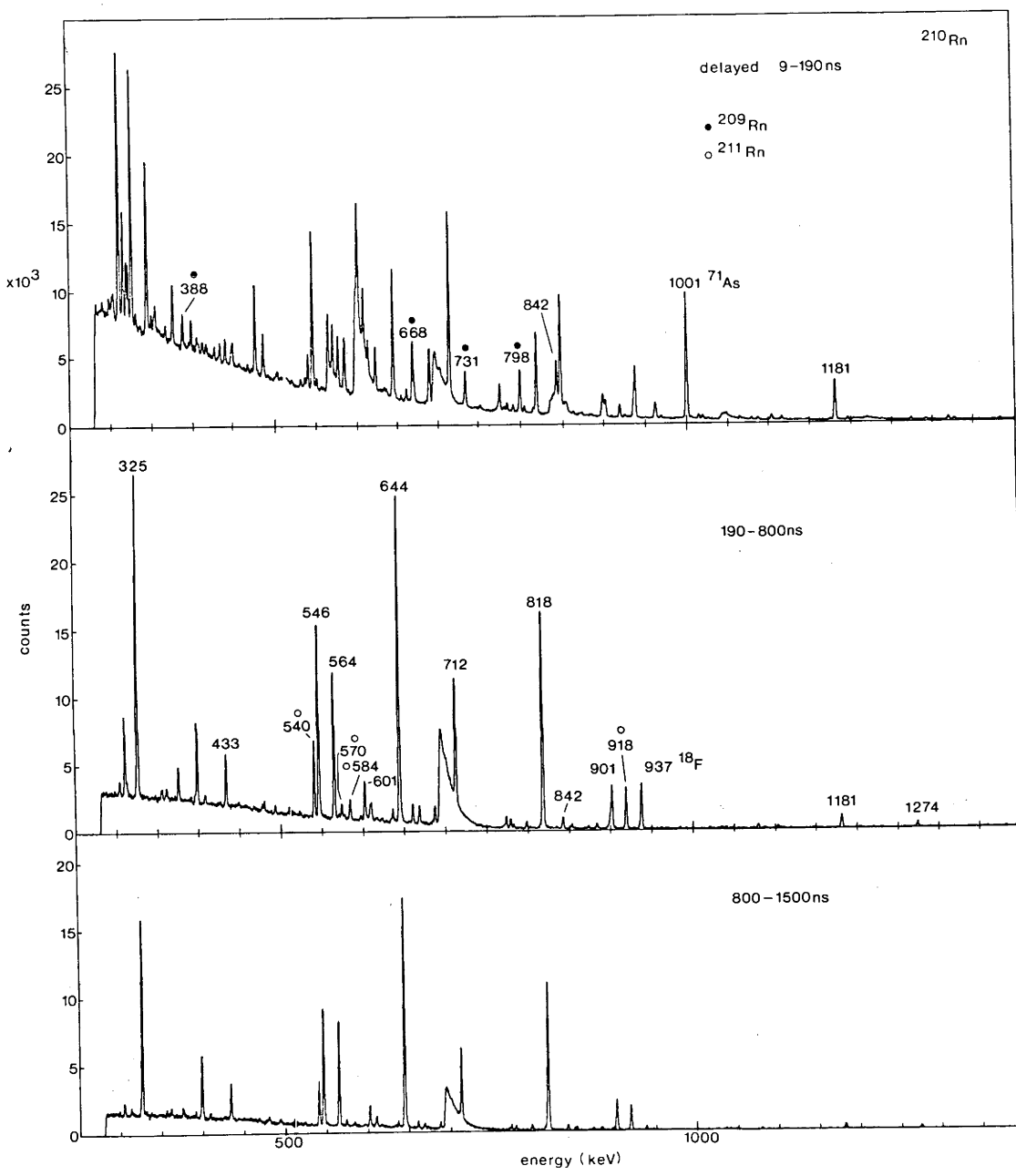

Fig. 3.9: Delayed γ-ray spectra, for different time regions. Contaminant lines are marked.

the intensity will be due to Compton events which result from γ-rays which have interacted with the edges of the germanium crystal and consequently have a different time distribution to the γ-rays interacting in the centre of the crystal. Using the prompt peaks and from other experiments (such as the timing experiment described below), the expected difference between the "background" time zero and the true time zero was estimated and a displaced second curve was drawn to estimate the true time zero as a function of energy (see fig. 3.10). Another factor which will mock up a phase shift is the rotation of the reaction plane caused by the beam bending in the magnetic field. This was calculated by Stuchbery (Stu85) to be 6.7(1)° where the errors reflect uncertainties in the fringing field determination and target position.

Finally the ratio functions will depend on the sidefeeding intensities which were determined by fitting the areas under the ^{210}Rn γ-ray peaks and correcting for the intensity vetoed out at time zero.

The ratio functions were fitted using a least squares fitting program, written by Andrew Stuchbery, based on the multiple feeding formula given by Hausser et al. (Hau76). For long lived isomers the Larmor frequency can be determined without reference to time zero. Thus to eliminate possible errors in the determination of the effective time zero and the calculation of the beam bending, the g-factors of these states were determined with the time zero taken as a free parameter. Checks were made by extrapolating the fitted curves back to time zero in cases of single isomers that the time zero values and beam bending corrections were reasonable. For the 14^+ and 20^+ states both of which are relatively short lived and fed by longer lived higher isomers, it was possible to determine their g-factors more accurately by fixing the time zero. Figures 3.11-3.13 show the

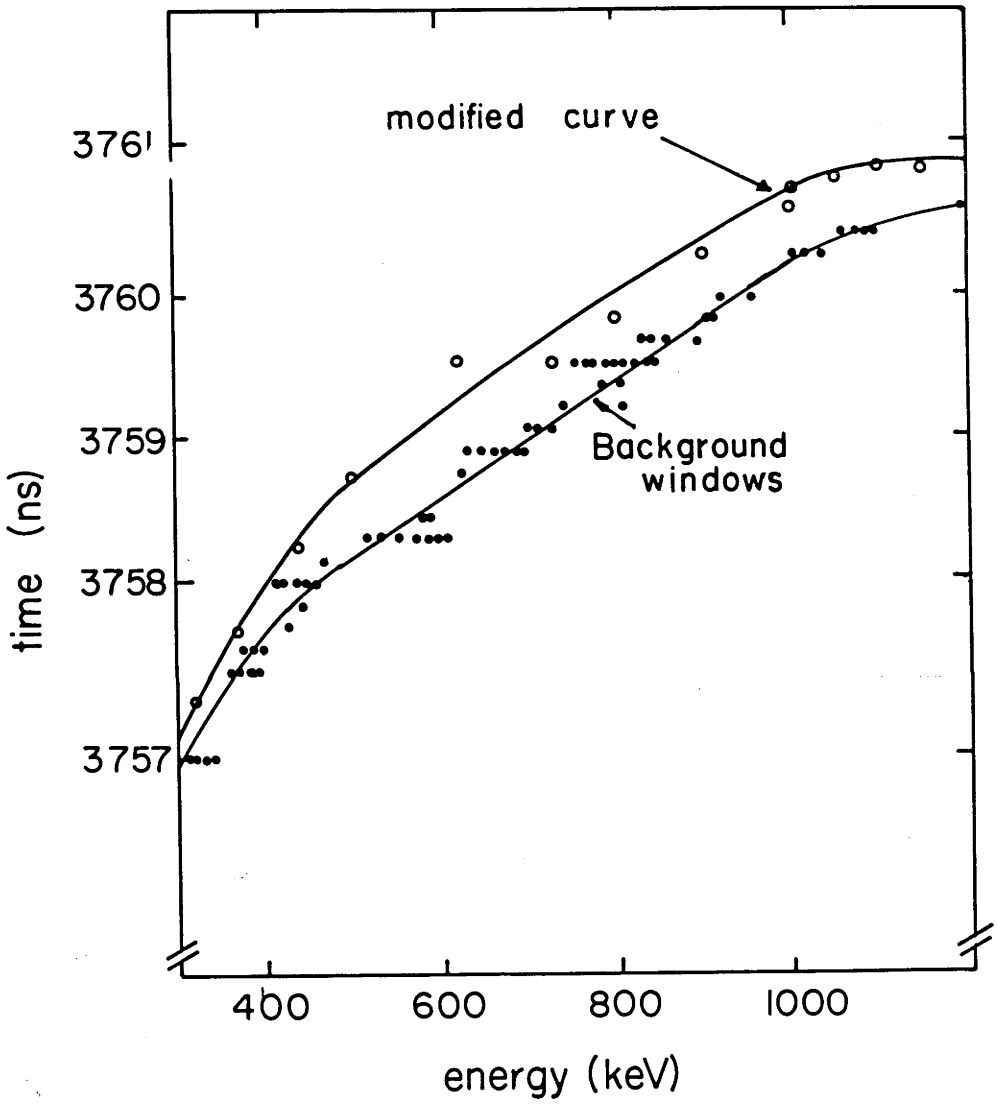

Fig. 3.10: Curves illustrating "time walk". The lower curve is the time zero for the background windows while the higher curve is the estimated "true" time zero.

ratio functions together with the fits. Since the properties of any higher isomers feeding the state of interest are needed in the fitting procedure the ratio functions were fitted in descending order from the top-most isomer. The A_4 coefficients should be small compared to the A_2 coefficients and so were ignored in the fitting procedure. To check that this is indeed a good approximation several "test" cases were fitted with a non-zero A_4.

The ratio functions of γ-rays decaying directly from a short lived isomer which is fed by a long lived isomer could be used to independently determine the g-factor of the higher isomer. This was done by noting that the short lived isomer essentially causes a phase shift away from the origin, so that the g-factor of the long lived isomer could be ascertained by allowing the time zero to vary in the fitting procedure. Thus the g-factor of the 22^+ state could be determined from the ratio function in the long time region of the 1181 keV line which decays directly from the 20^+ state.

As a check on possible systematic errors in the experiment, the g-factors of the 937 keV line in ^{18}F (which decays in the same environment as the ^{210}Rn) was fitted (fig. 3.14). The value obtained for the g-factor of the 5^+ state in ^{18}F was 0.568(8) which is close to the accepted value of 0.572(6) (Led78). (The diamagnetic and Knight shift corrections are negligible for F in Hg.) Similarly, the value obtained for the g-factor of the 1001 keV state in ^{71}As was 1.148(10) which compares to the accepted value of 1.144(20) (Led78). The g-factor of the $17/2^-$ state in ^{211}Rn could also be determined by fitting the ratio function of the 540 keV line which is fed by the $17/2^-$ state. The value obtained (0.914(8)) is in excellent agreement with the value of 0.912(7) reported by Poletti et al. (Pol85), which ensures that the relative values of the g-factors in ^{210}Rn and ^{211}Rn

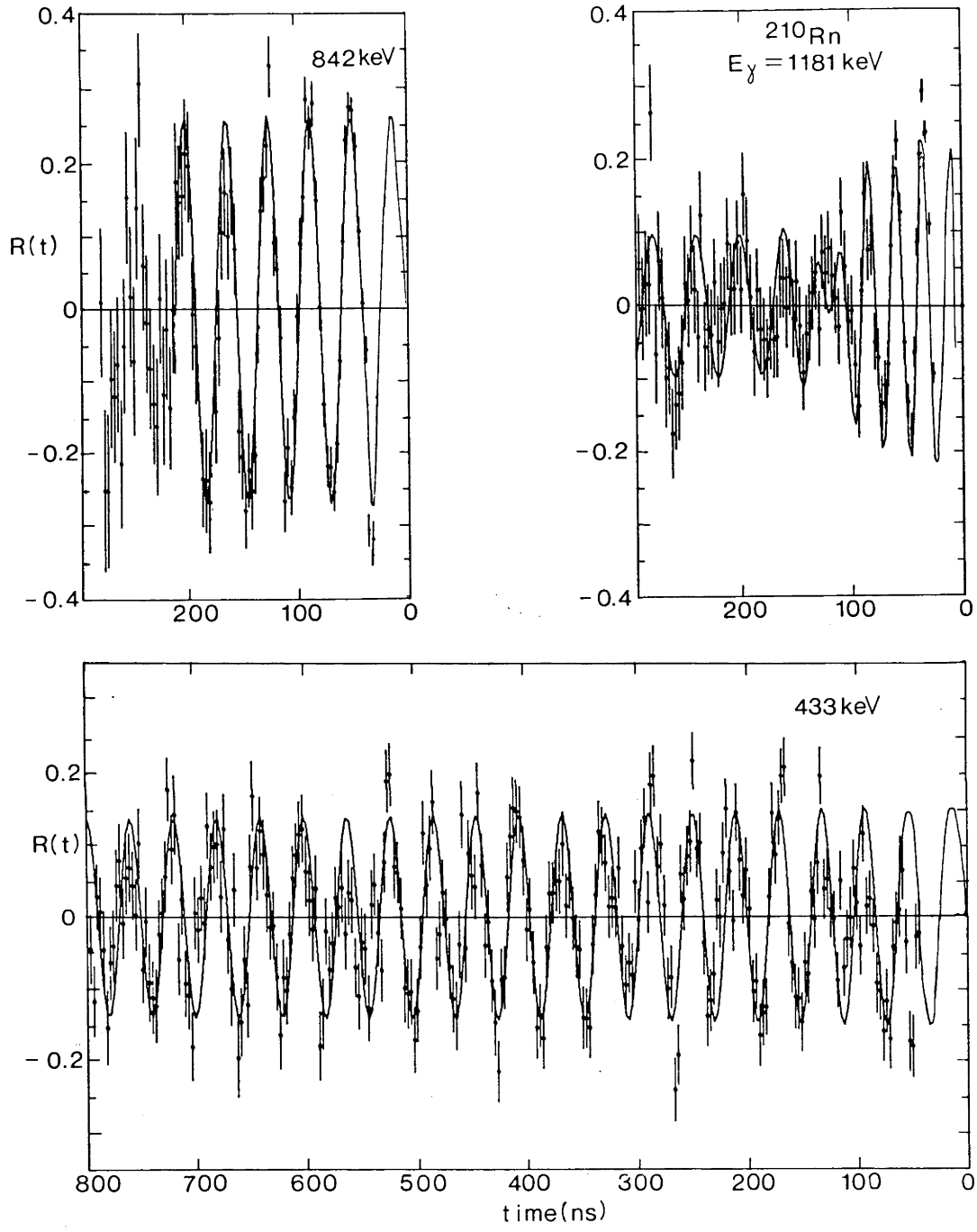

Fig. 3.11: Ratio functions for γ-rays decaying from the three highest isomers in ^{210}Rn. Note the interference patterns evident in the ratio function of the 1181 keV transition.

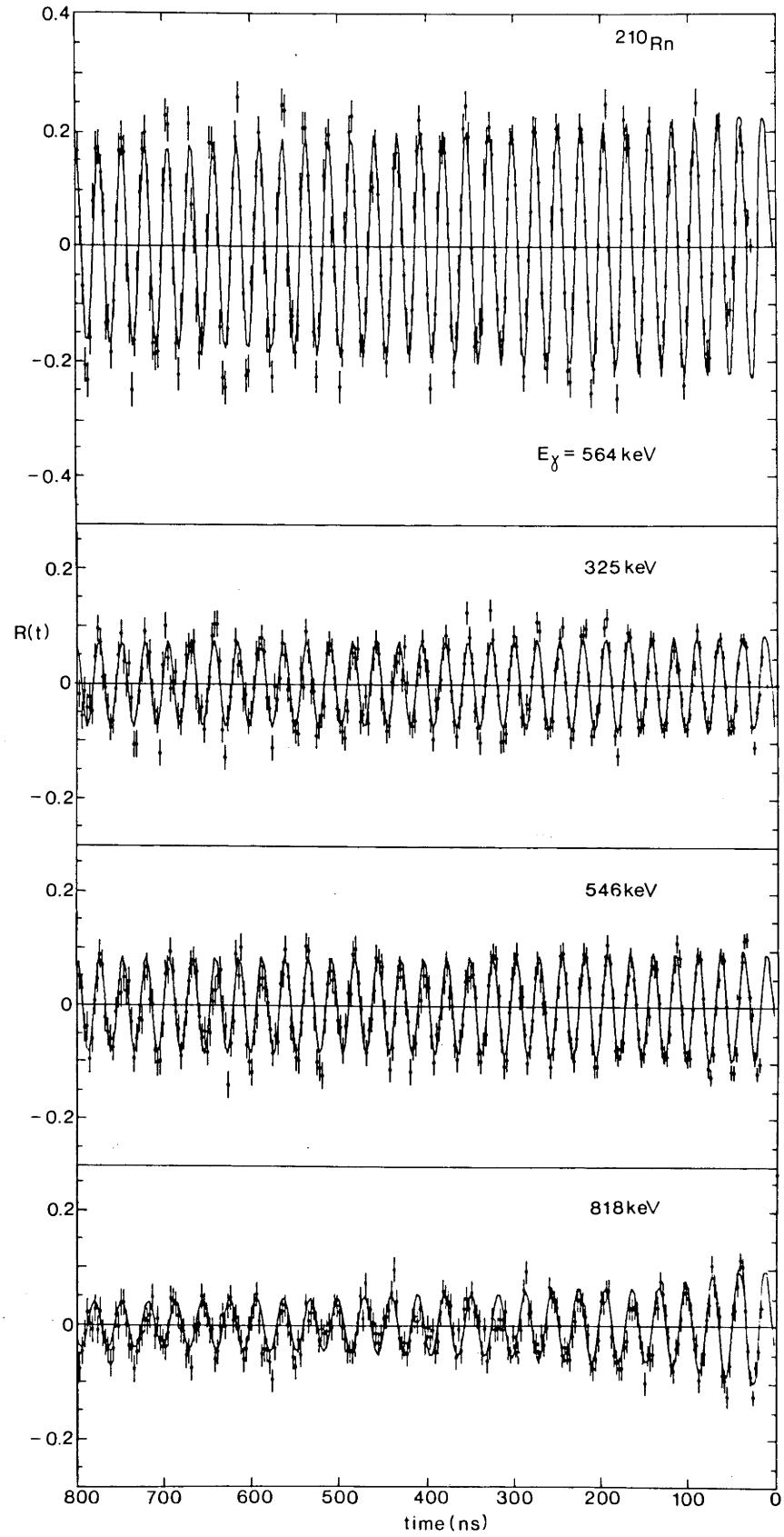

Fig. 3.12: Ratio functions for γ-rays decaying from the 17^-, 14^+ and 8^+ states. Note that both the 546 and the 325 ratio functions were used to determine the g-factor of the 14^+ state.

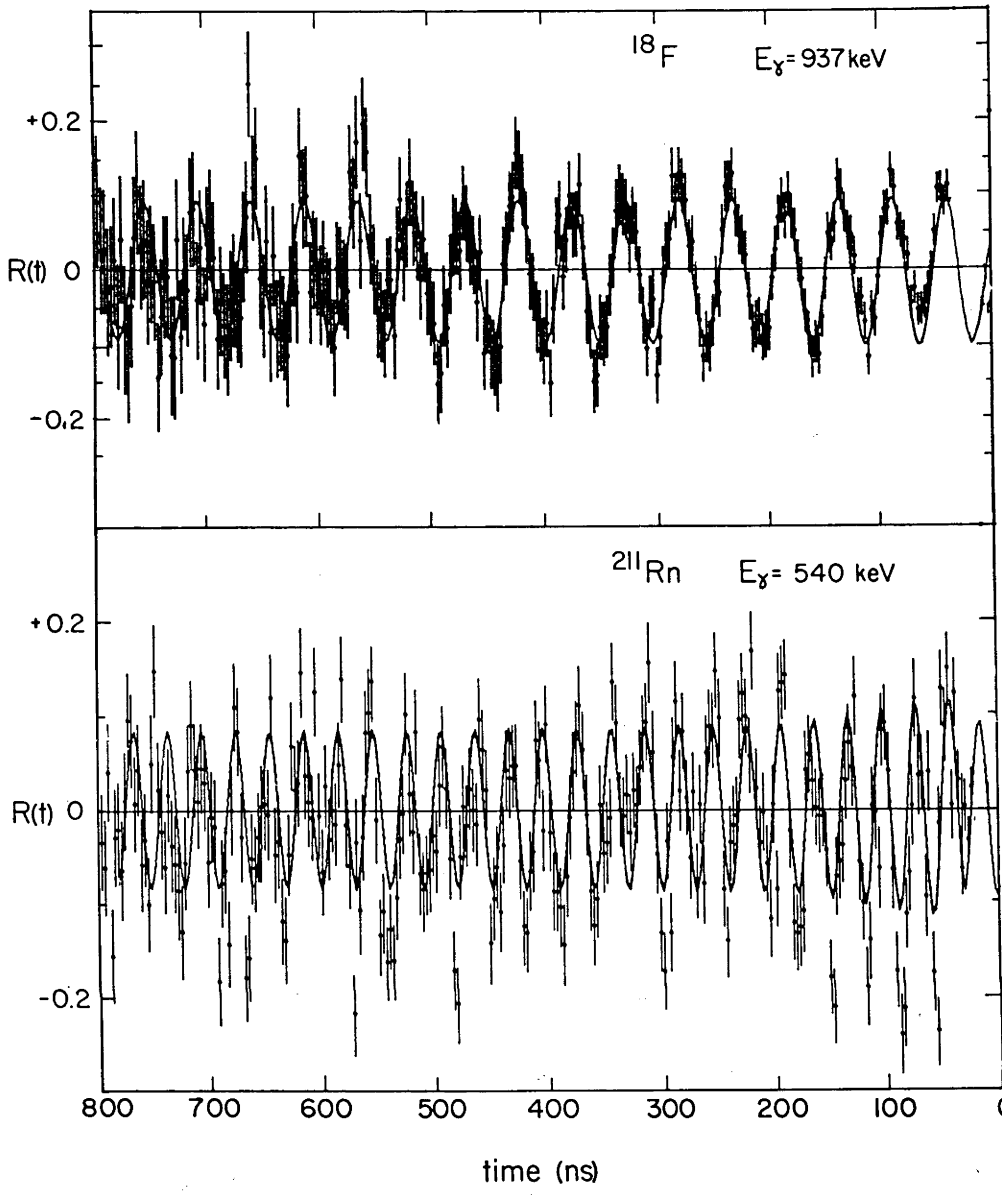

Fig. 3.13: Ratio functions used to check the field and time calibration. The 937 keV line decays from the 5^+ state in ^{18}F while the 540 keV line was used to determine the g-factor of the $17/2^-$ state in ^{211}Rn.

are known accurately. The experiment reported by Poletti et al. was part of the same series of experiments as that described in this thesis so there could be systematic errors common to the two experiments. However, in the experiment of Poletti et al. the g-factors of several isomeric states in ^{212}Rn were found to be in good agreement with the values reported by Horn et al. (Hor77). Further in the experiment of Byrne et al. (Byr85), which was also part of the

same series of experiments but with a different target arrangement, the g-factor of the $29/2^+$ state in ^{213}Fr was measured as 1.041(10) which compares to the value obtained by the Chalk River group of 1.0383(8) (Bee77). All of these checks are consistent with the contention that the systematic errors, for example in the time or field calibrations, are small.

In table 3.1 the measured g-factors are presented. Most of the quoted error is due to uncertainties in the magnetic field and the time calibrations which have nominal uncertainties of 1% and 0.1% respectively. However because the independent checks that were made on possible calibration errors, as described above, were consistent with the systematic errors being small the total error in the field and time calibrations was taken as one half of one per cent. Since the g-factor of the 14^+ state is essentially determined from phase shift information the quoted error reflects uncertainty in the time zero calibration. Although the lifetime of the 20^+ state is relatively short the expected ratio function of the 1181 keV line is not overly sensitive to the time zero determination. The reason for this is that the g-factor of the 20^+ state and the 22^+ state feeding it are very different, hence there are noticeable interference effects (see fig. 3.11). Also in table 3.1 the g-factor values obtained here are compared to the values obtained by Maier et al. (Mai81). The measurements agree within the quoted errors, although there could be a slight systematic difference.

In the same table the g-factors of the configurations proposed by Poletti et al. (Pol82) are compared with the experimental g-factors. The g-factors of the configurations are calculated using the experimental g-factors of the single particle states (if available) and additivity.

TABLE 3.1

I	E(keV)	g (exp)[a]	g (Mai81)	A_2	Configuration	g(calc)
25^-	842	0.733(9)	-	0.42(3)	$\pi(h^3i)_{17}-\nu(jp^{-1})_8+$	0.70
					$\pi(h^2i^2)_{20}+\nu(gp^{-1})_5-$	0.86
22^+	433	0.701(7)	-	0.22(4)	$\pi(h^3i)_{17}-\nu(gp^{-1})_5-$	0.76
	1181	0.703(7)				
	average	0.702(6)				
20^+	1181	1.115(5)	-	0.36(4)	$\pi(h^2i^2)_{20}+$	1.11
17^-	564	1.051(5)	1.049(10)	0.35(2)	$\pi(h^3i)_{17}-$	1.04
	325	1.052(8)				
	546	1.053(8)				
	average	1.052(5)				
14^+	325	1.065(8)		0.12(2)	$\pi(h^3f)_{14}+$	1.07
	546	1.062(10)		0.14(2)		
	average	1.064(7)	1.043(20)			
8^+	818	0.900(9)		0.14(2)	$\pi(h^4)_8+$	0.91
	644	0.897(9)		0.12(2)		
	average	0.898(7)	0.883(10)			

[a] Corrected values. $g_{corr} = g_{uncorr} \times 1.0186$.

It can be seen that the theoretical g-factors for the lower spin states are in good agreement with the experimental values. It should be noted that the g-factor of the h^4 configuration is overestimated due to core polarisation blocking (spin flip admixtures $(h_{9/2}h_{11/2}^{-1})$ contributing to the single particle $h_{9/2}$ g-factor are blocked) (Tow76). For the high-spin states the g-factors are certainly consistent with the contention that these are core excited states. Notwithstanding this the calculated g-factors (assuming pure configurations) are sometimes quite different from the experimental values. In Chapter 4 the reasons for the discrepancies will be investigated.

As well as the g-factor information, the A_2 values are listed in the table. These are all consistent with the spin assignments of Poletti et al. ((Pol82), see fig. 3.7). For aligned E3 transitions in the m = 0 angular momentum substate the expected A_2 should be about 0.68. Since the reaction populates the m substates with an approximately Gaussian distribution around the m = 0 substate the observed A_2 should be less. In fact calculations predict that the measured A_2 for a heavy ion reaction should be approximately 0.5. We attribute the difference between the observed and expected values, not to relaxation effects, but to time zero drifts in the pulsing system. During the experiment an electronic feedback system was used to automatically corect time zero drifts, however it was still being developed and occasionally had to be adjusted manually. Hence the prompt peaks were effectively 3 ns wide, compared to the nominal 1 ns width. (This will of course change only the measured A_2 values and not the g-factors.) In a later g-factor experiment with the electronic feedback more developed, using the same experimental apparatus to measure the g-factors of states in ^{213}Rn (Stu85) all of the expected alignment was seen.

3.5 TIMING MEASUREMENTS

The expected lifetime of the 1245 keV ($28^+ \rightarrow 25^-$) E3 transition in ^{210}Rn of 3-6 ns, is less than the limits set by previous experiments (Pol82). To determine its lifetime accurately and hence its B(E3) value, which is crucial to the nuclear structure interpretation advanced in chapter 4, a fast timing experiment was carried out. A pulsed ^{17}O beam of width ~ 1 ns and pulse separation of 108 ns was used to bombard a ^{198}Pt target (96% pure). Two hyperpure germanium detectors were used at $\pm 56°$, one of which was much more efficient for the lower energy γ-rays. The pulsing system was tuned and monitored

in the same way as that described in the g-factor experiment. Time drifts of the pulsing system were automatically corrected using the feedback system referred to above.

The data were recorded in event-by-event mode on magnetic tape and the background subtracted time spectra were generated in a manner similar to that described in the g-factor experiment. To obtain the lifetimes of the short lived isomers it was necessary to take into account the width of the prompt response function (PRF) (Lew85). The variation of the PRF width and time zero needed in the fitting procedure was established using γ-rays which are known to be prompt.

3.5.1 The Results

The lifetime of the 28^+ state was determined from the time spectrum of the 1245 keV transition. In fig. 3.14 the fit is shown together with the line shape expected for a prompt γ-ray of the same energy. As well as the 28^+ state the lifetimes of several other states were ascertained with a greater accuracy than previous experiments (Pol82). These results are presented in table 3.2. Since the main motivation for the measurements was to accurately determine the enhanced E3 strengths for the yrast transitions in ^{210}Rn, the B(E3) values are also listed in table 3.2. It should be noted that a sidebranch decay from the 28^+ state with an intensity as high as 10% would not have been seen by Poletti et al. (Pol82) so in this respect the quoted B(E3) is an upper limit. The measured value for the mean life of the 25^- state deduced from the decay curve of the 842 keV transition is 52(5) ns compared to the previous value of 49(2) ns. Similarly the measured lifetime of the 20^+ state of 19(2) ns is slightly higher than the previous determination of 17(1) ns.

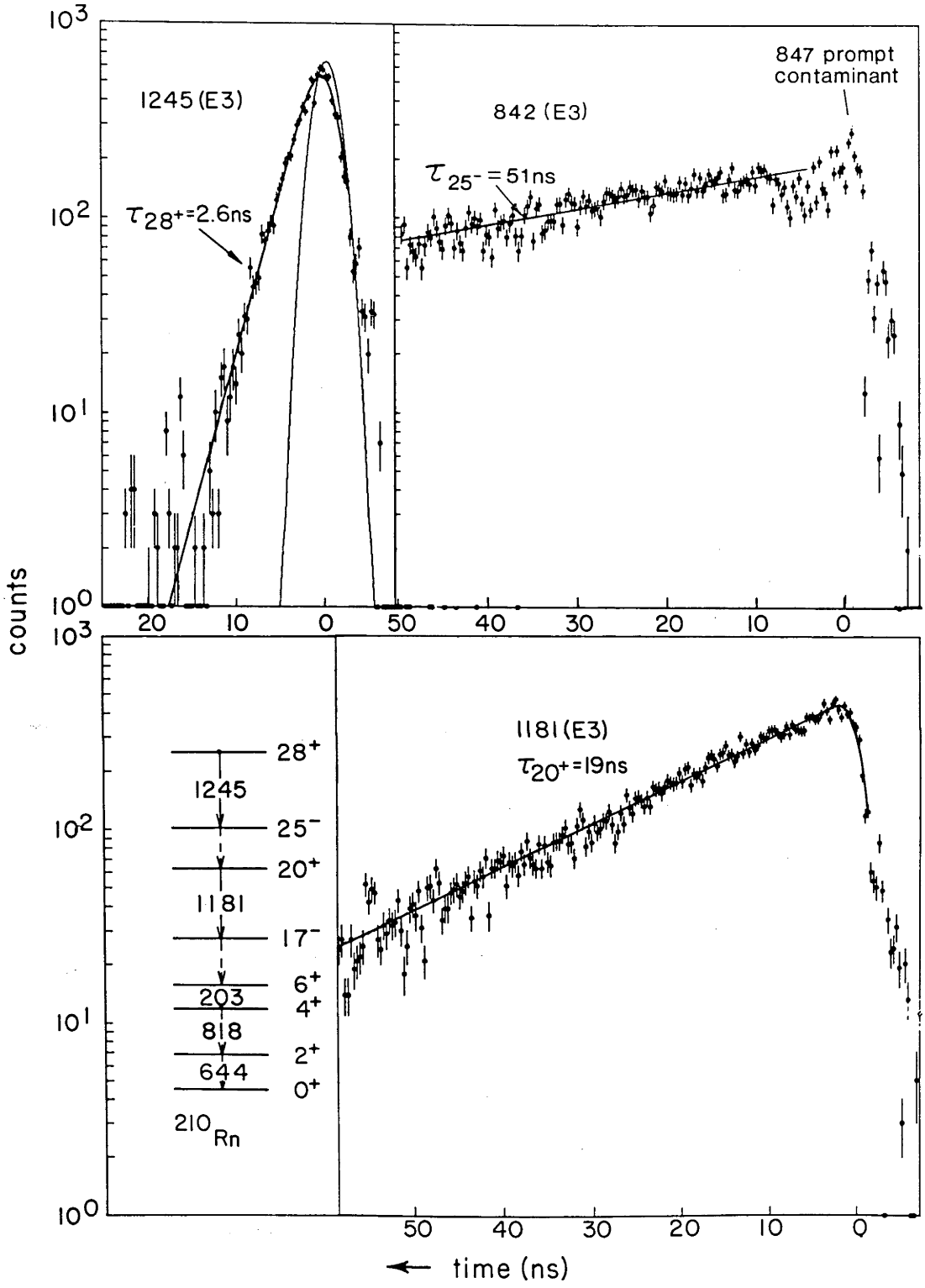

Fig. 3.14: Time spectra for transitions in ^{210}Rn (discussed in the text). The P.R.F. is illustrated for the 1245 keV transition.

Table 3.2: Measured mean lifetimes and deduced B(E3) values. The B(E3) values were calculated using the branching ratios, which were obtained from the g-factor data, and the given electron conversion coefficients for the main γ-ray (α) and the branch γ-ray (α_β) (Po182).

I	τ_m (ns)	$I_i \rightarrow I_f$	Branching Ratio (γ)	α_β	α	B(E3) ($\times 10^3$) e^2fm^6
28^+	2.6(3)	$28^+ \rightarrow 25^-$	100%	-	0.01	145(17)
25^-	52(5)	$25^- \rightarrow 22^+$	89%	0.7	0.02	91(9)
20^+	19(2)	$20^+ \rightarrow 17^-$	100	-	0.01	27(2)

CHAPTER 4

CALCULATIONS

4.1 INTRODUCTION

In Chapter 2 we looked at several interpretations of the high spin states in ^{210}Rn, ^{211}Rn and ^{212}Rn. It was seen that none of the models could explain the g-factor, B(E3) and excitation energy information simultaneously. Recently it has been suggested that some of the high-spin "shell model" states in this region are substantially mixed (Pol85, Byr85, Ber85, Kal85). Since many of the "single particle" states in the lead region mix considerably with particle-vibration coupled states, to calculate the energies and the wave-functions of the many particle states consistently, we need to include the particle-vibration components explicitly. In the rest of the chapter we will see how the particle-vibration states are included and what the effect of this is. Initially states with an even number of neutron holes will be examined. Later we will look at states with an odd number of neutron holes.

4.2 PARTICLE-VIBRATION COUPLING TO SINGLE PARTICLE STATES

It is well known that some of the single particle states around the lead region will mix with particle vibrational states involving the 3^- phonon (Boh75, Ham74, Ham77). In chapter 2 it was noted that the amplitudes of the different components can be calculated directly. Here, for completeness, we briefly consider how this is done.

A vibrational phonon gives rise to fluctuations in the average field which can cause excitations of single particle states. The

potential variation of a vibrational state of multipolarity λ has the same form as that obtained by a deformation of the average static potential of the same multipolarity as λ. Hence the particle-vibration Hamiltonian is:

$$H^{\lambda}_{pv} = k_{\lambda}(r) \sum Y^{*}_{\lambda\mu}(\theta,\phi)\alpha_{\lambda\mu}$$

where α_λ is the vibrational amplitude and $k_\lambda(r)$ is the radial form. $k_\lambda(r)$ is obtained by assuming that the deformed potential is:

$$V_0(r(1 + \sum_{\mu} \alpha_{\lambda\mu} Y^{*}_{\lambda\mu}(\theta,\phi))^{-1})$$

which can be expanded as

$$V_0\,(r(1 + \sum_{\mu} \alpha_{\lambda\mu} Y^{*}_{\lambda\mu}(\theta,\phi))^{-1}) = V_0(r) - r \sum_{\mu} \alpha_{\lambda\mu} Y^{*}_{\lambda\mu}(\theta,\phi)\frac{\partial V_0}{\partial r} + \ldots \ .$$

and so $k_\lambda(r) \sim -R \frac{\partial V_0}{\partial r}$. Hence the coupling matrix is:

$$h(j_1,j_2) = \langle j_1|H_{pv}|j_2\rangle$$

$$= -i^{\ell_1+\lambda-2}\left(\frac{2\lambda+1}{4\pi}\right)\langle j_1\tfrac{1}{2}\lambda 0|j_2\tfrac{1}{2}\rangle\langle j_2|R_0 \frac{\partial V_0}{\partial r}|j_1\rangle\langle n = 1|\alpha_\lambda|n = 0\rangle$$

n being the number of phonons.

Since the $B(E3)_{3^- \to 0^+}$ in ^{208}Pb depends on $\langle n = 1|\alpha_\lambda|n = 0\rangle$, the matrix element of $\alpha\lambda$ can be taken from experiment, while $\langle j_1|R_0 \frac{\partial V_0}{\partial r}|j_2\rangle$ is calculated using a realistic potential such as the Woods-Saxon potential. Hamamoto (Ham74) has calculated the numerical values $h(j_1; j_2\, \lambda = 3^-)$ for the single particle states around the lead region (which are listed in appendix 2).

Given the matrix elements, the wavefunctions of the "single particle" states can be calculated. For example $h(\nu j_{15/2};\nu g_{9/2}3^-)$ = -770 keV while $h(\nu g_{9/2};(\nu j_{15/2} \otimes 3^-)_{9/2}))$ = -970 keV. Consequently the unperturbed $\nu j_{15/2}$ and $\nu g_{9/2}$ configurations will be pushed down by the mixing with the relevant particle-vibration states. Since the energy separation between the experimental states is known (1420 keV),

the amount that the pure single particle states have been depressed can be calculated. More explicitly if the energies relative to the "$g_{9/2}$" state are taken as x for the $\nu g_{9/2}$ configuration and 1420+y for that of the unperturbed $\nu j_{15/2}$ particle, then the matrix for the "$j_{15/2}$" state is (in keV):

$\nu j_{15/2}$	$\nu g_{9/2} \otimes 3^-$
1420+y	-770
-770	x+2600

while that of the "$g_{9/2}$" state is

$\nu g_{9/2}$	$(\nu j_{15/2} \otimes 3^-)_{9/2}$
x	-980
-980	2600+1420+y

Demanding that the eigenvalue of the matrix returns the observed energies gives the unperturbed single particle energies and the following wavefunctions:

$$\text{"}j_{15/2}\text{"} = .89\,|\nu j_{15/2}> + .51\,|\nu g_{9/2} \otimes 3^->$$

$$\text{"}g_{9/2}\text{"} = .98\,|\nu g_{9/2}> + .2\,|(\nu j_{15/2} \otimes 3^-)_{9/2}>$$

(where the E3 transitions between the components are marked). The B(E3) value can now be calculated directly using an appropriate value for the pure single particle transition matrix element (Ham74). There are of course other "single particle" states which mix considerably with particle-vibration coupled states. In table 4.1 we list the unperturbed energies of some of the single particle states in the lead region. The wavefunctions of the observed states are also listed.

In the table the energies are relative to the ground state energy of the relevant nucleus while dE is the difference between the pure particle energy and that of the observed state.

TABLE 4.1: "SINGLE PARTICLE" STATES

Nucleus	State	E (MeV)	dE (keV)	Wave Function
^{209}Bi	$\pi i_{13/2}$	2.220	410	$.912\|\pi i_{13/2}\rangle+.365\|\pi f_{7/2}\otimes 3^-\rangle$ $+.19\|h\otimes 3^-\rangle$
	$\pi f_{7/2}$	1.284	387	$.952\|\pi f_{7/2}\rangle+.307\|(\pi i_{13/2}\otimes 3^-)_{7/2}\rangle$
	$\pi h_{9/2}$	0.15	15	$.998\|\pi h_{9/2}\rangle-.061\|(\pi i_{13/2}\otimes 3^-)_{9/2}\rangle$
^{209}Pb	$\nu g_{9/2}$	0.213	213	$.977\|\nu g_{9/2}\rangle+.214\|(\nu j_{15/2}\otimes 3^-)_{9/2}\rangle$
	$\nu j_{15/2}$	1.848	426	$.875\|\nu j_{15/2}\rangle+.484\|\nu g_{9/2}\otimes 3^-\rangle$

4.2.1 g-Factors of "Single Particle" States

The g-factors of the "single particle" states will reflect the particle vibration coupled admixtures. Since most calculated single-particle g-factors do not take such mixing into account the calculated g-factors have to be corrected. Hamamoto (Ham76b) has tabulated the corrections for many of the single particle states in the lead region. What will be useful later in the chapter is the opposite approach; given the experimental g-factor, what is the single particle g-factor? Since the g-factor of the 3^- state is known in ^{208}Pb, given the wavefunctions in table 4.1 it is straightforward to disentangle the two contributions to obtain the g-factor of the pure particle state. In appendix 1 the single particle g-factors obtained in this way are tabulated.

4.3 "TWO PARTICLE" STATES

How does the octupole coupling change the energies of the two nucleon states around the lead region?

One way we can think of these "single particle" states is to imagine a nucleon continuously emitting and absorbing phonons. We could represent such a state (say the "$j_{15/2}$" state) by the following

diagram, where a wavy line is a phonon and a straight line signifies a particle.

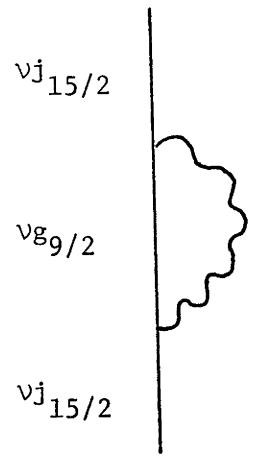

Fig. 4.1: The "$\nu j_{15/2}$" state.

When two "single particles" are coupled together to form a "two particle" state a phonon can be emitted by one particle and absorbed by the other.

For concreteness we will look at the "$(\pi i_{13/2}\nu g_{9/2})_{11}^{+}$" state in ^{210}Bi. The $(\pi i_{13/2}\ \nu g_{9/2})_{11}^{+}$ particle configuration will mix with the $(\pi f_{7/2}\nu j_{15/2})_{11}^{+}$ configuration via the exchange of a 3^{-} phonon. Pictorially the octupole contribution to the matrix element connecting the two configurations is:

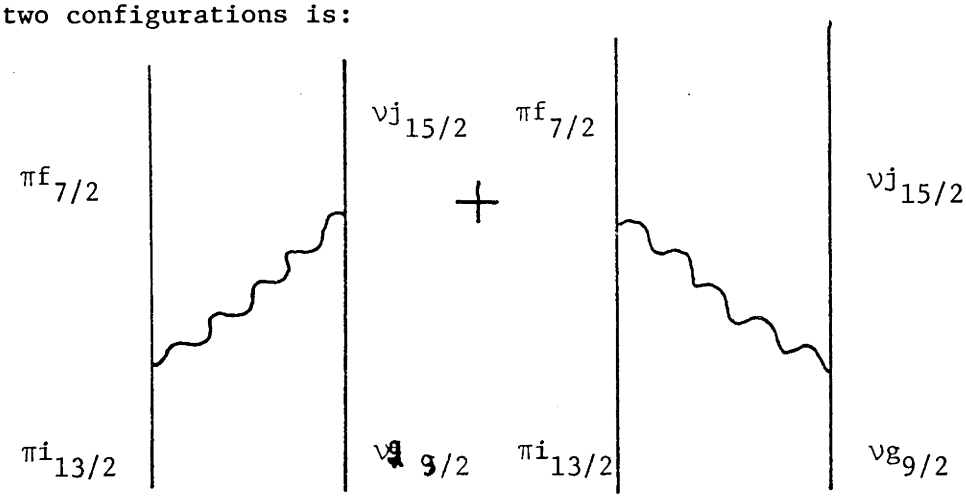

Fig. 4.2: The $\langle \pi f_{7/2}\nu j_{15/2}|V_{oct}|\pi i_{13/2}\nu g_{9/2}\rangle$ matrix element.

Using standard perturbation theory and remembering that:

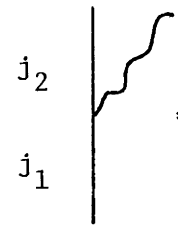

$= h(j_1, j_2 3^-)$ and

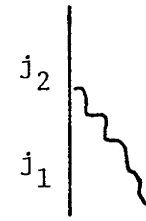

$= h(j_1 3^-, j_2)$

the above matrix element can be calculated.

The contribution of the first diagram in fig. 4.2 is:

$$\langle \pi f_{7/2} \nu j_{15/2} | V_{pv} | (\pi f_{7/2} \otimes 3^-) \nu g_{9/2} \rangle$$

$$\times \langle (\pi f_{7/2} (\nu g_{9/2} \otimes 3^-) | V_{pv} | \pi i_{13/2} \nu g_{9/2} \rangle / (E(ig) - [E(fg) + E(3^-)])$$

$$= h(\nu j_{15/2}; \nu g_{9/2} \otimes 3^-) h(\pi i_{13/2}, \pi f_{7/2} \otimes 3^-) / (-1.9 \text{ MeV})$$

$$= -369 \text{ keV}$$

where we have used the particle vibration matrix elements listed in appendix 2.

In the second diagram of fig. 4.1 the intermediate state must be recoupled:

$$((\pi i (\nu j \otimes 3^-)_{9/2})_{11}^+) = W(13/2,3,11,15/2;7/2,9/2) \hat{7}/2, \hat{9}/2 \times ((\pi i \otimes 3^-)_{7/2} \nu j)_{11}^+$$

so the second diagram contributes

$$(.597) h(j3^-; g) h(i3^-; f) / -4\text{MeV} = -185\text{keV} .$$

Hence in the perturbation approximation the octupole contribution to the off-diagonal matrix element $\langle (\pi f_{7/2} \nu j_{15/2}) | V_{pv} | (\pi i_{13/2} \nu g_{9/2}) \rangle$, is the sum of the two diagrams which is equal to -554 keV. As well as the particle-vibration contribution to the residual interaction there is the shell model "two-body" residual interaction which is calculated by Kuo and Herling to be -310 keV (Kuo71). Adding the two contributions to the residual interaction together, the value of the off-diagonal matrix element becomes -864 keV. (For illustrative purposes we will assume the matrix element reverses.) In the

perturbation approach the wavefunctions are assumed to be 100% pure. In the case considered here such an approximation is not a good one so a more realistic estimate of the value of the off-diagonal matrix element is obtained by multiplying the calculated value by the amplitude for the "$(\pi i_{13/2}{}^{\nu}g_{9/2})$" and "$(\pi f_{7/2}{}^{\nu}j_{15/2})$" states to be in their pure two nucleon configurations. From table 4.1 this amplitude is (.913)(.89)(.98)(.92) = .713 so multiplying -864 keV by .713 we find that the $\langle \pi i_{13/2}{}^{\nu}g_{9/2} | V_{sh} + V_{pv} | \pi f_{7/2}{}^{\nu}j_{15/2} \rangle$ matrix element is -620 keV. To see the effect that the octupole mixing has on the "$(\pi i_{13/2}{}^{\nu}g_{9/2})$" state, for the moment we will ignore the diagonal shell model contribution to the residual interaction ($\langle j_1 j_2 | V_{sh} | j_1 j_2 \rangle$). Therefore the energy change due to mixing is obtained by diagonalising the following matrix:

	"$(\pi i \nu g)$"	"$(\pi f \nu j)$"
	$E(\pi i)+E(\nu g)$	-620
	-620	$E(\pi f)+E(\nu j)$

where the "single particle" energies are those of the experimental states. From the eigenvalue of the matrix we find that the "mixing" lowers the energy by -359 keV compared to the value -150 keV which is obtained in the pure shell model approximation using the value for $\langle \pi i \nu g | V_{sh} | \pi f \nu j \rangle$ quoted above (-310 keV). We shall see below that including the octupole induced mixing improves the agreement with experiment.

The particle vibration coupling is very strong in this example so the perturbative approach we used to calculate the matrix element is not a good approximation. What we have done is to "prediagonalise" the single particle energies and hence the particle-vibration effects have not been included consistently. To include such effects as well

as the shell model interactions in a coherent way it is necessary to use an expanded basis.

4.4 INCLUDING PARTICLE-VIBRATION STATES EXPLICITLY

Using the language of matrix mechanics, the $(\pi i_{13/2}\nu g_{9/2})_{11}^{+}$ and $(\pi f_{7/2}\nu j_{15/2})_{11}^{+}$ configurations couple to non-orthogonal particle-vibration states and hence mix. For example the $(\pi i_{13/2}\nu g_{9/2})_{11}^{+}$ configuration couples to the $(\pi i_{13/2}(\nu j_{15/2} \otimes 3^{-}))_{11}^{+}$ particle-vibration state while the $(\pi f_{7/2}\nu j_{15/2})_{11}^{+}$ configuration couples to the octupole coupled state, $((\pi i_{13/2} \otimes 3^{-})_{7/2}\ \nu j_{15/2})_{11}^{+}$. These two particle-vibration states are not orthogonal. However to set up a matrix we need to choose an orthogonal basis. There are seven orthogonal states that can be made by coupling $(\pi i\ \nu j \otimes 3^{-})_{11}^{+}$ in different ways and in principle all of these would need to be included.

One such basis is $[\pi i\ ((\nu j \otimes 3^{-})_{J})]$ for J = 9/2 ... 21/2.

However a better choice is to take the two states used in the perturbation treatment and form an orthonormal set:

$$[\psi^{+},\ \psi^{-},\ \theta_1,\ \ldots.,\ \theta_5]$$

where

$$\delta = \frac{[((\pi i_{13/2} \otimes 3^{-})_{7/2}\nu j_{15/2}) \pm (\pi i_{13/2}(\nu j_{15/2} \otimes 3^{-})_{9/2})]}{\sqrt{2(1 \pm \delta)}}$$

where $\delta = \langle((\pi i_{13/2} \otimes 3^{-})_{7/2}\nu j_{15/2})|(\pi i_{13/2}(\nu j_{15/2} \otimes 3^{-})_{9/2})\rangle$ is the overlap integral and $[\theta_1,\ldots,\theta_5]$ are chosen in any way to complete the orthonormal set.

Each θ_i will have a zero matrix element with the particle states. (For example to compute $\langle(\pi f_{7/2}\nu j_{15/2})|V_{pv}|\theta_i\rangle$, θ_i would need to be recoupled in terms of $((\pi i \otimes 3^{-})_{7/2}\nu j)$. But each θ_i is, by choice orthogonal to this state, hence the matrix element is zero.)

There will be off-diagonal matrix elements between the $\psi^{\pm}$ and the θ_i but to a good approximation these can be ignored, as they will be much smaller than the particle-vibration matrix elements. Consequently in the calculation we need not include the states θ_i.

Hence a good basis is the set of states $[(\pi i_{13/2}\nu g_{9/2}), (\pi f_{7/2}\nu j_{15/2}), (\pi f_{7/2}\nu g_{9/2} \otimes 3^-), \psi^+, \psi^-]$. Having found a basis the next step is to calculate the matrix elements needed of which there are two kinds, the shell model residual interactions, and the particle-vibration matrix elements, some of which were used above. (All the matrix elements used have been collected together in appendix 2.)

The shell model matrix elements determine the energy change due to two valence particles interacting. More explicitly, in the shell model the valence particles are placed in an average field which determines the extreme weak coupling energy and the spatial part of the single particle orbitals. Two valence nucleons will interact via the two-body nucleon-nucleon force changing the energy and wavefunction of the state. The shell model matrix elements that we use where possible are those calculated by Kuo and Herling (Kuo71), which include a 1p-1h polarisation contribution as well as the bare nucleon-nucleon force. The polarisation contribution does not include collective effects such as the octupole coupling that we are considering here, however for phenomenological matrix elements such as those of Ma and True (Ma73), some of the particle-vibration effects are included implicitly through a $P_3(\cos\theta)$ contribution.

Using the two-body and particle-vibration matrix elements listed in appendix 2 and recoupling the wavefunction where necessary, the following matrix is obtained for the yrast 11^+ state in ^{210}Bi (MeV): Since the matrix is symmetric only the top half has been listed. The

$(\pi i_{13/2}\nu g_{9/2})$	$(\pi f_{7/2}\nu j_{15/2})$	$(\pi f_{7/2}\nu g_{9/2} \otimes 3^-)$	ψ^+	ψ^-
-(6.11 +.44)	-.31	-.91	-.44	-.87
+(.41 +.213)				
	-(5.42 +.38)	-.77	.50	-1.1
	+(.387 +.426)			
		-(6.84 +.65)	0	0
		+(2.6 +.213 +.387)		
			-(3.89 +.966)	0
			+(2.6 +.426 +.41)	
				$E(\psi^+)=E(\psi^-)$

diagonal energies have been corrected for the octupole mixing as can be seen above. In the diagonal energy sum the first entry is the weak coupling energy, the second entry is the shell model residual interaction while the last two components are the octupole "corrections" to give the pure configuration energy. The energies and wavefunctions for the lowest "$(\pi i_{13/2}\nu g_{9/2})$" and "$(\pi f_{7/2}\nu j_{15/2})$" states calculated from the matrix are listed below:

-6868 keV -5222 keV

with the wavefunctions

$(\pi i \nu g)$	.77	-.54
$(\pi f \nu j)$	.43	.79
$(\pi f \nu g \otimes 3^-)$	.4	.13
(ψ^-)	.03	-.21
(ψ^+)	.25	.14

The calculated energies above correspond to total effective residual interactions of -744 keV for the "$(\pi i \nu g)_{11}+$" state and +194 keV for the "$(\pi f \nu j)_{11}+$" state, compared to the values of -560 keV and -260 keV obtained by Kuo and Herling (Kuo71) in the pure shell model

approximation. The "$(\pi f\nu j)_{11}+$" state has not been identified experimentally, however from the energy of the 11^+ member of the $(\pi i\nu g)_{11}+$ muliplet in ^{210}Bi (Dae77) the "$(\pi i\nu g)_{11}+$" residual interaction is -961. Inclusion of the particle-vibration coupling has improved the comparison between calculation and experiment. Although we have included the main configurations in the basis used so far there are other configurations which could be included. The "$i_{13/2}$" particle has been depressed ~ 40 keV by mixing with the $(\pi h \otimes 3^-)$ particle vibration state so another configuration that needs to be included is the $((\pi h \otimes 3^-)_{9/2}\nu g_{9/2})$ one. Including the $(\pi h\nu j)_{11}+$ and $(\pi i_{13/2}\nu i_{11/2})_{11}+$ configurations as well gives a value of -803 keV for the "$(\pi i\nu g)$" residual interaction and +167 for the "$(\pi f\nu j$") interaction. (The matrix and wave functions obtained with the expanded basis are listed in appendix 3.) Although inclusion of the particle- vibration states explicitly improves the agreement between the theoretical and experimental residual interaction for the "$(\pi i\nu g)$" state, in later calculations we will need to know these residual interactions more accurately. It should be noted that Kuo and Herling's matrix elements generally underestimate the proton-neutron interaction if the two particles are coupled to the maximum possible spin (see e.g. (Lon80b)). With this in mind we scale the $(\pi i\nu g)_{11}+$ and $(\pi f\nu j)_{11}+$ diagonal matrix elements to obtain agreement with experiment. The energies needed to give this agreement with experiment correspond to a diagonal residual interaction contribution of -637 keV and -570 keV respectively for the two configurations compared to Kuo and Herling's values of -440 keV and -380 keV. Since we have no experimental estimate of the value of the off-diagonal matrix element we have not adjusted it. However it is probable that the $\langle(\pi i_{13/2}\nu g_{9/2})|V_{sh}|(\pi f_{7/2}\nu j_{15/2})\rangle$ should be also scaled since for

most phenomenological interactions, scaling of the diagonal matrix elements affects the values of the off-diagonal elements. (The value of the off-diagonal matrix elements affects the electromagnetic properties of the state, hence the value of the off-diagonal element could be deduced from the decay properties of the 11^+ yrast state in ^{210}Bi, assuming the character of the octupole phonon remains the same. However to date the information is not available. Later, we will calculate the wavefunction of a related state in ^{210}At which decays via an E 3 transition. Although the calculated value obtained using the matrix elements given above is consistent with experiment, the experimental errors on the transition rate are too large to draw firm conclusions as to how the matrix elements should be scaled. Until accurate evidence is available on the electromagnetic properties of such states, in the calculations below we will use the values given above for the matrix elements.)

4.5 MANY-PARTICLE STATES IN THE RADON NUCLEI

The energies of the yrast states in the radon nuclei can be calculated, as explained in chapter 2, using the empirically determined residual interactions. However if the two-body residual interactions are obtained from mixed states the procedure can break down. A well known example illustrating this is in ^{212}Rn (Lon80, Ho77), where the $\pi(h^2if)_{18^-}$ state is ~ 400 keV above the $\pi(h^2if)_{17^-}$ state. The energy difference which would be expected from the shell model is about 50 keV. The large discrepancy arises because the proton in the $\pi i_{13/2}$ orbital cannot mix with the $(\pi f \otimes 3^-)$ particle-vibration state due to Pauli blocking (which shows that particle vibration states are real!). The calculated energy depression of the $\pi i_{13/2}$ particle due to particle-vibration coupling is ~410 keV (see table 4.1).

Section 4.2 showed that the "$(\pi i\nu g)"_{11}+$ state is far from pure so the mixing needs to be explicitly included to calculate many-particle states involving this mixed configuration as a component.

The problem then is to calculate the wavefunctions of the high-spin states in the radon nuclei including all the particle-vibration states and the relevant particle configurations explicitly.

The method used to do this is:

1. The energies of the available shell model states are calculated using empirical residual interactions. From these first order calculations we can identify those particle and particle-vibration configurations which will contribute to the wavefunction of the yrast state considered, thus a basis can be chosen. However for non-maximally aligned configurations, only the important couplings are selected (see discussion in section 4.3 above) to minimise computation.
2. The energies of the configurations are calculated using empirical residual interactions (if possible), except where there is substantial mixing in the parent state. For example for the residual interaction of the $(\pi i\nu g)_{11}+$ state we use the "corrected" value given above. In the states that we will look at below the only corrected "empirical" values used are for the $(\pi i_{13/2}{}^{\nu}g_{9/2})_{11}+$ and $(\pi f_{7/2}{}^{\nu}j_{15/2})_{11}+$ states, which have been discussed above.
   For example the energy of the $(\pi(h^2i^2)\nu g)_{49/2}-$ $(\nu p_{1/2}^{-2})_{0}+$ configuration is calculated by using the experimental energy of the $(\pi(h^2i^2)_{20}+)$ state in ^{210}Rn. A $g_{9/2}$ neutron is added and the residual interactions $\langle h_8^2+|g\rangle$, $\langle(p_{1/2}^{-2})_0+|g\rangle$ are calculated using known two-body residual interactions. (A note on notation, $\langle\ |\ \rangle$ stands for the residual interaction between the component groups, hence $\langle h^2|\ g\rangle = \langle h^2g|V_{sh}|h^2g\rangle - \langle h^2|V_{sh}|h^2\rangle$ etc.) The residual

interaction $\langle i^2|g\rangle$ is calculated using the value for the two-body matrix element $\langle ig|V_{sh}|ig\rangle_{11}^{+}$ of -637 keV. For the $\langle ig|V_{sh}|ig\rangle_{10}^{+}$ matrix element the theoretical value of Kuo and Herling is used which is close to zero (the experimental state has not been identified).

3. The off-diagonal elements are calculated by recoupling in terms of the matrix elements given in appendix 1.
4. The final matrix is diagonalised to give the energies and the wavefunctions.

Apart from the approximations involved in selecting the basis, the other aproximations are: the diagonal residual interaction of the 3^- phonon with the particle component of a particle-vibration state is ignored. The energy of the two phonon state is taken as 2×2600 keV; most calculations agree that the energy of the phonon state will be within a few hundred keV of this value (see e.g. (Ham74)). We have only included double octupole 3^- states coupled to 6^+ in the basis. The other coupling that could have been considered is the 0^+ coupling, however particle vibration states that include this coupling would not be favoured energetically or geometrically (i.e. the recoupling coefficients are small). Some of the experimental residual interaction is due to configuration mixing. Where the parent states are reasonably pure this has been ignored, however in a sense we are double counting by calculating mixing using such empirical interactions. We shall see below that this approximation is not serious.

We will look at the high spin yrast states in the radon and astatine nuclei shown schematically in fig. 4.3.

4.5.1 The $\pi(h^2i^2)_{20^+}$ $(\nu p_{1/2}^{-2})_{0^+}$ and the
$\pi(h^3i)_{17^-}$ $(\nu p_{1/2}^{-2})_{0^+}$ states in ^{210}Rn

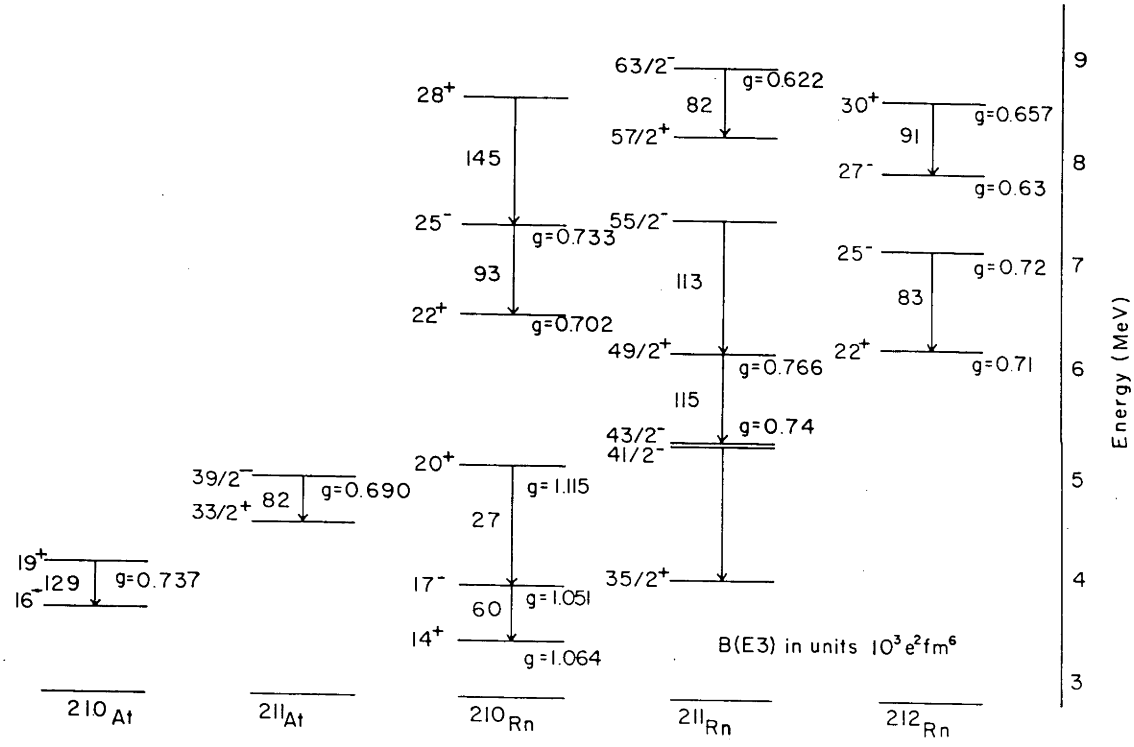

Fig. 4.3: The high spin states discussed in the text. E3 transitions connecting states are marked.

The B(E3) between these two states is 26.6×10^3 e^2fm^6 (10.4 s.p.u) (see chapter 3). If the states were pure the transition strength would be 7500 e^2fm^6. [To calculate the transition strength in terms of the "$i_{13/2} \rightarrow h_{9/2}$" transition the wave function needs to be recoupled; (using Lawson's (Law80) definition of the matrix element, and T3 being the transition operator):

$$\sqrt{(B(E3)[\ (h^2i^2)_{20^+} \rightarrow (h^3i))_{17^-}]} = [(\hat{I}_f/\hat{I}_i)\langle \pi h^3 i \,|T3|\, \pi h^2 i^2\rangle]$$

Now

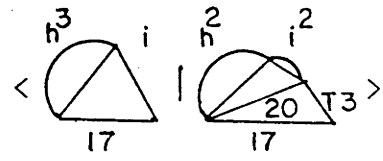

$$= (.88)\sqrt{((2)(3)(25)(10)(41)(22)}(2J+1)W(13/2,13/2,J,3;12,9/2)$$
$$W(8,9/2,17,13/2;21/2,J)W(8,12,17,3\ ;20,J)(-1)(-1)^{11-J}\langle \pi h_{9/2}|T3|\pi i_{13/2}\rangle$$
$$= -.65\langle \pi h_{9/2}|T3|\pi i_{13/2}\rangle$$

so that

$$(B(E3)[(h^2i^2)_{20^+} \rightarrow (h^3i)_{17^-}]$$
$$= [(35)(14)/(41)(10)](-.65)^2 = (.50)\ (B(E3)[i_{13/2} \rightarrow h_{9/2}]\ .$$

With the experimental "single particle" value of $15(5) \times 10^3$ e^2fm^6 (Her69, Bro70) gives the calculated rate as 7500 e^2fm^6.

The large difference between the experimental B(E3) (26600 e^2fm^6) and the calculated B(E3) (7.5×10^3 e^2fm^6), indicates that the states are not pure. In fact the $\pi(h^3i)_{17^-}$ state can mix with the $\pi(h^3if)_{17^-}$ state. We will now calculate the wavefunction of the "$\pi(h^3i)_{17^-}$" state. A good basis is the set, [$\pi(h^3i)$, $\pi(h^3f \otimes 3^-)$, $\pi(h^2if)$, $\pi(h^2f^2 \otimes 3^-)$, $\pi(h^2(i^2 \otimes 3^-)_{9/2^-})_{17^-}$]. To calculate the diagonal residual interactions for the $(\pi(h^3f)\nu(p^{-2}_{1/2})_{0^+})_{14^+}$, $(\pi(h^3i)\nu(p^{-2}_{1/2})_{0^+})_{17^-}$ and the $(\pi(h^2i^2)\nu(p^{-2}_{1/2})_{0^+})_{20^+}$ configurations we

used the experimental energies for the states in ^{210}Rn. As was pointed out above this procedure is an approximation and only justified if the mixing is small. The experimental $(\pi(h^2if)\nu(p_{1/2}^{-2})_{0^+})_{17^-}$ and $(\pi(h^2f^2)\nu(p_{1/2}^{-2})_{0^+})_{14^+}$ states have not been identified so these were calculated (including core polarisation effects) from parent states in ^{212}Rn or using solely two-body matrix elements say (see for example (Byr85)). Once the diagonal residual interactions are obtained the energies are corrected for the octupole depression using table 4.1. To illustrate the recoupling procedure we calculate some of the off-diagonal matrix elements in detail. The matrix elements on the left hand side of the equalities are recoupled in terms of the matrix elements on the right hand side, the numerical values of which are found in appendix 2. It should be remarked that some of the matrix elements listed in appendix 3 have been calculated using the surface delta interaction (S.D.I.). It might be argued that the S.D.I. matrix elements contain an octupole contribution implicitly, however the parameter values we used were obtained by fitting to the low spin states in ^{210}Po (Pol81), most of which would not be affected by octupole induced mixing, and for those that are, the effect is small.

The off-diagonal matrix elements are worked out as follows (in the notation below the $\nu(p_{1/2}^{-2})_{0^+}$ spectator configuration has been suppressed):

1. $\langle\pi(h^3i)|V_{pv}|\pi(h^3f)\otimes 3^-\rangle = \langle\pi i|V_{pv}|\pi f\otimes 3^-\rangle = -910$ keV.
2. The $\langle\pi(h^3i)|V_{sh}|\pi(h^2if)\rangle$ matrix element is calculated in terms of the $\langle\pi(h^2)|V_{sh}|\pi(hf)\rangle_{J=8^+,6^+}$ and the $\langle\pi(hi)|V_{sh}|\pi(if)\rangle_{J=8^+}$ matrix elements. For example the $\langle\pi(hi)|V_{sh}|\pi(if)\rangle_{J=8^+}$ component is: $(0.88)\sqrt{(3)}\ W(89/21713/2;21/29)(\hat{21}/2)(\hat{9})$.
3. $\langle h^2if|V_{pv}|h^3f\otimes 3^-\rangle =$ 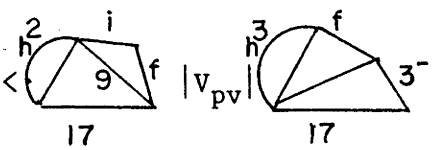

$= W(8,13/2,17,7/2;27/2,9)(\hat{27}/2)(\hat{9})$ 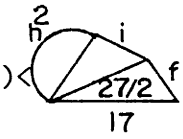 $|V_{pv}|$ 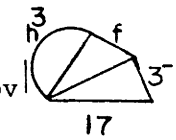

the above matrix element $=\sqrt{(3)}(.88)$ 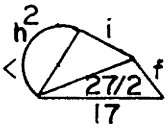 $|V_{pv}|$ 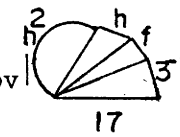

the last matrix element = W(16/2,9/2,27/2,3;21/2,13/2)($2\hat{1}$/2)($1\hat{3}$/2))

multiplied by

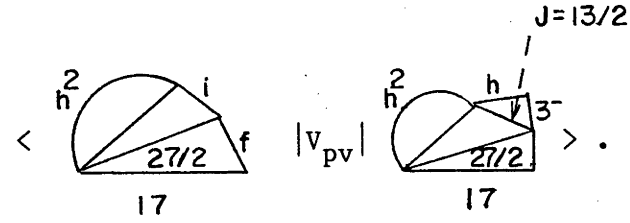

Now using the fact that the projection of any state onto itself is unity the last matrix element is just $\langle \pi i | V_{pv} | \pi h \otimes 3^- \rangle$ = -210 keV, and inserting numerical values for the Racah coefficients gives the result.

4. $\langle \pi(h^2 if) | V_{pv} | \pi(h^2(i^2 \otimes 3^-)_9 -) \rangle$

$= \sqrt{(2)} W(13/2,13/2,9,3;12,7/2)(1\hat{2})(\hat{7}/2) \langle \pi f | V_{pv} | \pi i \otimes 3^- \rangle$.

The other matrix elements were calculated in a similar manner to give the matrix for the 17^- states reproduced below.

$V_{sh}+V_{pv}$	$\pi(h^3i)$	$\pi(h^3f) \otimes 3^-$	$\pi(h^2if)$	$\pi(h^2f^2) \otimes 3^-$	$\pi(h^2(i^2 \otimes 3^-)_9-)$
$\pi(h^3i)$	4.222	-.91	.05	0	-0.13
$\pi(h^3f) \otimes 3^-$		6.235	-.09	-0.1	0
$\pi(h^2if)$			5.27	-1.13	-1.23
$\pi(h^2f^2) \otimes 3^-$				7.618	0
$\pi h^2(i^2 \otimes 3^-)_9-$					8.40

(energies in MeV)

The resultant energies and wave functions of the two lowest states, the "$\pi(h^3i)$" and the "$\pi(h^2if)$" states are:

energy (MeV)	3.845	4.455
$\pi(h^3i)$	.912	-.200
$\pi(h^3f) \otimes 3^-$	.357	-.040
$\pi(h^2if)$	.173	.728
$\pi(h^3f^2) \otimes 3^-$	.064	.325
$\pi h^2((i^2 \otimes 3^-)_9-)$	.082	.304

We discussed earlier some of the approximations that are involved in these calculations. From the difference between the calculated energies and the observed energies above we can evaluate the effects of the approximations. Since we "fed" the experimental energy of the 17^- state into the matrix we should get the experimental energy back again. (The reason we did the calculation was to obtain the wavefunction and not to calculate the energy!) Hence a self-consistency test here is to see how close the energies are to the experimental values. The experimental 17^- state is at 3812 keV, 33 keV lower than the "calculated" state. Although the $(\pi(h^2if)\nu(p^{-2}_{1/2})_{0^+})$ state has not been identified in ^{210}Rn, when the same calculation is performed in ^{212}Rn the energy difference is 20 keV. From examples such as this it can be concluded that the calculational technique is "self-consistent" to within about 50 keV. The experimental energies are not exactly reproduced because of factors such as: part of the experimental residual interaction energy is due to the $\pi i_{13/2}$ particle in the $\pi(h^3i)$ configuration not being able to mix with the $\pi(h_{9/2} \otimes 3^-)_{13/2}$ particle-vibration configuration, which pushes the energy up by $\sim$40 keV (in effect we count this twice). Another part of the experimental $\pi(h^3i)$ residual interaction is due to the (slight) mixing with the $\pi(h^2if)$ state. Still another part of the residual interaction is due to the fact that the $\pi(h^3f) \otimes 3^-$ configuration is $\sim$ 2050 keV higher than the πh^3i state. (The $\pi f \otimes 3^-$,

$\pi i_{13/2}$ energy separation in ^{209}Bi is ~ 1900 keV.) Ideally we should disentangle all these contributions to the residual interaction, however that would be very hard to do and so we have to be content with the approximations involved in neglecting such effects.

In appendix 4 the matrix, energy and wave function of the $(h^2i^2)_{20^+}$ state are given. Using the wavefunctions for the yrast 20^+ and 17^- states the expected B(E3) can be calculated.

To calculate the B(E3) value the following fact is useful: If $(\psi \otimes j) \rightarrow (\psi \otimes 1)$ and if $(\psi \otimes j)$, $(\psi \otimes 1)$ are maximally aligned then:

$$\sqrt{(B(E3)(\psi \otimes j) \rightarrow (\psi \otimes 1))} = \sqrt{(B(E3) j \rightarrow 1))}$$

We will denote the $((B(E3)\phi \rightarrow W)$ by (W/ϕ). So

$$\begin{aligned}(h^3i/h^2i^2) = {} & (.918)(.851)(h^3i/h^2i^2) + (.851)(.173)(h^2if/h^2i^2) \\ & + (.480)(.357)(h^3f/h^2if) + (.480)(.064)(h^2f^2/h^2if) \\ & + (.134)(.357)(f/i) + \text{the octupole contribution} .\end{aligned}$$

Note that the octupole coupled states also contribute via single particle transitions e.g. $(\pi(h^3f \otimes 3^-)/\pi(h^3i \otimes 3^-)) = (\pi f/\pi i)$. The octupole contribution is:

$$\begin{aligned}= {} & [(.480)(.173)W(13/2,7/2,12,3;9,13/2)(\hat{9})(\hat{13}/2) \\ & + (0.134)(.912)+(.154)(.063)\sqrt{(2)} + (0.066)(.357)\sqrt{(2)} \\ & + [(0.082)(.851)W(8,12,17,3;9,20)(9)(20)\ (34/41)](0^+/3^-) .\end{aligned}$$

The pure single particle matrix elements are calculated using the expression given by Bohr and Mottelson (Boh69):

$$\langle j_2 \| i^{\lambda} M(E\ ) \| j_1 \rangle = e(-1)^{j_1 - j_2 + \lambda}\ i^{\ell_1 - \ell_2 + \lambda} \left(\frac{(2\lambda+1)(2j_1+1)}{4\pi} \right)$$

$$\times \langle j_1 \tfrac{1}{2} \lambda 0 | j_2 \tfrac{1}{2} \rangle \langle j_2 | r^{\lambda} | j_1 \rangle .$$

Values of 238 fm^3 (Boh75) and 197 fm^3 (Blo60) were used for the

radial matrix elements $\langle \pi h | r^3 | \pi i \rangle$ and $\langle \pi f | r^3 | \pi i \rangle$. An effective charge of 1.3 for the proton is used (Ham74). (The effective charge includes the effects of even higher lying collective 3^- states.) Hence the values for the single particle matrix elements are, $(\pi h/\pi i) = -27$ e fm^3 and $(\pi f/\pi i) = 94$ e fm^3. Using these values gives a calculated value for the B(E 3) "$(\pi h^2 i^2)$" $\rightarrow$ "$(\pi h^3 i)$" of 1680 e^{2}fm^6, compared to the experimental value of 26.6×10^3 e^{2}fm^6, which is in much better agreement than the previous estimate assuming pure configurations (7500 e^{2}fm^6). However there is still a significant disagreement. It should be noted that if the wavefunctions for the "$\pi i_{13/2}$" and "$\pi h_{9/2}$" states are used, together with the single particle transition matrix elements quoted above, the calculated "$\pi i_{13/2}$" $\rightarrow$ "$\pi h_{9/2}$" transition in ^{209}Bi is underestimated (9000 e^{2}fm^6 compared to the experimental value of 15000 e^{2}fm^6). Consequently the calculated "$(h^2 i^2)_{20^+}$" $\rightarrow$ "$(h^3 i)_{17^-}$" transition rate will be somewhat underestimated.

The energies and wavefunctions of the other states shown in fig. 4.3 were calculated in a similar way. The matrices and the wavefunctions are given in appendix 3. In the following we consider states in different nuclei to be related if the basis in the calculations for the two nuclei are related by the addition of "spectator" particles. The addition of such particles means that the off-diagonal shell model matrix elements in the matrices need not be the same, but for the states considered here the addition of the "spectator" particle does not change the matrix dramatically. The diagonal energies have been calculated by using the experimental proton-component energy, then adding the extra neutron particles, and calculating the relevant residual interactions in terms of the two-body matrix elements. A brief summary of the results follows:

i) The "$(\pi(h^3i)\nu g)_{43/2^-}$" state

We identify "$(\pi(h^3i)(\nu g))_{43/2^-}$" coupled to $\nu(p^{-2}_{1/2})_{0^+}$ with the $43/2^-$ yrast state in ^{211}Rn, while the 27^- state in ^{212}Rn is identified with the related "$\pi(h^3i)_{17^-}\nu((g_{9/2}i_{11/2})(p^{-2}_{1/2})_{0^+})_{10^+})$" state. From section 4.2 it is apparent that the $(\pi(h^3i)\nu(g))$ configuration will mix strongly with the $(\pi(h^3f)\nu(j))$ configuration despite the large energy separation (~ 1 MeV).

ii. The "$[(\pi(h^2i^2)\nu g) + (\pi(h^3i)\nu j) + (\pi(h^2if)\nu j)]_{49/2^+}$" state

When two neutron holes in the 0^+ configuration are added the state can be identified with the yrast $49/2^+$ state in ^{211}Rn, while adding an extra $i_{11/2}$ neutron as well, gives a 30^+ state in ^{212}Rn. The configuration with the lowest energy is the $\pi(h^2i^2)\nu g$. Again this will mix with the "fj" coupling strongly (i.e. $\pi(h^2if)\nu j$). The $(\pi(h^2i^2)\nu g)$ will also mix with the $(\pi(h^3i)\nu j)$ state since the two configurations both couple to the same particle vibration state $(\pi(h^3i)\nu g) \otimes 3^-))$. Although the coupling induced by this is weak (due to the spin flip) it is enough to cause strong mixing as the states are close in energy. Finally, the $(\pi(h^3i)\nu j)$ and the $(\pi(h^2if)\nu j)$ will mix as seen above in the discussion of the 17^- state in ^{210}Rn. Part of the reason these two configurations mix is that they both couple to the particle-vibration state $(\pi(h^3f)\nu g \otimes 3^-)$. It turns out, somewhat surprisingly, that the three configurations have similar amplitudes in the final state. The above general considerations apply, by implication, to the related states in ^{212}Rn and ^{210}Rn.

iii. The "$(\pi(h^2i^2)\nu j)"_{55/2^-}$ state

This state will be yrast in ^{211}Rn (coupled to $\nu(p^{-2}_{1/2})_{0^+}$), we identify it with the $55/2^-$ state at 6.4 MeV excitation.

The question now is the following, how well do the calculated

properties of the states agree with reality, and in particular are the E3 strengths reproduced? In the tables below we compare the calculated properties of the states with the observed properties.

Table 2.2 shows the B(E(3)) values calculated for transitions between these states (using the wave functions obtained in appendix 2).

TABLE 4.2

Nucleus	I_f	I_i	B(E3) calc.[e]	B(E3) exp.[e]
^{210}Rn[a]	17^-	20^+	17	27(3)
	14^+	17^-	63	60(3)
^{211}Rn[b]	$43/2^-$	$49/2^+$	79	115(7)
	$49/2^+$	$55/2^-$	122	113(27)
^{212}Rn[c]	27^-	30^+	60	91(8)
^{210}At[d]	16^-	19^+	81	129(60)

[a] (see chapter 3) and (Pol85).
[b] from (Pol85).
[c] from (Hor77).
[d] from (Rah77).
[e] in units of 10^3 e^2fm^6.

Table 4.3 compares the calculated energies with the experimental values.

The calculations above are in reasonable agreement with experiment, however the differences are more than would be expected from the approximations involved in the calculations. Is this due to the character of the octupole state changing and hence affecting the energies of the energies of the state or are some of the matrix elements used in the calculations incorrect? The problem is discussed further in Chapter 5.

TABLE 4.3: ENERGIES AND g-FACTORS OF HIGH SPIN STATES IN THE Rn NUCLEI

Nucleus	Spin	Energy (calc.)[e]	Energy (exp.)[e]	g (calc.)	g (exp.)
^{210}Rn	20^+	-	4994+Δ'	1.116(20)	1.115(15)
	17^-	-	3812+Δ'	1.049	1.051(5)
	14^+	-	3248+Δ'	1.058(8)	1.064(7)
^{211}Rn	$43/2^-$	5206+Δ	5247+Δ'	0.735	0.74(2)
	$49/2^+$	6102+Δ	6101+Δ'	0.782	0.766(8)
	$55/2^-$	7410+Δ	7400+Δ'	-	-
^{212}Rn	27^-	7761+Δ	7849+Δ'	0.616	0.63(3)
	30^+	8571+Δ	8550+Δ'	0.664	0.657(4)
^{210}At	19^+	4028	4006	0.707	0.737(25)
	16^-	3655	3691	-	-

[a] (Pol81 and chapter 3).
[b] (Pol80, Pol85).
[c] (Hor77).
[d] (Rah77).
[e] units (keV).

4.6 STATES WITH AN ODD NUMBER OF NEUTRON HOLES

In the previous section we did not consider neutron holes explicitly, in fact for states with two neutron holes we took the core to be ^{206}Pb rather than ^{208}Pb. By ignoring possible neutron hole excitations the problem of calculating the wavefunctions of the high-spin states considered above was simplified considerably. Because of the strong proton-neutron hole repulsive interaction for spin-aligned states it is not advantageous to break a 0^+ neutron hole pair and align the spin of the neutron holes with that of the particles. Consequently for the high-spin states we are looking at in the radon nuclei the configurations with neutron-hole excitations are in general non-yrast. (If the neutron holes are not aligned with that

of the particles, the small increase in spin possible does not compensate for the energy lost by breaking a neutron hole pair.) There will be little mixing between configurations based on neutron-hole excitations and configurations coupled to a 0^+ neutron-hole pair, since if two such configurations couple to the same spin they will usually differ by at least three orbits. Experimental evidence for the assertion is seen in nuclei such as ^{208}At (Fan84) where the level scheme shows two disconnected cascades, one based on neutron-hole excitations, the other on proton excitations. Such considerations suggest that the approximation of taking ^{206}Pb to be a "non-interacting" core is a good one for the states we are interested in in the radon nuclei.

However, for states where there are an odd number of neutron-holes we must consider the neutron-holes explicitly. For states with three neutron-holes the arguments above suggest that the "core" should be taken as ^{206}Pb. The problem then is the following, how do we deal with a "spare" neutron-hole? A first approximation might be to select the energetically most favoured single hole orbital and couple this as a "spectator" particle to each of the basis configurations. The diagonal residual interactions of the neutron-hole with each basis configuration could be calculated, while a few of the off-diagonal matrix elements would need to be modified slightly, but essentially, the states with a neutron-hole would be related to the "parent state" in the neighbouring nucleus by the simple addition of a neutron hole.

Such a procedure is not a good approximation when it comes to calculating the g-factor of the state. The reason is that around ^{208}Pb, the neutron-hole orbitals near the Fermi surface include the spin orbit pairs $\nu p_{1/2}^{-1}$, $\nu p_{3/2}^{-1}$ and $\nu f_{5/2}^{-1}$, $\nu f_{7/2}^{-1}$. The g-factor of a

state is sensitive to even small admixtures of spin orbit pairs due to the off-diagonal contribution. For example Hausser et al. (Hau76) have calculated the wavefunction, using shell model interactions, of the $17/2^-$ ^{209}Po yrast state to be:

$$|17/2^-> = .953|8^+ \otimes \nu p_{1/2}^{-1}> - .263|8^+ \otimes \nu f_{5/2}^{-1}> - .125|8^+ \otimes \nu f_{3/2}^{-1}> + \ldots .$$

and find that the off-diagonal term corresponding to the $\nu p_{1/2}^{-1} \rightarrow \nu p_{1/2}^{-1}$ transition reduces the g-factor by .03. The off-diagonal contribution can be readily calculated by writing the magnetic moment explicitly as $\mu = \sqrt{\frac{4\pi}{3}}\,M1$.

Then the magnetic moment of a state $|\phi_I> = \alpha|\psi_J \otimes j_1> \beta|\psi_J \otimes j_2>$ which is defined as $<\phi_{1M}|\sqrt{\frac{4\pi}{3}}M1|\phi_{1M}>_{M=I}$ will contain off-diagonal terms such as $\alpha\beta\sqrt{\frac{4\pi}{3}}<\psi_J \otimes j_1 |M1|\psi_J \otimes j_2>$ which can be expressed using the Wigner-Eckart theorem as

$$\alpha\beta\sqrt{\frac{4\pi}{3}}(I\ I\ 1\ 0|I\ I)<\psi_J \otimes j_1 \| M1 \| \psi_J \otimes j_2> = \alpha\beta\sqrt{\frac{4\pi}{3}}W(J,j_2,I,1;I,j_1)\hat{I}\hat{j}<j_1\|M1\|j_2>\frac{1}{\sqrt{I(I+1)}} .$$

For the transitions we are interested in the M1 matrix elements have been measured experimentally (Bab72).

The problem now is, how can the neutron hole mixing be calculated? Of course one way to do it would be to enlarge the configuration space by including the $\nu p_{1/2}^{-1}$, $\nu p_{3/2}^{-1}$, $\nu f_{5/2}^{-1}$ and $\nu f_{7/2}^{-1}$ neutron orbitals. However the size of the matrix would increase by at least a factor of 16, and the task of calculating the wavefunction would become formidable.

An alternative approach is to "freeze out" the core and then calculate the average effect that the valence particles have on the neutron-hole. That is we calculate the diagonal energies assuming the basis configurations are coupled to a particular "spectator" neutron hole. Strictly speaking the modifications to the off-diagonal matrix

elements should also be calculated but we have not done so due to time constraints. In fact the two-body particle-hole off-diagonal matrix elements are expected to be small (Kuo68), so it is a good approximation to ignore them. The next step is to calculate the average effect that the valence particles have on the odd neutron-hole. We do this by assuming that the valence particles distort the average field in an oblate-quadrupole manner, and it is the quadrupole distortion of the field which mixes the different neutron hole orbitals with the same m-projection. (Of course the deformation needs to be estimated somehow.) It turns out that the amount of mixing is sensitive to the quadrupole deformation and for even quite small deformations ($\beta = -.05$) the $K = 1/2^-$ state which comes out of the $\nu p^{-1}_{1/2}$ orbital is substantially mixed.

We shall see below how to calculate the mixing, but for now we note that Matsuyanagi et al. (Mat78) have calculated the deformation for the $17/2^-$ state in ^{209}Po referred to earlier, to be $\approx\beta = -.015$. For such a deformation we calculate the relevant $K = 1/2^-$ neutron orbital to have the wavefunction:

$$K = |1/2^-\rangle = .96\nu p^{-1}_{1/2} + .246\ \nu f^{-1}_{5/2} - .133\nu p^{-1}_{3/2} + \ldots$$

Coupling this state to the 8^+ state in ^{210}Po gives the wavefunction of the $17/2^-$ state in ^{209}Po:

$$|17/2^-\rangle = .96|8^+ \otimes \nu p^{-1}_{1/2}\rangle + .246|8^+ \otimes \nu f^{-1}_{5/2}\rangle - .133|8^+ \otimes \nu p^{-1}_{3/2}\rangle + \ldots$$

which is in excellent agreement with the explicit shell model calculation cited above. We are using a different phase convention to Hausser et al.

4.6.1 Calculation of the Neutron Hole Mixing

The Nilsson Hamiltonian is usually taken as:

$$\frac{H}{h\omega_0} = \frac{1}{2}(-\nabla^2 + \rho^2) - \beta\rho^2 Y_{20}(\theta,\phi) - 2K\underset{\sim}{\ell}.\underset{\sim}{s} - \mu K(\underset{\sim}{\ell}.\underset{\sim}{\ell} - \langle\ell^2\rangle_N) \ ,$$

where $\rho^2 = \frac{m\omega_0}{h} r^2$. Since for zero deformation the eigenvalues are the single particle energies the Hamiltonian can be written as:

$$\frac{H}{h\omega_0} = \frac{H_{sp}}{h\omega_0} - \beta\rho^2 Y_{20}(\theta,\phi) \ .$$

We will take the single neutron-hole energies from the experimental energy spectrum of the "core" of interest (^{207}Pb or ^{205}Pb). The reason being that the single particle energies obtained with the Nilsson model at zero deformation are not accurate enough for our purposes. Having obtained the single particle energies (listed in appendix 5) only the matrix elements of $-\beta\rho^2 Y_{20}(\theta,\phi)$ need now be calculated:

$$\langle\phi_{j'K'N'}|\phi^2 Y_{20}|\phi_{jKN}\rangle = \langle\phi_{jK'N'}|\rho^2|\phi_{jKN}\rangle\langle\phi_{j'K'}|Y_{20}(\theta,\phi)|\phi_{j'K'}\rangle$$

and

$$\langle\phi_{j'K}|Y_{20}|\phi_{j'K}\rangle = (j\ 2\ K\ 0\ |\ j\ K)\langle\phi_{j'K}\|Y_{20}\|\phi_{jK}\rangle$$

$$= (-1)\left(\frac{(2.2+1)(2j+1)(2j'+1)}{4\pi}\right)\begin{pmatrix} j & 2 & j' \\ K & 0 & -K \end{pmatrix}\begin{pmatrix} j & 2 & j' \\ \frac{1}{2} & 0 & -\frac{1}{2} \end{pmatrix}$$

(see e.g. Lawson (Law80)). Using radial matrix elements calculated with a harmonic oscillator potential (see appendix 5) the matrix elements of $-\beta\rho^2 Y_{20}(\theta,\phi)$ can be computed, and the matrix diagonalised to give the wavefunction. In appendix 5 the wavefunctions and energies of the K = 1/2, and K = 3/2 neutron-hole states in ^{205}Pb and ^{207}Pb for the values of β used here are listed.

Although we do not make use of the energies of the Nilsson orbitals, since the shift in energy as a function of deformation is included implicitly by using empirical residual interactions it is interesting to plot the Nilsson energies. In the ^{205}Pb core initially

the $\nu p_{1/2}$ and $\nu f_{5/2}$ orbitals are almost degenerate for zero deformation. When the energy of configurations in ^{210}Rn, based on the $43/2^-$ configurations in ^{211}Rn discussed above, are calculated it is found that it is energetically more favourable for the unpaired neutron-hole to occupy the "$\nu p_{1/2}^{-1}$" orbital, however from fig. 4.4 we see that energy of this orbital increases much more rapidly with deformation than the K = 3/2 "$\nu p_{5/2}^{-1}$" orbital. Hence as the deformation increases we would expect to see states coupled to the K = 3/2 "$\nu f_{5/2}^{-1}$" orbital intrude below the "$\nu p_{1/2}^{-1}$" coupling. For the ^{207}Pb core, since there are two less neutron holes the trend will be for the "$\nu p_{1/2}^{-1}$" coupling to become even more favoured as the deformation increases.

4.6.2 Calculation of the Energy and Wavefunctions for States with An Odd Number of Neutron Holes

In calculating the energies of the core excited states with an odd number of neutron holes, one needs the residual neutron-(neutron-hole) interactions. These are taken from the relevant core excited states in ^{208}Pb. It should be remembered that the "$(\nu g_{9/2} p_{1/2}^{-1})$" and the "$(\nu j_{15/2} \nu p_{1/2}^{-1})$" states in ^{208}Pb are not pure. For example the wavefunction of the 5^- state in ^{208}Pb is (Rin73):

$$|5^-\rangle = .87|\nu g p^{-1}\rangle + .234|\nu i p^{-1}\rangle + .118|\nu j i^{-1}\rangle - .145|\pi h d^{-1}\rangle$$
$$- .209|\pi h s^{-1}\rangle - .135|\pi f d^{-1}\rangle - .116|\pi i h^{-1}\rangle + \ldots$$

while the 8^+ state will contain small admixtures of id^{-1} and if^{-1} etc. The mixing pushes down the energy of the final state. For the high-spin states in the radon nuclei with four aligned protons many of the proton particle, particle-hole components will be quenched due to the exclusion principle. Thus we would expect in such nuclei the 5^- and 8^+ states to be more pure and consequently pushed down less in energy. Since the complexity of the calculations would be increased

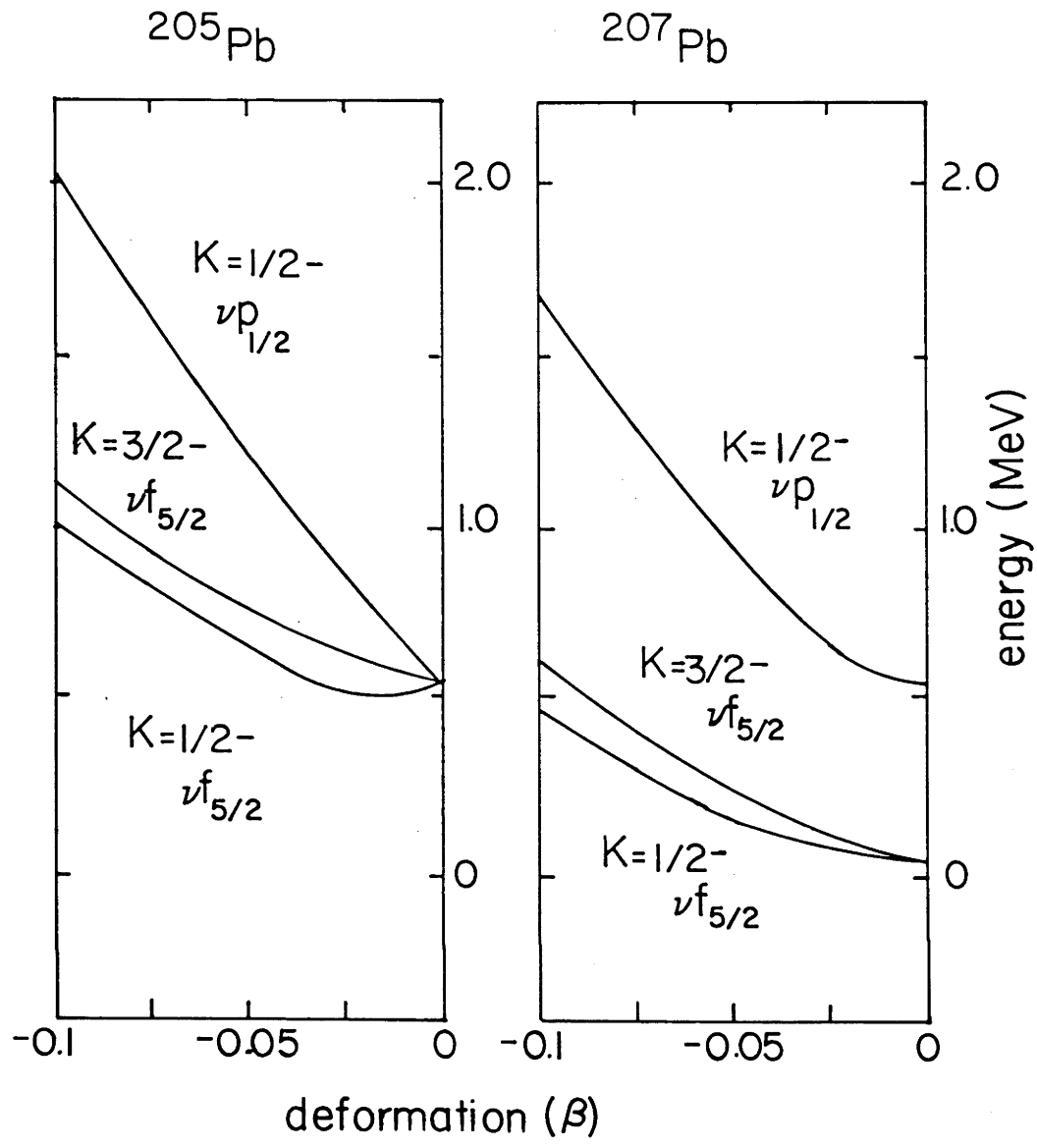

Fig. 4.4: Energies of the K = 1/2 and K = 3/2 neutron hole Nilsson orbitals.

considerably if such effects were included explicitly we have assumed the 5^- and 8^+ states to be pure, however one consequence of taking the "$(\nu g p^{-1})$" and "$(\nu j p^{-1})$" residual interactions from ^{208}Pb, where there is no Pauli blocking, is that the calculated energies for the core excited energies will be underestimated for configurations which include the $\nu p_{1/2}$ orbital. Since the process applies to both the "$(\nu g p^{-1})$" and the "$(\nu j p^{-1})$" configurations we would not expect the

difference between the two residual interactions to change substantially, so the wavefunctions should not be affected much by the approximation of treating the "νgp^{-1}" and "νjp^{-1}" states as pure. The quenching of the proton particle-hole pair components is also consistent with using the pure single-particle g-factors rather than using say the experimental g-factor for the 5^- state. Another consequence of ignoring such mixing is that the $8^+ \rightarrow 5^-$ B(E3) should be different (and probably less) than that of a pure $j \rightarrow g$ transition. However the difference should not be more then 10% in ^{208}Pb.

With the approximations discussed above the energies and wavefunctions of high spin states in ^{210}Rn, ^{211}Rn, ^{212}Rn and ^{211}At were computed. In tables 4.5 and 4.6 the calculations are compared with the experimental information (the wavefunctions etc. are listed in appendix 4 and appendix 5). The wavefunctions were obtained as explained above, for the deformations of the configuration we used typical values given by Matsuyanagi (Mat78) for ^{212}Rn at the same spin as the state being considered. The adopted deformation together with the off-diagonal contribution to the g-factor are also listed. It should be remembered that using the mixed neutron hole wavefunctions changes the diagonal contribution from that obtained if we had just used a pure neutron hole.

We see from table 4.5 that, as expected, the energies of the states which include an odd "$\nu p_{1/2}$ neutron-hole" are underestimated. It must be remembered that many of the two-body residual interactions that include the $\nu f_{5/2^-}$ neutron-hole are not known experimentally and had to be estimated from states in ^{210}At and ^{209}Po. It is seen that introducing neutron-hole mixing as described above satisfactorily explains the difference in the g-factors between configurations coupled to even and odd cores. The wavefunction for the $35/2^+$ state

TABLE 4.5: B(E3) VALUES

Nucleus	I_f	I_i	B(E3) calc.[c]	B(E3) exp.[c]
^{210}Rn[a]	22^+	25^-	80	97(4)
	25^-	28^+	117	145(17)
^{211}Rn[b]	$57/2^+$	$63/2^-$	70	82(5)
^{212}Rn[d]	22^+	25^-	81	83(8)
^{211}At[e]	$33/2^+$	$39/2^-$	71	82(9)

[a] (Pol82).
[b] (Pol85b).
[c] units of 10^3 e^2fm^6.
[d] (Hor77).
[e] (Mai71).

TABLE 4.6: g-FACTORS AND ENERGIES

Nucleus	Spin	Energy (calc.)	Energy (exp.)	g (calc.)	g (exp)
^{210}Rn[a]	22^+	6302+Δ	6469+Δ'	0.697	0.702(7)
	25^-	7239+Δ	7310+Δ'	0.741	0.733(9)
	28^+	8479+Δ	8555+Δ'	-	-
^{211}Rn[a]	$25/2^+$	-	-	1.020	1.017(13)
	$57/2^+$	8064+Δ	8169+Δ'		~~0.626(6)~~
	$63/2^-$	8882+Δ	8856+Δ'	0.610	0.622(6)
^{212}Rn[a]	22^+	5893+Δ	6180+Δ'	0.705	0.72(1)
	25^-	6844+Δ	7113+Δ'	0.747	0.71(2)
^{211}At[a]	$33/2^+$	3996	4381	-	-
	$39/2^-$	4551	4816	0.681	0.690(7)

[a] (Pol81, chapter 4 this work).
[b] (Pol85, Pol80).
[c] (Hor77).
[d] (Mai71, Ber85).

TABLE 4.7: THE NEUTRON HOLE

Nucleus	Spin	β	Neutron-Hole Orbital Occ.	Δg (off-diag.)
^{210}Rn	22^+	-.05	"$p_{1/2,1/2}$"	-.028 -.026
^{212}Rn	25^-	-.05	"	-.025 -.023
^{211}Rn	$35/2^+$	-.025	"	-.025
	$57/2^+$	-.08	"$f_{5/2,3/2}$"	-.016
	$63/2^-$	-.08	"	-.016
^{211}At	39/2	-.025	"$p_{1/2,1/2}$"	-.027

in ^{211}Rn essentially consists of the 17^- state in ^{210}Rn coupled to the "$\nu p_{1/2}$" neutron hole the difference in the g-factors between the two states is nicely explained, which increases our confidence in the calculational method.

CHAPTER 5

CONCLUDING COMMENTS

Perhaps the most interesting result to emerge from the systematic study of the high-spin states in the radon nuclei of which this work is part, is that contrary to naive expectations these states are very mixed. By including particle-vibration coupled states explicitly within the framework of the shell model it was found that the mixing between states arises in a natural way. Their wavefunctions were found to contain large admixtures of particle-vibration configurations. In fact from the wavefunctions in appendix 3 it can be seen that in ^{210}Rn the amount of time for which a state consists of particle-vibration configurations is 13% for the 17^- state, 20% for the 22^+ state, 34% for the 25^- state and 40% for the 28^+ state. Hence it is not surprising that to explain the properties of the high-spin states consistently the particle-vibration states need to be considered explicitly.

Another interesting effect is the difference in the g-factors of states related by the addition of a neutron hole. It was noted that the magnetic moments of states with an "odd neutron hole" are very sensitive to possible admixtures of spin-orbit partners in the "neutron hole" part of the wavefunction. The Nilsson orbitals that arise from the spherical $p_{1/2}$ and $f_{5/2}$ configurations, when expressed in the $|ljm\rangle$ basis, are very mixed even for small deformations. Hence it was considered appropriate to use the Nilsson wavefunctions for the "neutron hole" orbitals, which were calculated using typical

deformations suggested by Matsuyanagi et al. (Mat78). The differences between states related by the addition of a neutron hole were then reproduced in a satisfactory manner.

Although progress has been made in understanding the structure of the high-spin states considered here, the differences between the calculated and the experimental B(E3) values are certainly larger than one might expect. What is the reason for this? It could be argued that some of the matrix elements used in the calculations are underestimated. However we do not consider this is to be the complete explanation, for the following reasons. The particle-vibration model has been tested extensively and is firmly established. Consequently the particle-vibration matrix elements should be correct, except possibly for the spin flip cases which are sensitive to spin dependent components in the vibrational field (Bor75). Certainly when the wavefunctions in table 4.1 are used to calculate the $i_{13/2^-} \rightarrow h_{9/2}$ transition the B(E3) is underestimated, which could be an indication that the $\langle (h_{9/2} \otimes 3^-) | H_{pv} | i_{13/2} \rangle$ matrix element is larger than the calculated value. If this were the reason for the discrepancy and the matrix elements were adjusted to agree with experiment for the "single proton transition" the calculated B(E3) values would change for the multi particle states by no more than 10%-15%. This would still leave a significant discrepancy between the calculations and experiment. Similarly if the off-diagonal shell model matrix elements are varied within reasonable limits the wavefunctions do not change dramatically. For example if the $\langle (ig)_{11}+ | V_{sh} | (fj)_{11}+ \rangle$ matrix element is changed from -310 keV to -410 keV the wavefunctions essentially remain the same (appendix 6). It is worth noting that in ^{210}Rn both the $28^+ \rightarrow 25^-$ and the $25^- \rightarrow 22^+$ transition strengths are underestimated. This may be significant since changes in the shell model matrix elements used to

calculate the wavefunction of the 25^- state would usually result in the calculated strength of one of the transitions being increased at the expense of the strength of the other.

The source of the overall underestimation may lie in the approach of using the properties of the 3^- state in ^{208}Pb to describe the vibrational phonon. For nuclei with several valence particles, the properties of the 3^- state may change. Microscopically the wavefunction of the octupole vibration state in ^{208}Pb can be written (Ham77) as:

$$|3^-\rangle \sim .36|\pi(h_{9/2}\, d_{3/2}^{-1})\rangle + .27|\pi(f_{7/2}\, s_{1/2}^{-1})\rangle + .27|\pi(i_{13/2}\, h_{1/2}^{-1})\rangle + .44|\nu(g_{9/2}\, p_{3/2}^{-1})\rangle + .37|\nu(i_{11/2}\, f_{5/2}^{-1})\rangle + .3|\nu(j_{15/2}\, i_{13/2}^{-1})\rangle + \ldots\ldots$$

With the addition of valence particles the energies of the particle hole excitations will change. For example if the 3^- state is coupled to an $f_{7/2}$ proton in ^{209}Bi the energy of the $(\pi f_{7/2} \otimes (\nu(g_{9/2} p_{3/2}^{-1}))$ configuration is nearly 300 keV less than its weak coupling energy. Similarly the energies of the other p-h pairs will be modified by the presence of the $f_{7/2}$ particle. By using the properties of the 3^- state in ^{208}Pb we are "pre-diagonalising". Since the states considered here have up to 6 particles outside the core the energies of the p-h pairs could change substantially, and it may not be a reasonable approximation to use the octupole state in ^{208}Pb. In fact in ^{210}Po the energy of the 3^- state is 2387 keV compared to the energy of the octupole state in ^{208}Pb of 2614 keV. The effective energy of the 3^- state could be depressed through interactions with the valence particles. Hamamoto (Ham77) has calculated the diagonal residual interaction due to the quadrupole interaction between an octupole phonon coupled to a particle state. Using the measured value for the

quadrupole moment of the 3^- state of -.34(15)b (Sph83), and a typical value of -3b for the quadrupole moment of a high-spin multi-particle state, results in energy shifts of -400 keV for the maximal and minimal angular momentum couplings of a particle-vibration of spin $49/2^+$.

What effect would a lower octupole energy have on the calculated wavefunctions and energies of the states discussed in chapter 4? Although lowering the energy of the 3^- phonon would depress the "single particle" energies, the effect would already be included in the empirical residual interactions. Hence we would not notice any discrepancy in our excitation energy calculations. However the relative proportions of particle and particle-vibration states in the wavefunctions would change resulting in increased E3 transition rates.

To quantify this assertion, in appendix 6 the wavefunctions of the $43/2^-$ and $49/2^+$ states have been calculated assuming that the energy of the octupole phonon is 2 MeV. In calculating the energies of the configurations we corrected for the "extra" energy depression caused by using a lower value for the energy of the 3^- phonon. Consequently the calculated energies do not change. What is interesting though is that the calculated B(E3) ($49/2^+ \rightarrow 43/2^-$) changes from 79×10^3 e^2fm^6 to 120×10^3 e^2fm^6 compared to the experimental value of 115(5) 10^3 e^2fm^6, while the calculated g-factor of the $49/2^+$ state changes from .781 to .764 compared to the measured value of .766(8). (The g-factor of the 22^+ state remains the same.) Similar changes would occur for the other states discussed in chapter 4.

Thus although some of our approximations may have been too simplistic, we have certainly made progress in understanding the structure of the high-spin core excited states in the radon region. Perhaps what is required is a more formal self consistent approach

which seeks to describe the states from a microscopic viewpoint and so treats the particle and phonon configurations on an equal footing.

Finally it should be noted that it is only when all the properties, including both E3 and magnetic moment information is considered together can one arrive at a satisfactory understanding of the high-spin states in the radon nuclei.

ARIVIDERCI!

APPENDIX 1

SINGLE PARTICLE G-FACTORS

We collect here all the single particle g-factors that were used to calculate the g-factors of states disscussed in the main text. As noted in section 5.2.1 the empirical single particle g-factors include contributions from admixtures of particle-vibration states. The wavefunctions of the multiparticle states were calculated including explicitly configurations coupled to the 3^- state. Here the experimental g-factors used to calculate the g-factors of the multiparticle states need to be corrected for the octupole contribution. This was done using the wavefunctions given in table 4.1 (see chapter 4) and the measured values for the g-factors of the 3^- state in ^{208}Pb of .60(1) and the the single particle states (Sch80). Table A1 lists the values obtained for the g-factors of the unperturbed states. If the magnetic moment of a single particle state is not known we use the theoretical values of Bauer et al. (Bau73), which do not include corrections for possible particle vibration admixtures.

The g-factors of multiparticle configurations were calculated using additivity.

TABLE A1: SINGLE PARTICLE G-FACTORS

nucleus	state	g (exp)	g (corrected)
^{209}Bi	$h_{9/2}$	0.913	0.913
	$i_{13/2}$	1.246	1.287
	$f_{7/2}$		1.525
^{209}Pb	$j_{15/2}$		-.164
	$g_{9/2}$	-.316	-.303
	$i_{11/2}$		0.126
^{207}Pb	$p_{1/2}$	1.175	1.175
	$f_{5/2}$	0.316	0.316
	$p_{3/2}$	-.818	-.818
	$f_{7/2}$		-.362
	$h_{9/2}$		0.154

APPENDIX 2

MATRIX ELEMENTS

2.1 PARTICLE-VIBRATION MATRIX ELEMENTS

The particle-octupole-vibration matrix elements $h(j_1;j_2 3^-)$ used in this thesis were calculated by Hamamoto (Ham74, Ham77, see also Boh75) and are listed in Table A2.1.

TABLE A2.1: PARTICLE-VIBRATION MATRIX ELEMENTS

j_1	$\nu g_{9/2}$	$\pi f_{7/2}$	$\pi h9/2$
j_2	$\nu j_{15/2}$	$\pi i_{13/2}$	$\pi i_{13/2}$
$h(j_1;j_2 3^-)$	-.77	-.91	-.21

2.2 SHELL MODEL MATRIX ELEMENTS

The matrix elements for the $J = 11^+$ proton-neutron interaction were extracted from the wavefunctions of Kuo and Herling (Kuo71). The values obtained are listed in Table A2.2.

The two-body matrix elements for the other p-n angular momentum couplings, which contributed less to the many-body off-diagonal matrix elements, were calculated using the Surface Delta Interaction (SDI) formula (Bru77):

TABLE A2.2: MATRIX ELEMENTS FOR THE p-n INTERACTION J = 11^+ (MeV)

$j_1 j_2$	$j_3 j_4$	$\langle j_1 j_2 \lvert V_{sh} \rvert j_3 j_4 \rangle$
$(\pi h_{9/2} \nu j_{15/2})$	$(\pi f_{7/2} \nu j_{15/2})$	-0.12
$(\pi h_{9/2} \nu j_{15/2})$	$(\pi i_{13/2} \nu i_{11/2})$	0.08
$(\pi h_{9/2} \nu j_{15/2})$	$(\pi i_{13/2} \nu g_{9/2})$	-0.05
$(\pi f_{7/2} \nu j_{15/2})$	$(\pi i_{13/2} \nu g_{9/2})$	-0.31
$(\pi f_{7/2} \nu j_{15/2})$	$(\pi i_{13/2} \nu i_{11/2})$	0.10
$(\pi i_{13/2} \nu g_{9/2})$	$(\pi i_{13/2} \nu i_{11/2})$	0.05

$$\langle j_1 j_2 | V^{SDI}(1,2) | j_3 j_4 \rangle_{JT} = \tfrac{1}{2} A_T (-1)^{n_1+n_2+n_3+n_4} \sqrt{\frac{(2j_1+1)(2j_2+1)(2j_3+1)(2j_4+1)}{(1+\delta_{12})(1+\delta_{34})}}$$

$$\times \left\{ (-1)^{j_2+j_4+j_2+j_4} \begin{pmatrix} j_1 & j_2 & J \\ \frac{1}{2} & -\frac{1}{2} & 0 \end{pmatrix} \begin{pmatrix} j_3 & j_4 & J \\ \frac{1}{2} & -\frac{1}{2} & 0 \end{pmatrix} [1 - (-1)^{J+T+l_3+l_4}] \right.$$

$$\left. - \begin{pmatrix} j_1 & j_2 & J \\ \frac{1}{2} & \frac{1}{2} & -1 \end{pmatrix} \begin{pmatrix} j_3 & j_4 & J \\ \frac{1}{2} & \frac{1}{2} & -1 \end{pmatrix} [1 + (-1)^T] \right. .$$

with the value of .12 MeV for A_0 (which gives a reasonable fit to the Kuo and Herling 11^+ matrix elements). SDI two-body proton-proton matrix elements with A_1 = .159 MeV (Pol80) were used.

APPENDIX 3

THE $(\pi i_{13/2}\ \nu g_{9/2})$ STATE IN ^{210}Bi

The basis (in order) used to calculate the energy and wavefunction of the yrast 11^+ state in ^{210}Bi is:

$$(\pi i_{13/2}\nu g_{9/2}),\ (\pi f_{7/2}\nu j_{15/2}),\ (\pi h_{9/2}\nu j_{15/2}),\ (\pi f_{7/2}\nu g_{9/2}\otimes 3^-),$$
$$|\psi^+>,\ |\psi^->,\ |\chi^+>,\ |\chi^->,\ (\pi i_{13/2}\nu i_{11/2}),\ ((\pi i_{13/2}\otimes 3^-)_{7/2}\nu i_{11/2})$$

where

$$|\psi_\pm> = \frac{(\pi i(\nu j\otimes 3^-)_{9/2})_{11}+> \pm ((\pi i\otimes 3^-)_{7/2}\nu j)_{11}+>}{\sqrt{2(1\pm\delta)}} \qquad \delta = 0.6$$

and

$$|\chi_\pm> = \frac{((\pi h\otimes 3^-)_{13/2}\nu g)_{11}+> \quad (\pi h(\nu g\otimes 3^-)_{15/2})_{11}+>}{\sqrt{2(1\pm\delta)}} \qquad \delta = 0.8$$

In Table A3.1 the matrix elements are listed. The diagonal entries were taken from experiment (see e.g. Lon80b), except for the $<ig|V_{sh}|ig>_{J=11}+$ and $<fj|V_{sh}|fj>_{J=11}+$ matrix elements which were calculated by Kuo and Herling (Kuo71). The wavefunctions and energies are also listed in Table A3.1.

In Table A3.2 the energies and wavefunctions obtained using the modified values of -6.14 MeV and -5.19 MeV for the diagonal $(ig)_{11}+$ and $(fj)_{11}+$ matrix elements are presented.

TABLE A3.1

MATRIX AND WAVEFUNCTIONS FOR 11+ STATES IN 210BI (KUO AND HERLING)

-5.927	-0.310	-0.050	-0.910	-0.440	-0.870	0.070	-0.200	0.050	0.000
-0.310	-4.990	-0.720	-0.770	0.550	-1.100	0.000	0.000	0.100	0.000
-0.050	-0.120	-5.930	0.000	0.000	0.000	-0.240	-0.730	0.080	0.000
-0.910	-0.770	0.000	-4.290	0.000	0.000	0.000	-0.100	0.000	0.000
-0.440	0.550	0.000	0.000	-2.260	0.000	0.000	0.000	0.000	0.000
-0.870	-1.100	0.000	0.000	0.000	-2.260	0.000	0.000	0.000	0.000
0.070	0.000	-0.240	0.000	0.000	0.000	-5.000	0.000	0.000	0.000
-0.200	0.000	-0.730	-0.100	0.000	0.000	0.000	-5.000	0.000	0.000
0.050	0.100	0.080	0.000	0.000	0.000	0.000	0.000	-4.950	-0.910
0.000	0.000	0.000	0.000	0.000	0.000	0.000	0.000	-0.910	-3.470

Energies (MeV) (relative to 208Pb) are :

-6.929	-6.321	-5.398	-5.249	-4.979	-4.551	-3.837	-3.036	-2.114	-1.662

Wavefunctions are :

0.737	-0.224	-0.205	-0.458	-0.159	0.133	-0.228	0.004	0.176	-0.170
0.413	-0.097	0.272	0.723	0.156	-0.074	-0.245	0.011	-0.111	-0.347
0.223	0.844	-0.012	0.053	0.036	0.481	0.045	0.013	0.003	0.011
0.381	-0.117	0.010	0.129	0.000	-0.072	0.890	-0.009	-0.034	0.161
0.021	-0.011	-0.076	-0.201	-0.057	0.043	0.022	-0.006	-0.954	-0.194
0.235	-0.074	0.039	0.133	0.012	0.015	-0.297	0.020	-0.212	0.887
0.001	0.165	0.028	0.180	-0.940	-0.236	-0.023	-0.001	0.004	-0.004
0.181	0.424	-0.123	-0.161	0.249	-0.825	-0.065	-0.005	-0.012	0.003
-0.055	-0.043	-0.839	0.323	0.020	0.032	-0.010	0.430	-0.001	-0.015
-0.015	-0.014	-0.396	0.165	0.012	0.027	-0.024	-0.902	0.001	0.008

TABLE A3.2

MATRIX AND WAVEFUNCTIONS FOR THE 11+ STATES IN 210BI (ADJUSTED)

-6.140	-0.310	-0.050	-0.910	-0.440	-0.870	0.070	-0.200	0.050	0.000
-0.310	-5.190	-0.720	-0.770	0.550	-1.100	0.000	0.000	0.100	0.000
-0.050	-0.120	-5.930	0.000	0.000	0.000	-0.240	-0.730	0.080	0.000
-0.910	-0.770	0.000	-4.290	0.000	0.000	0.000	-0.100	0.000	0.000
-0.440	0.550	0.000	0.000	-2.260	0.000	0.000	0.000	0.000	0.000
-0.870	-1.100	0.000	0.000	0.000	-2.260	0.000	0.000	0.000	0.000
0.070	0.000	-0.240	0.000	0.000	0.000	-5.000	0.000	0.000	0.000
-0.200	0.000	-0.730	-0.100	0.000	0.000	0.000	-5.000	0.000	0.000
0.050	0.100	0.080	0.000	0.000	0.000	0.000	0.000	-4.950	-0.910
0.000	0.000	0.000	0.000	0.000	0.000	0.000	0.000	-0.910	-3.470

Energies (MeV) (relative to 208PB) are:

-7.083	-6.331	-5.475	-5.351	-4.985	-4.555	-3.860	-3.036	-2.123	-1.691

Wavefunctions are :

-0.761	-0.188	0.456	-0.221	-0.110	0.113	-0.220	0.004	0.166	0.165
-0.417	-0.067	-0.698	0.385	0.088	-0.052	-0.234	0.011	-0.105	0.332
-0.175	0.855	-0.009	0.040	0.026	0.483	0.046	0.013	0.003	-0.011
-0.368	-0.088	-0.090	0.088	-0.007	-0.075	0.900	-0.009	-0.032	-0.156
-0.022	-0.011	0.182	-0.100	-0.035	0.034	0.020	-0.005	-0.957	0.193
-0.232	-0.058	-0.115	0.075	0.000	0.018	-0.281	0.019	-0.210	-0.895
0.005	0.164	-0.072	0.072	-0.950	-0.243	-0.023	-0.001	0.004	0.004
-0.152	0.434	0.159	-0.017	0.273	-0.826	-0.070	-0.005	-0.011	-0.003
0.049	-0.048	0.428	0.791	0.010	0.034	-0.010	0.430	-0.001	0.015
0.012	-0.015	0.194	0.383	0.006	0.028	-0.022	-0.902	0.001	-0.007

APPENDIX 4

MATRICES, ENERGIES AND WAVEFUNCTIONS

The method used to calculate the wavefunctions of states which have substantial admixtures of particle-octupole-vibration configurations was described in Chapter 4. The matrix elements used in the calculations, which were obtained by recoupling in terms of the particle-vibration and two-body matrix elements given in appendix 2, are listed in this appendix.

The angular momentum recoupling procedure is straightforward and the reader is referred to Lawson (Law80) for the formalism, however a comment on phases is pertinent. Since the transition rates depend critically on the relative phases of the components it is essential to calculate the phases correctly. Hence the phases were calculated using Lawson's formalism and again using the following set of rules (which were easier to apply). When interchanging two particles coupled to spin J, a geometric phase factor of $(-1)^{j_1+j_2-J}$ is introduced. If the two particles are identical an extra phase factor of (-1) is introduced. Note that in this scheme there this no extra phase factor associated with the fractional parentage coefficients.

The diagonal energies of the core excited states were calculated by coupling extra neutrons to the empirical many-particle proton-neutron-hole "core". Thus, for example, the energy of the $(\pi(h^3i)_{17}\text{-}\nu(gp^{-1})_5)_{49/2^+}$ configuration is calculated using the 17^- state in ^{210}Rn as the "core". The extra residual interactions are then calculated in the usual way (see for example Byr82). Finally the

energies are corrected for the octupole contributions to the single particle energies (see Table 4.1).

The empirical residual interactions we used can be obtained elsewhere (see for example the compilation of Lonnroth (Lon82, Byr82), however as explained in chapter 4 we have used for the $\langle(ig)_{11}^{+}|(ig)_{11}^{+}\rangle$ and $\langle(fj)_{11}^{+}|(fj)_{11}^{+}\rangle$ residual interactions the values of -637 keV and -570 keV respectively. For some states the many-particle proton neutron "core" has not been identified and had to be calculated in terms of the two-body residual interactions. For the two-body residual interactions not known from experiment, we used the calculated values of Kuo and Herling (Kuo71, and see Lon82). However in some cases it was possible to obtain them indirectly from experiment. Thus the $(\pi i_{13/2}\nu i_{11/2})_{12}^{+}$ residual interaction was deduced from the known energy of the $45/2^{-}$ state in ^{211}Rn (which is expected to have a fairly pure $(\pi(h^3i)_{17}\text{-}\nu i_{11/2})$ configuration), while the proton-$\nu f_{5/2}^{-}$ interactions needed to calculate the energies of the $57/2^{+}$ and $63/2^{-}$ configurations in ^{211}Rn were obtained using states in ^{208}At and ^{207}Po. Finally the $(\pi h^2((if)_{10}^{-}\ \nu g)_{33/2^{-}})_{43/2^{-}}$ and $(\pi h^2((if)_{10}^{-}\ \nu j))_{49/2^{+}}$ configurations were not corrected for the octupole depression of the $g_{9/2}$ and $j_{15/2}$ neutrons since the relevant octupole vibrational states were not included in the basis.

The basis used for each state (in order) and the diagonal energies used are listed in Tables A4.1-A4.7. The matrices are in MeV (unless otherwise specified), the energies and the wavefunctions are also listed. The B(E3) values and the g-factors listed in chapter 4 were calculated using these wavefunctions. The values for the radial matrix elements used to calculate the single particle T3 matrix elements were: $\langle\pi h|r^3|\pi i\rangle$ = 238 fm^3, $\langle\pi f|r^3|\pi i\rangle$ = 197 fm^3, and $\langle\nu g|r^3|\nu j\rangle$ = 254 fm^3 with effective charges of 1.3 for the protons and 0.9 for the neutrons.

TABLE A4.1: BASES AND UNPERTURBED ENERGIES OF RELATED CORE EXCITED STATES IN ^{210}Rn, ^{211}Rn, ^{212}Rn

Basis States[a]	ENERGIES (keV)				
	$^{211}Rn\ 43/2^-$	$^{210}Rn\ 22^+$	$^{212}Rn\ 22^+$	$^{212}Rn\ 27^-$	$^{211}Rn\ 57/2^+$
	$+(\nu)^{-2}_0$	$+(\nu^{-1})_{1/2}$	$+(\nu^{-1})_{1/2}$	$+(\nu i_{11/2})$	$+(\nu^{-1}_{(3/2)} i_{11/2})_7$
$\pi(h^3 i)_{17}-\nu g$	6170	7223	6880	8619	8877
$\pi(h^3 f)_{14}+\nu j$	6980	8110	7647	9660	10019
$\pi(h^2(if)_{9^-})_{17}-\nu g$	7030	8162	7680	9680	9970
$\pi(h^3 f)\nu g \otimes 3^-$	8160	9310	8762	10970	11520
$\|\psi_1>-$	9785	10820	10554	12104	12354
$\|\psi_1>+$	9785	10820	10554	12104	12354
$\pi(h^2 f^2)_{14}+\nu g \otimes 3^-$	9340	10470	9940	12440	12760
$\pi(h^2(i^2 \otimes 3^-)_{9^-})\nu g$	10188	12420	11030	12495	12865
$\|\chi>_-$	10840	11970	11485	13430	13620
$\|\chi>_+$	10840	11970	11485	13430	13620
$\pi(h^2 f^2)_{14}+\nu j$	8335	9470	8950	11320	11614
$\pi(h^2(if)_{10}-\nu g)_{27/2}$	7325	8490	7970	10050	10270

$$|\psi_1>_\pm = (\pi h^3(i \otimes 3^-)_{7/2}\nu j \pm \pi(h^3 i)_{17^-} \otimes (\nu j \otimes 3^-)_{9/2}) \frac{1}{\sqrt{2(1+\delta_1)}}, \quad \delta_1 = 0.6$$

$$|\chi>_\pm = \pi h^2((i \otimes 3^-)_{7/2}\nu f_{7/2})_6 \nu j \pm \pi h^2(if)_{9^-}(\nu j \otimes 3^-)_{9/2} \frac{1}{\sqrt{2 \pm \delta_2}}, \quad \delta_2 = 0.53$$

TABLE A4.2: BASES AND UNPERTURBED ENERGIES OF RELATED CORE EXCITED STATES IN ^{210}Rn, ^{211}Rn, ^{212}Rn

Basis States	ENERGIES (keV)				
	^{211}Rn $49/2^+$	^{210}Rn 25^-	^{212}Rn 25^-	^{211}Rn $63/2^-$	^{212}Rn 30^+
	$+(\nu^{-2})_0$	$+(\nu^{-1})_{1/2}$	$+(\nu^{-1})_{1/2}$	$+(\nu^{-1}i_{11/2})_{14/2}$	$+\nu i_{11/2}$
$\pi(h^2i^2)_{20}+\nu g$	7588	8653	8432	10265	9895
$\pi(h^3i)_{17}-\nu j$	7186	8216	7954	9753	9504
$\pi(h^3i)_{17}-\nu g)_{43/2^-}\otimes 3^-$	8770	9823	9480	11477	11220
$(\pi(h^3f)_{14}+\nu j)_{43/2^-}\otimes 3^-$	9580	10700	10247	12620	12260
$\|\psi\rangle_-$	9620	10775	10280	12570	12280
$\|\psi\rangle_+$	9620	10775	10280	12570	12280
$\pi(h^3f)_{14}+\nu g\otimes(3^-)^2$	10760	11900	11360	14120	13570
$\pi(h^2(if)_{9^-})_{17}-\nu j$	8235	9365	8886	11020	10760
$\pi(h^2f^2)_{14}+\nu j\otimes 3^-$	10935	12070	11548	14215	13850
$\pi(h^2f^2)_{14}+\nu g\otimes(3^-)^2$	11940	13070	12540	15355	14970
$\|\chi\rangle_-$	11100	12140	12010	13620	13280
$\|\chi\rangle_+$	11100	12140	12010	13620	13280
$\pi h^2((if)_{10}-\nu j_{15/2})_{33/2}$	8540	9630	9170	11430	11275

$$|\psi\rangle_\pm = (\pi(h^2(if)_{9^-})_{17}-\nu g)\otimes 3^- \pm \pi(h^2(i(f\otimes 3^-)_{13/2})_{12}+)\nu g \times 1/\sqrt{2(1\pm\delta_1)} \quad ; \quad \delta_1 = 0.84$$

$$|\chi\rangle_\pm = (\pi(h^2(i^2\otimes 3^-)_9-\nu j \pm \pi(h^2i^2)_{20}+(\nu j\otimes 3^-)_{9/2}) \times 1/\sqrt{2(1\pm\delta_2)} \quad ; \quad \delta_2 = 0.69$$

TABLE A4.3: BASES AND UNPERTURBED ENERGIES OF RELATED CORE EXCITED STATES IN ^{210}Rn, ^{211}Rn, ^{212}Rn

Basis States	ENERGIES (keV) ^{211}Rn $55/2^-$ $+(\nu^{-2})_0$	^{210}Rn 28^+ $+(\nu^{-2})_0(\nu^{-1})_{1/2}$
$\pi(h^2i^2)_{20}+\nu j$	8500	9545
$\pi(h^2i^2)_{20}-\nu g \otimes 3^-$	10188	11250
$\pi(h^3i)_{17}-\nu j \otimes 3^-$	9786	10815
$\|\psi\rangle_-$	10914	11965
$\|\psi\rangle_+$	10914	11965
$\|\chi\rangle_-$	12300	13370
$\|\chi\rangle_+$	12300	13370
$\pi(h^2f^2)_{14}+\nu j \otimes (3^-)^2$	13610	14670
$\pi(h^3f)_{14}+\nu j \otimes (3^-)^2$	12180	13300
$\pi(h^3i)_{17}-\nu g \otimes (3^-)^2$	11370	12420
$\pi(h^2f^2)_{14}+\nu g \otimes (3^-)^3$	14610	15670

$$|\psi\rangle_\pm = \frac{\pi h^2(if)_9-\nu j \otimes 3^- \pm \pi h^2(if \otimes 3^-)_{12}\nu j}{\sqrt{2(1 \pm \delta_1)}} \qquad \delta = 0.84$$

$$|\chi\rangle_\pm = \frac{\pi(h^2(if)_{9^-})_{17}-\nu g \otimes (3^-)^2 \pm \pi h^2(i(f \otimes (3^-)^2)_{15/2})_{15}\nu g)}{\sqrt{2(1 \pm \delta_2)}}$$

$$\delta = 0.77$$

TABLE A4.4: BASES AND UNPERTURBED ENERGIES OF RELATED CORE EXCITED STATES IN ^{211}At AND ^{210}At

Basis States	ENERGIES (keV) ^{211}At $39/2^-$ $+\nu p^{-1}_{1/2}$	^{210}At 19^+ $+\nu(p^{-2}_{1/2})_{0^+}$
$\pi(h^2i)_{29/2^+}\nu g$	5493	4923
$\pi(h^2f)_{23/2^+}\nu j$	6293	5737
$\pi(h^2f)_{23/2^+}\nu g \otimes 3^-$	7992	6910
$\|\psi\rangle_-$	9165	8541
$\|\psi\rangle_+$	9165	8541

$$|\psi\rangle_\pm = \frac{\pi(h^2i)_{29/2^+}(\nu j \otimes 3^-)_{9/2^+} \pm \pi(h^2(i \otimes 3^-)_{7/2^+})\nu j}{\sqrt{2(1 \pm \delta)}} \qquad \delta = 0.6$$

TABLE A4.5: BASES AND UNPERTURBED ENERGIES OF RELATED CORE EXCITED STATES IN ^{211}At AND ^{210}At

Basis States	ENERGIES (keV) ^{211}At $33/2^+$ $+\nu p^{-1}_{1/2}$	^{210}At 16^- $+\nu(p^{-2}_{1/2})_{0^+}$
$\pi(h^2f)_{23/2}\nu g$	4792	4310
$\pi(h^3)_{21/2^-}\nu i$	4264	3957
$\pi(h^2(i \otimes 3^-)_{7/2})_{23/2^-}\nu g$	8073	7523
$\pi(h^2f)_{23/2^-}(\nu j \otimes 3^-)_{9/2^+}$	8893	8337

TABLE A4.6: BASES AND ENERGIES FOR 20^+ IN ^{210}Rn

Basis	ENERGIES (keV) $^{210}Rn\ 20^+ + \nu(p_{1/2}^{-2})_{0^+}$
$\pi(h^2 i^2)$	5814
$\pi(h^2(i(f \otimes 3^-)_{7/2})_{9^-})$	7891
$\pi(h^3 i) \otimes 3^-$	6822
$\pi(h^2 f^2) \otimes 3^{-2}$	10251
$\pi(h^3 f) \otimes 3^{-2}$	8835

TABLE A4.7: BASES AND ENERGIES FOR RELATES STATES IN ^{210}Rn AND ^{211}Rn

Basis	ENERGIES (keV) $^{210}Rn\ 17^- + \nu(p_{1/2}^{-2})_{0^+}$	$^{211}Rn\ 35/2^+ + \nu(p_{1/2}^{-1})$
$\pi(h^3 i)_{17^-}$	4222	4337
$\pi(h^3 f)_{14^+} \otimes 3^-$	6235	6231
$\pi(h^2(if)_{9^-})_{17^-}$	5291	5309
$\pi(h^2 f^2)_{14^+} \otimes 3^-$	7471	7533
$\pi(h^2(i^2 \otimes 3^-)_{9^-})_{17^-}$	7891	7909

MATRIX FOR THE 22+ AND 43/2- STATES

6.170	-0.310	-0.090	-0.910	-0.440	-0.870	0.000	-0.130	0.000	0.000	0.000	-0.050
-0.310	6.980	-0.020	-0.770	0.550	-1.100	0.000	0.000	0.000	0.000	-0.150	-0.010
-0.090	-0.020	7.030	-0.090	0.000	0.000	-1.130	-1.230	-0.490	-0.870	-0.330	-0.100
-0.910	-0.770	-0.090	8.160	0.000	0.000	-0.140	0.000	0.000	0.000	0.000	0.000
-0.440	0.500	0.000	0.000	9.785	0.000	0.000	0.000	0.000	0.000	0.000	0.000
-0.870	-1.100	0.000	0.000	0.000	9.785	0.000	0.000	0.000	0.000	0.000	0.000
0.000	0.000	-1.130	-0.140	0.000	0.000	9.340	0.000	0.000	0.000	-0.770	0.000
-0.130	0.000	-1.230	0.000	0.000	0.000	0.000	10.188	-0.040	-0.270	0.000	0.000
0.000	0.000	-0.490	0.000	0.000	0.000	0.000	-0.040	10.840	0.000	0.890	0.000
0.000	0.000	-0.870	0.000	0.000	0.000	0.000	-0.270	0.000	10.840	-1.580	0.000
0.000	-0.150	-0.330	0.000	0.000	0.000	-0.770	0.000	0.890	-1.580	8.335	0.000
-0.050	-0.010	-0.100	0.000	0.000	0.000	0.000	0.000	0.000	0.000	0.000	7.325

THE 22+ STATES IN 210RN

Energies (MeV) are :

6.294	6.972	7.879	8.489	8.769	9.657	10.795	10.958	11.434	12.143	12.800	13.043

Wavefunctions are :

0.759	0.193	-0.525	0.042	0.077	0.197	0.003	0.171	-0.186	-0.009	0.019	-0.007
0.431	0.092	0.794	-0.042	-0.088	0.182	0.000	-0.115	-0.345	0.002	-0.003	-0.018
0.183	-0.780	-0.068	-0.026	-0.435	0.057	-0.178	-0.017	0.009	0.155	0.318	0.062
0.348	0.056	0.090	0.010	-0.052	-0.902	-0.075	-0.044	0.208	0.001	-0.005	0.010
0.026	0.010	-0.214	0.017	0.038	-0.004	0.047	-0.963	-0.147	0.004	-0.005	-0.003
0.251	0.070	0.142	-0.004	-0.014	0.319	0.091	-0.156	0.882	0.005	-0.007	0.012
0.077	-0.328	0.007	0.035	0.059	-0.083	0.898	0.052	-0.048	-0.068	-0.175	-0.165
0.055	-0.184	-0.032	-0.004	-0.128	0.037	-0.187	-0.002	-0.003	0.197	-0.913	0.192
0.003	-0.014	-0.031	-0.036	-0.285	0.016	-0.002	-0.008	-0.007	-0.890	-0.074	0.345
0.054	-0.259	0.024	0.051	0.255	0.021	-0.315	-0.015	0.039	-0.367	-0.159	-0.775
0.084	-0.357	0.106	0.127	0.778	-0.008	-0.104	0.000	0.009	-0.079	0.064	0.459
0.028	-0.044	-0.041	-0.987	0.145	-0.015	0.008	-0.002	0.004	-0.004	-0.008	-0.001

THE 43/2- STATES IN 211RN

Energies (MeV) are :

5.206	5.798	6.776	7.325	7.612	8.521	9.593	9.921	10.383	10.653	11.087	11.904

Wavefunctions are :

0.739	0.219	0.539	-0.045	-0.085	-0.207	-0.015	0.168	0.185	-0.029	-0.003	-0.005
0.439	0.123	-0.786	0.046	0.099	-0.189	-0.003	-0.114	0.336	-0.006	-0.003	-0.019
0.216	-0.770	0.061	0.018	0.411	-0.047	0.105	-0.014	-0.014	-0.255	-0.311	0.110
0.353	0.076	-0.080	-0.011	0.047	0.902	0.089	-0.039	-0.195	0.008	0.003	0.009
0.023	0.009	0.209	-0.017	-0.040	0.003	-0.028	-0.965	0.145	0.011	0.000	-0.003
0.246	0.082	-0.132	0.004	0.016	-0.307	-0.082	-0.154	-0.888	0.037	0.004	0.012
0.089	-0.317	-0.013	-0.034	-0.077	0.091	-0.868	0.036	0.047	0.235	0.170	-0.188
0.076	-0.225	0.041	0.002	0.169	-0.055	0.346	0.004	0.021	0.839	0.292	0.038
0.004	-0.017	0.034	0.032	0.280	-0.011	-0.029	-0.009	0.002	-0.354	0.824	0.336
0.064	-0.251	-0.031	-0.047	-0.258	-0.023	0.294	-0.010	-0.041	-0.218	0.324	-0.789
0.097	-0.340	-0.120	-0.115	-0.783	0.001	0.115	0.001	-0.008	-0.029	0.071	0.464
0.030	-0.042	0.046	0.989	-0.132	0.014	-0.004	-0.002	-0.004	0.008	0.008	-0.002

THE 22+ STATES IN 212RN

Energies (MeV) are :

5.893	6.452	7.460	7.970	8.245	9.146	10.224	10.686	11.132	11.432	11.755	12.542

Wavefunctions are:

0.727	0.231	0.546	-0.050	-0.092	0.218	-0.019	0.164	-0.182	0.029	-0.007	0.005
0.444	0.133	-0.782	0.051	0.105	0.202	-0.006	-0.111	-0.327	0.006	-0.003	0.019
0.231	-0.763	0.067	0.022	0.420	0.050	0.132	-0.013	0.013	0.191	-0.339	-0.107
0.362	0.086	-0.077	-0.011	0.050	-0.901	0.091	-0.034	0.178	-0.009	0.005	-0.009
0.021	0.008	0.204	-0.018	-0.040	-0.004	-0.016	-0.967	-0.144	-0.011	0.001	0.004
0.240	0.085	-0.124	0.005	0.016	0.292	-0.070	-0.154	0.896	-0.036	0.008	-0.013
0.097	-0.320	-0.013	-0.035	-0.070	-0.091	-0.882	0.024	-0.037	-0.165	0.184	0.184
0.077	-0.213	0.041	0.003	0.161	0.051	0.298	0.010	-0.026	-0.805	0.424	-0.045
0.004	-0.015	0.037	0.034	0.280	0.013	-0.020	-0.010	0.000	0.475	0.761	-0.337
0.070	-0.252	-0.033	-0.048	-0.254	0.022	0.299	-0.006	0.038	0.244	0.297	0.791
0.106	-0.345	-0.127	-0.120	-0.779	-0.004	0.115	0.002	0.006	0.041	0.063	-0.462
0.031	-0.042	0.051	0.987	-0.140	-0.015	-0.005	-0.002	0.004	-0.006	0.009	0.002

MATRIX FOR THE 49/2+ AND 25- STATES

7.858	-0.032	-0.150	0.000	0.360	-1.230	0.000	-0.290	0.000	0.000	-0.380	-0.890	-0.260
-0.032	7.506	-0.770	-0.910	0.000	0.000	0.000	-0.100	0.000	0.000	0.050	-0.120	-0.085
-0.150	-0.770	8.320	-0.310	-0.030	-0.090	-1.290	0.000	0.000	0.000	0.000	0.000	0.000
0.000	-0.910	-0.310	9.250	-0.010	-0.020	-1.090	-0.090	-0.150	0.000	0.000	0.000	0.000
0.360	0.000	-0.030	-0.010	9.240	0.000	-0.040	-0.220	-0.080	0.440	0.000	0.000	-0.040
-1.230	0.000	-0.090	-0.020	0.000	9.240	-0.130	-0.740	-0.320	-1.510	0.000	0.000	-0.160
0.000	0.000	-1.290	-1.090	-0.040	-0.130	9.660	0.000	0.000	-0.140	0.000	0.000	0.000
-0.290	-0.100	0.000	-0.090	-0.220	-0.740	0.000	8.625	-1.130	0.000	0.520	-1.130	0.200
0.000	0.000	0.000	-0.150	-0.080	-0.320	0.000	-1.130	10.770	-1.090	0.000	0.000	0.000
0.000	0.000	0.000	0.000	0.440	-1.510	-0.140	0.000	-1.090	11.000	0.000	0.000	0.000
-0.380	0.050	0.000	0.000	0.000	0.000	0.000	0.520	0.000	0.000	10.900	0.000	0.000
-0.890	-0.120	0.000	0.000	0.000	0.000	0.000	-1.130	0.000	0.000	0.000	10.900	0.000
-0.260	-0.085	0.000	0.000	-0.040	-0.160	0.000	0.200	0.000	0.000	0.000	0.000	8.960

THE 25- STATES IN 210RN

Energies (MeV) are :

7.187	7.574	8.759	9.475	9.728	10.349	10.749	10.873	12.077	12.392	12.736	12.974	14.385

Wavefunctions are :

0.548	0.425	0.518	0.043	0.256	0.276	0.091	-0.045	-0.054	0.264	0.104	0.069	0.092
0.462	-0.677	-0.002	0.512	0.139	-0.054	-0.154	-0.041	-0.006	-0.008	-0.015	0.132	-0.007
0.267	-0.318	0.093	-0.664	-0.108	0.164	-0.468	0.074	-0.048	0.037	0.069	-0.325	0.017
0.203	-0.269	-0.025	-0.182	-0.050	-0.095	0.820	0.003	0.025	0.019	0.091	-0.400	0.029
-0.038	-0.046	-0.162	-0.014	-0.144	0.351	0.020	-0.896	-0.032	0.072	-0.074	-0.009	0.105
0.349	0.256	0.016	-0.060	-0.078	-0.576	-0.125	-0.329	0.344	-0.296	0.054	-0.088	-0.361
0.133	-0.153	0.026	-0.441	-0.100	-0.012	0.229	0.012	0.064	-0.085	-0.183	0.809	-0.049
0.391	0.250	-0.702	0.040	-0.142	0.243	-0.010	0.193	0.043	-0.130	0.346	0.084	0.165
0.146	0.093	-0.257	-0.021	-0.114	-0.239	-0.005	-0.012	-0.627	0.493	-0.167	0.013	-0.411
0.123	0.089	-0.042	-0.047	-0.058	-0.473	-0.074	-0.052	-0.142	0.069	-0.280	-0.017	0.797
-0.004	0.014	0.166	-0.011	0.068	-0.010	0.034	-0.091	-0.675	-0.668	0.234	0.029	0.023
0.199	0.127	-0.098	0.054	0.035	0.287	0.037	0.137	0.004	-0.343	-0.808	-0.207	-0.119
0.065	0.021	0.311	0.237	-0.906	0.083	0.006	0.114	-0.013	-0.018	0.012	0.001	0.013

THE 49/2+ STATES IN 211RN

Energies (MeV) are :

6.102	6.510	7.653	8.406	8.637	9.222	9.645	9.724	10.977	11.319	11.670	11.855	13.252

Wavefunctions are :

0.561	0.387	0.527	0.040	0.257	0.290	0.090	0.046	0.088	-0.250	0.106	0.080	-0.093
0.420	-0.696	-0.002	0.518	0.151	-0.061	-0.155	0.039	0.005	0.009	-0.027	0.134	0.007
0.249	-0.337	0.090	-0.647	-0.116	0.164	-0.478	-0.097	0.051	-0.032	0.100	-0.324	-0.017
0.191	-0.287	-0.025	-0.185	-0.054	-0.084	0.816	0.028	-0.024	-0.021	0.124	-0.390	-0.029
-0.040	-0.044	-0.168	-0.010	-0.153	0.363	-0.017	0.889	0.047	-0.068	-0.067	-0.014	-0.105
0.368	0.240	0.028	-0.065	-0.079	-0.571	-0.131	0.333	-0.376	0.247	0.051	-0.084	0.360
0.127	-0.166	0.026	-0.447	-0.110	-0.003	0.220	-0.008	-0.070	0.076	-0.253	0.786	0.049
0.413	0.233	-0.698	0.047	-0.135	0.241	-0.005	-0.203	-0.073	0.136	0.324	0.109	-0.167
0.156	0.087	-0.255	-0.020	-0.114	-0.238	-0.002	0.011	0.689	-0.414	-0.134	0.007	0.412
0.130	0.084	-0.037	-0.050	-0.058	-0.471	-0.070	0.055	0.159	-0.060	-0.273	-0.039	-0.796
-0.005	0.013	0.163	-0.013	0.065	-0.007	0.030	0.088	0.578	0.757	0.223	0.043	-0.024
0.203	0.114	-0.093	0.056	0.038	0.279	0.038	-0.133	-0.029	0.312	-0.802	-0.279	0.126
0.064	0.015	0.309	0.255	-0.902	0.081	0.010	-0.122	0.008	0.020	0.011	0.001	-0.013

THE 25- STATES IN 212RN

Energies (MeV) are :

6.844	7.254	8.363	9.101	9.291	9.902	10.323	10.390	11.662	12.177	12.434	12.575	13.872

Wavefunctions are :

0.527	0.372	-0.541	0.012	-0.280	0.318	0.097	0.047	0.151	0.212	0.021	0.145	0.103
0.424	-0.680	0.012	0.515	-0.206	-0.061	-0.156	0.036	0.002	-0.015	-0.117	0.082	-0.007
0.257	-0.342	-0.088	-0.615	0.171	0.167	-0.485	-0.118	0.057	0.030	0.303	-0.167	0.016
0.201	-0.291	0.028	-0.176	0.072	-0.089	0.808	0.058	-0.018	0.035	0.363	-0.200	0.029
-0.036	-0.042	0.175	0.006	0.169	0.362	-0.050	0.884	0.073	0.053	-0.036	-0.048	0.105
0.374	0.253	-0.063	-0.062	0.059	-0.552	-0.143	0.336	-0.427	-0.144	0.094	-0.031	-0.365
0.137	-0.174	-0.027	-0.443	0.155	-0.004	0.216	-0.002	-0.082	-0.078	-0.720	0.387	-0.048
0.433	0.262	0.674	0.069	0.151	0.244	0.004	-0.214	-0.134	-0.128	0.145	0.267	0.174
0.167	0.100	0.247	-0.009	0.120	-0.249	-0.007	0.008	0.772	0.239	-0.068	-0.019	-0.408
0.137	0.092	0.022	-0.049	0.051	-0.479	-0.077	0.059	0.174	0.027	-0.169	-0.219	0.788
-0.009	0.008	-0.153	-0.020	-0.064	-0.002	0.025	0.079	0.364	-0.887	0.145	0.156	0.027
0.195	0.115	0.077	0.052	-0.038	0.262	0.043	-0.121	-0.048	-0.249	-0.398	-0.780	-0.154
0.062	0.013	-0.344	0.340	0.862	0.062	0.012	-0.121	0.000	-0.019	0.006	0.005	0.013

MATRIX FOR THE 55/2- AND 28+ STATES

9.545	-0.770	-0.150	0.360	-1.230	0.000	0.000	0.000	0.000	0.000	0.000
-0.770	11.250	-0.035	-0.100	-0.290	0.510	-1.210	0.000	0.000	0.000	0.000
-0.150	-0.035	10.815	-0.030	-0.100	0.000	0.000	0.000	-1.290	-1.090	0.000
0.360	-0.080	-0.030	11.965	0.000	0.000	-0.280	0.440	-0.030	0.000	0.000
-1.230	-0.290	-0.100	0.000	11.965	-0.410	-0.970	-1.510	-0.120	0.000	0.000
0.000	0.510	0.000	0.000	-0.410	13.370	0.000	-0.075	-0.010	-0.010	0.540
0.000	-1.210	0.000	-0.280	-0.970	0.000	13.370	-0.310	-0.020	-0.090	-1.850
0.000	0.000	0.000	0.440	-1.510	-0.075	-0.310	14.670	-0.150	0.000	-1.330
0.000	0.000	-1.290	-0.030	-0.120	-0.010	-0.020	-0.150	13.300	-0.310	0.000
0.000	0.000	-1.090	0.000	0.000	-0.010	-0.090	0.000	-0.310	12.420	0.000
0.000	0.000	0.000	0.000	0.000	0.540	-1.850	-1.330	0.000	0.000	15.670

28+ STATES IN 210RN

Energies (MeV) are :

8.473	9.806	10.627	11.343	11.986	12.875	13.156	13.730	13.875	15.046	17.423

Wavefunctions are:

-0.779	0.117	0.503	0.216	0.139	-0.048	0.188	-0.125	0.054	0.055	0.038
-0.351	0.066	-0.565	0.546	-0.203	0.074	-0.407	0.098	-0.001	0.162	-0.081
-0.119	-0.841	0.023	0.046	-0.014	0.304	0.038	-0.115	-0.409	0.017	0.006
0.072	-0.032	-0.226	0.151	0.943	-0.014	0.050	0.077	-0.005	0.148	0.019
-0.424	0.027	-0.158	-0.620	0.129	0.043	-0.287	0.402	-0.139	-0.305	-0.187
0.007	-0.009	0.124	-0.238	0.130	0.006	-0.634	-0.671	0.133	0.177	-0.103
-0.206	0.020	-0.506	-0.143	-0.003	-0.084	0.319	-0.502	0.070	-0.405	0.388
-0.137	0.004	-0.150	-0.381	-0.109	0.010	0.114	0.113	0.009	0.763	0.440
-0.050	-0.344	-0.012	-0.034	0.000	0.276	0.023	0.155	0.879	-0.059	-0.014
-0.041	-0.391	-0.013	0.023	-0.034	-0.901	-0.096	0.098	0.114	0.013	-0.007
-0.079	0.008	-0.239	-0.148	-0.060	-0.052	0.432	-0.214	0.039	0.271	-0.775

55/2- STATES IN 211RN

Energies (MeV) are :

7.410	8.762	9.566	10.246	10.870	11.820	12.050	12.627	12.772	13.947	16.323

Wavefunctions are :

-0.774	0.116	0.506	0.223	0.142	-0.050	0.183	0.135	0.052	-0.054	0.038
-0.350	0.066	-0.559	0.545	-0.207	0.079	-0.409	-0.111	0.000	-0.165	-0.082
-0.117	-0.839	0.024	0.047	-0.016	0.294	0.036	0.109	-0.424	-0.017	0.006
0.073	-0.033	-0.235	0.156	0.940	-0.014	0.058	-0.071	-0.003	-0.148	0.019
-0.431	0.027	-0.159	-0.618	0.133	0.045	-0.261	-0.419	-0.131	0.300	-0.187
0.007	-0.010	0.127	-0.243	0.137	0.010	-0.660	0.646	0.115	-0.170	-0.102
-0.207	0.020	-0.503	-0.134	-0.010	-0.089	0.292	0.512	0.059	0.414	0.394
-0.140	0.004	-0.152	-0.380	-0.108	0.008	0.125	-0.096	0.014	-0.765	0.437
-0.050	-0.351	-0.012	-0.033	-0.001	0.294	0.030	-0.131	0.874	0.058	-0.014
-0.041	-0.392	-0.012	0.023	-0.034	-0.897	-0.101	-0.104	0.132	-0.013	-0.007
-0.080	0.008	-0.240	-0.144	-0.064	-0.058	0.423	0.244	0.037	-0.261	-0.774

MATRIX FOR THE 27- AND 57/2+ STATES

8.877	-0.310	-0.040	-0.910	-0.440	-0.870	0.000	-0.130	0.000	0.000	0.000	-0.050
-0.310	10.019	-0.020	-0.770	0.550	-1.100	0.000	0.000	0.000	0.000	-0.080	-0.010
-0.040	-0.020	9.970	-0.090	0.000	0.000	-1.130	-1.230	-0.490	-0.870	-0.330	-0.100
-0.910	-0.770	-0.090	11.520	0.000	0.000	-0.070	0.000	0.000	0.000	0.000	0.000
-0.440	0.500	0.000	0.000	12.354	0.000	0.000	0.000	0.000	0.000	0.000	0.000
-0.870	-1.100	0.000	0.000	0.000	12.350	0.000	0.000	0.000	0.000	0.000	0.000
0.000	0.000	-1.130	-0.070	0.000	0.000	12.760	0.000	0.000	0.000	-0.770	0.000
-0.130	0.000	-1.230	0.000	0.000	0.000	0.000	12.865	-0.040	-0.270	0.000	0.000
0.000	0.000	-0.490	0.000	0.000	0.000	0.000	-0.040	13.620	0.000	0.890	0.000
0.000	0.000	-0.870	0.000	0.000	0.000	0.000	-0.270	0.000	13.620	-1.580	0.000
0.000	-0.080	-0.330	0.000	0.000	0.000	-0.770	0.000	0.890	-1.580	11.614	0.000
-0.050	-0.010	-0.100	0.000	0.000	0.000	0.000	0.000	0.000	0.000	0.000	10.270

THE 57/2+ STATES IN 211RN

Energies (MeV) are :

8.064	8.765	9.709	10.272	10.722	11.759	12.501	12.792	13.065	13.448	13.908	14.833

Wavefunctions are :

0.812	0.130	-0.479	-0.030	0.037	-0.140	0.182	0.008	-0.197	-0.025	0.008	0.002
0.392	0.052	0.816	0.025	-0.039	-0.111	-0.122	-0.054	-0.381	-0.005	0.003	0.011
0.120	-0.814	-0.026	-0.010	-0.366	-0.024	-0.009	0.027	0.002	-0.240	0.338	-0.121
0.305	0.024	0.105	-0.009	-0.029	0.890	-0.070	-0.017	0.311	0.009	-0.009	-0.005
0.038	0.009	-0.234	-0.012	0.022	-0.011	-0.957	-0.070	-0.146	0.008	-0.001	0.002
0.265	0.048	0.182	0.000	-0.007	-0.413	-0.164	0.118	0.826	0.024	-0.006	-0.006
0.040	-0.289	0.005	-0.028	0.095	0.039	-0.035	0.758	-0.105	0.421	-0.274	0.254
0.055	-0.258	-0.029	-0.010	-0.175	-0.047	0.044	-0.559	0.044	0.699	-0.301	-0.021
0.004	-0.028	-0.015	0.019	-0.308	-0.010	-0.009	0.063	-0.011	-0.392	-0.802	-0.321
0.034	-0.260	0.012	-0.039	0.306	-0.014	0.015	-0.286	0.054	-0.347	-0.263	0.750
0.043	-0.306	0.049	-0.076	0.792	0.005	0.008	-0.069	0.010	-0.025	-0.087	-0.505
0.026	-0.049	-0.033	0.995	0.078	0.007	-0.003	-0.001	0.005	0.008	-0.009	0.003

THE 27- STATES IN 212RN

Energies (MeV) are :

7.761	8.474	9.382	10.052	10.445	11.266	12.248	12.467	12.777	13.136	13.686	14.608

Wavefunctions are :

0.795	0.128	0.501	-0.028	0.038	0.168	0.178	-0.017	-0.193	-0.025	-0.005	-0.002
0.409	0.058	-0.808	0.022	-0.036	0.147	-0.119	0.045	-0.369	-0.004	-0.002	-0.010
0.120	-0.815	0.023	-0.005	-0.361	0.027	-0.012	-0.041	0.003	-0.282	-0.308	0.117
0.328	0.027	-0.103	-0.012	-0.035	-0.900	-0.052	0.025	0.258	0.008	0.007	0.004
0.033	0.008	0.229	-0.011	0.021	0.001	-0.958	0.082	-0.148	0.009	0.001	-0.002
0.263	0.048	-0.166	0.000	-0.004	0.368	-0.170	-0.094	0.853	0.025	0.004	0.005
0.041	-0.291	-0.006	-0.030	0.102	-0.034	-0.045	-0.741	-0.087	0.484	0.228	-0.238
0.055	-0.262	0.029	-0.008	-0.181	0.047	0.054	0.590	0.036	0.700	0.222	0.023
0.004	-0.028	0.014	0.021	-0.299	0.011	-0.011	-0.073	-0.011	-0.302	0.840	0.326
0.033	-0.254	-0.012	-0.041	0.300	0.009	0.018	0.266	0.045	-0.320	0.303	-0.759
0.043	-0.304	-0.048	-0.084	0.797	-0.010	0.011	0.083	0.011	-0.024	0.082	0.497
0.024	-0.047	0.029	0.994	0.087	-0.010	-0.003	0.002	0.005	0.010	0.009	-0.003

MATRIX FOR THE 63/2- AND THE 30+ STATES

10.265	-0.032	-0.150	0.000	0.360	-1.230	0.000	-0.290	0.000	0.000	-0.380	-0.890	-0.260
-0.032	9.753	-0.770	-0.910	0.000	0.000	0.000	-0.050	0.000	0.000	0.050	-0.120	-0.050
-0.150	-0.770	11.477	-0.310	-0.010	-0.040	-1.290	0.000	0.000	0.000	0.000	0.000	0.000
0.000	-0.910	-0.310	12.620	-0.010	-0.020	-1.090	-0.090	-0.050	0.000	0.000	0.000	0.000
0.360	0.000	-0.010	-0.010	12.570	0.000	-0.040	-0.220	-0.080	0.440	0.000	0.000	-0.040
-1.230	0.000	-0.040	-0.020	0.000	12.570	-0.130	-0.740	-0.320	-1.510	0.000	0.000	-0.160
0.000	0.000	-1.290	-1.090	-0.040	-0.130	14.120	0.000	0.000	-0.070	0.000	0.000	0.000
-0.290	-0.050	0.000	-0.090	-0.220	-0.740	0.000	11.020	-1.130	0.000	0.520	-1.130	0.200
0.000	0.000	0.000	-0.080	-0.080	-0.320	0.000	-1.130	14.215	-1.090	0.000	0.000	0.000
0.000	0.000	0.000	0.000	0.440	-1.510	-0.070	0.000	-1.090	15.355	0.000	0.000	0.000
-0.380	0.050	0.000	0.000	0.000	0.000	0.000	0.520	0.000	0.000	13.620	0.000	0.000
-0.890	-0.120	0.000	0.000	0.000	0.000	0.000	-1.130	0.000	0.000	0.000	13.620	0.000
-0.260	-0.050	0.000	0.000	-0.040	-0.160	0.000	0.200	0.000	0.000	0.000	0.000	11.430

THE 63/2- STATES IN 211RN

Energies (MeV) are :

8.882	9.176	10.442	11.228	11.509	12.207	12.615	12.658	13.705	14.163	14.430	15.070	16.551

Wavefunctions are :

-0.554	-0.449	0.515	0.043	0.223	-0.272	0.081	-0.013	-0.107	0.275	0.021	0.031	-0.073
-0.512	0.679	-0.014	0.481	0.081	0.020	-0.131	-0.095	0.009	0.008	-0.012	0.110	0.002
-0.268	0.294	0.079	-0.746	-0.080	-0.101	-0.389	-0.145	0.018	0.023	0.005	-0.300	-0.003
-0.193	0.233	-0.024	-0.163	-0.036	0.099	0.753	0.391	-0.018	0.019	-0.002	-0.387	-0.011
0.038	0.041	-0.158	-0.021	-0.134	-0.326	0.432	-0.800	-0.037	0.017	0.096	-0.009	-0.099
-0.319	-0.261	0.010	-0.022	-0.067	0.644	0.052	-0.324	-0.109	-0.353	-0.233	-0.065	0.329
-0.115	0.120	0.018	-0.396	-0.061	0.041	0.226	0.111	-0.017	-0.080	-0.002	0.860	0.014
-0.368	-0.277	-0.725	-0.002	-0.138	-0.195	-0.081	0.143	0.075	0.133	-0.367	0.022	-0.137
-0.120	-0.092	-0.230	-0.014	-0.085	0.218	-0.016	-0.024	0.254	0.486	0.631	0.031	0.411
-0.098	-0.081	-0.034	-0.016	-0.036	0.431	-0.041	-0.058	0.077	-0.014	0.318	0.001	-0.827
0.001	-0.014	0.180	-0.003	0.072	-0.002	0.079	-0.077	0.941	-0.064	-0.246	0.003	-0.015
-0.205	-0.142	-0.114	0.039	0.024	-0.325	-0.035	0.144	0.113	-0.730	0.491	-0.045	0.075
-0.057	-0.030	0.277	0.155	-0.936	-0.076	-0.048	0.098	0.027	0.004	-0.015	0.000	-0.011

THE 30+ STATES IN 212RN

Energies are :

8.571	8.885	10.149	10.921	11.334	11.886	12.271	12.363	13.364	13.821	14.090	14.584	16.183

Wavefunctions are :

-0.606	0.404	-0.510	0.056	-0.203	-0.256	0.076	0.037	-0.106	0.273	-0.017	-0.036	-0.074
-0.441	-0.717	0.010	0.498	-0.053	0.025	-0.145	0.055	0.008	0.004	0.012	-0.121	0.002
-0.241	-0.321	-0.079	-0.721	0.032	-0.113	-0.445	0.034	0.020	0.031	-0.004	0.315	-0.002
-0.175	-0.260	0.024	-0.178	0.029	0.099	0.818	-0.161	-0.016	0.029	0.002	0.403	-0.010
0.043	-0.039	0.157	-0.027	0.128	-0.331	0.189	0.888	-0.039	0.018	-0.099	0.010	-0.100
-0.339	0.227	0.008	-0.030	0.094	0.635	-0.045	0.321	-0.115	-0.364	0.228	0.072	0.335
-0.110	-0.142	-0.019	-0.427	0.042	0.037	0.243	-0.043	-0.018	-0.094	-0.002	-0.844	0.012
-0.379	0.229	0.736	-0.009	0.105	-0.204	-0.036	-0.158	0.074	0.125	0.377	-0.025	-0.141
-0.125	0.077	0.242	-0.020	0.086	0.219	-0.026	0.020	0.258	0.503	-0.611	-0.040	0.411
-0.106	0.071	0.042	-0.021	0.050	0.436	-0.060	0.044	0.077	-0.013	-0.316	0.002	-0.823
-0.002	0.016	-0.184	0.001	-0.066	0.005	0.054	0.102	0.938	-0.071	0.251	-0.004	-0.016
-0.217	0.121	0.121	0.042	-0.036	-0.327	0.010	-0.152	0.120	-0.713	-0.509	0.058	0.078
-0.058	0.024	-0.241	0.101	0.949	-0.105	-0.020	-0.120	0.030	0.004	0.017	0.000	-0.012

MATRIX FOR THE 16- AND 33/2+ STATES

4.792	0.028	-0.120	-0.974
0.028	4.264	0.000	0.000
-1.200	0.000	8.073	-0.250
-0.970	0.000	-0.250	8.893

MATRIX FOR THE 19+ AND 39/2- STATES

4.923	-0.310	-0.910	-0.440	-0.870
-0.310	5.737	-0.770	0.500	-0.110
-0.910	-0.770	6.910	0.000	0.000
-0.440	0.500	0.000	8.541	0.000
-0.870	-1.100	0.000	0.000	8.541

39/2- STATES IN 211AT

Energies (MeV) are :

4.553	6.109	7.783	9.297	9.746

Wavefunctions are :

0.770	-0.548	0.219	-0.164	0.181
0.454	0.795	0.202	0.111	0.330
0.370	0.089	-0.907	0.034	-0.178
0.024	-0.209	-0.003	0.967	0.147
0.253	0.130	0.298	0.159	-0.897

19+ STATES IN 210AT

Energies (MeV) are :

4.006	5.551	7.282	8.676	9.137

Wavefunctions are :

0.770	-0.547	0.211	-0.168	0.186
0.456	0.794	0.189	0.114	0.336
0.362	0.083	-0.907	0.037	-0.192
0.024	-0.213	-0.001	0.966	0.145
0.258	0.133	0.310	0.157	-0.891

16- STATES IN 210AT

Energies (MeV) are :

3.693	3.960	7.915	8.559

Wavefunctions are :

-0.924	-0.090	0.290	-0.231
0.098	-0.995	0.002	-0.001
-0.303	-0.032	-0.952	0.033
-0.209	-0.022	0.102	0.972

33/2- STATES IN 211AT

Energies (MeV) are :

4.179	4.272	8.459	9.111

Wavefunctions are :

0.890	-0.274	-0.287	-0.226
-0.295	-0.956	-0.002	-0.001
0.287	-0.090	0.953	0.027
0.198	-0.062	-0.093	0.974

MATRIX FOR THE 20+ STATES IN 210RN

5.814	-1.290	-0.150	0.000	0.000
-1.290	7.891	-0.050	-1.590	-0.120
-0.150	-0.050	6.822	0.000	-1.290
0.000	-1.590	0.000	10.071	-0.110
0.000	-0.120	-1.290	-0.110	8.835

20+ STATES IN 210RN

Energies (MeV) are :

5.063	6.218	7.693	9.475	10.984

Wavefunctions are :

0.851	-0.138	0.490	0.042	-0.123
0.480	-0.060	-0.720	-0.069	0.493
0.134	0.888	0.052	-0.437	-0.008
0.154	-0.012	-0.484	-0.019	-0.861
0.066	0.434	-0.064	0.896	0.021

MATRIX FOR THE 17- AND 35/2+ STATES

4.337	-0.910	-0.050	0.000	-0.130
-0.910	6.231	-0.900	-0.100	0.000
-0.050	-0.090	5.309	-1.130	-1.230
0.000	-0.100	-1.130	7.533	0.000
-0.130	0.000	-1.230	0.000	7.909

35/2+ STATES IN 211RN

Energies (MeV) are :

3.940	4.482	6.591	7.686	8.620

Wavefunctions are :

-0.900	-0.226	0.369	0.044	0.019
-0.369	-0.055	-0.925	-0.078	-0.005
-0.199	0.867	0.035	-0.105	0.443
-0.073	0.319	-0.057	0.823	-0.460
-0.091	0.303	0.069	-0.551	-0.770

17- STATES IN 210RN

Energies are :

3.845	4.455	6.579	7.638	8.593

Wavefunctions are :

-0.912	-0.200	0.354	0.043	0.019
-0.357	-0.040	-0.930	-0.080	-0.005
-0.173	0.872	0.036	-0.115	0.442
-0.064	0.325	-0.058	0.830	-0.445
-0.082	0.304	0.069	-0.538	-0.779

MATRIX FOR THE 14+ STATES

3.635	-0.100	-1.200	0.000
-0.100	4.933	0.000	-1.697
-1.200	0.000	6.937	-0.040
0.000	-1.697	-0.040	7.909

14+ STATES IN 210RN

Energies (MeV) are :

3.236	4.173	7.325	8.680

Wavefunctions are :

-0.947	0.092	-0.309	0.016
-0.092	-0.906	-0.011	-0.413
-0.307	0.034	0.950	-0.032
-0.036	-0.411	0.034	0.910

APPENDIX 5

"NEUTRON HOLE" ORBITALS

The matrix element $\langle j'1'k'n'|r^2Y_{20}|j\ 1\ k\ n\rangle$ needed in the calculation of the Nilsson orbitals is given by (Law80):

$$= (-1)\left(\frac{(2.2+1)(2j+1)(2j+1)}{4\pi}\right)^{\frac{1}{2}}\begin{pmatrix} j' & 2 & j \\ 1/2 & 0 & -1/2\end{pmatrix}\begin{pmatrix} j' & 2 & j \\ 3/2 & 0 & -3/2\end{pmatrix}\times\langle j'|r^2|j\rangle\ .$$

The radial wavefunctions listed in Table 5.1 were calculated using a harmonic oscillator potential, with the phase convention that the radial wavefunctions are positive at infinity.

TABLE A5.1: RADIAL MATRIX ELEMENTS

n'1'	nl	$\langle j'\|r^2\|j\rangle$ (fm^2)
ν1h	1h	39
ν1h	2f	28
ν2f	2f	39
ν2f	3p	36

The matrices for the K = 1/2 and K = 3/2 neutron orbitals in units of ħ are listed in Tables A5.2 and A5.3. The diagonal single particle energies, which are added to the diagonal terms listed in the tables, were taken from experiment (Table A5.4). The contribution of the off-diagonal contributions to the g-factors can be calculated using these wavefunctions (see chapter 4). The magnitude of the M1 matrix elements used were taken from experiment (Bab72), the sign being determined from the expression 3-41, p.337 in Bohr and Mottelson

(Boh75). The values used were $\langle \nu p_{1/2}^{-1} | M1 | \nu p_{3/2}^{-1} \rangle$ = -.64 nm and $\langle \nu f_{5/2}^{-1} | M1 | \nu f_{7/2}^{-1} \rangle$ = -.70 nm.

TABLE A5.2: MATRIX FOR NILSSON WAVEFUNCTIONS, K = 1/2

$p_{1/2}$	$p_{3/2}$	$f_{5/2}$	$f_{7/2}$	$h_{9/2}$	$h_{11/2}$
0	1.16β	-1.3β	0	0	0
	-0.82β	0.3β	-1.4β	0	0
		-0.94β	0.14β	-1.1β	0
			-0.85β	0.1β	0
				-0.99β	0.1β
					-0.92β

TABLE A5.3: MATRIX ELEMENTS FOR NILSSON WAVEFUNCTIONS, K = 3/2

$p_{3/2}$	$f_{5/2}$	$f_{7/2}$	$h_{9/2}$	$h_{11/2}$
0.82β	-0.74β	-1.04β	0	0
	-0.23β	0.38β	-0.95β	0
		-0.51β	0.28β	-1.0β
			-0.74β	0.29β
				-0.74β

TABLE A5.4: NILSSON ORBITALS ^{207}Pb K = 1/2, K = 3/2

		K = 1/2		K = 3/2
β		-.025	-.05	-.075
$\|nljK\rangle$	Energy (ħω)		amplitudes	
$\|\nu p^{-1}_{1/2}\rangle$	0	-.901	-.771	0
$\|\nu p^{-1}_{3/2}\rangle$	-.138	.218	.345	.391
$\|\nu f^{-1}_{5/2}\rangle$	-.088	-.375	-.528	-.882
$\|\nu f^{-1}_{7/2}\rangle$	-.360	.026	.073	.214
$\|\nu h^{-1}_{9/2}\rangle$	-.525	-.020	-.054	-.154
$\|\nu h^{-1}_{11/2}\rangle$	-1.141	.001	.003	.015

TABLE A5.5: NILSSON ORBITALS in ^{205}Pb K = 1/2, K = 3/2

		K = 1/2		K = 3/2
β		-.025	-.05	-.075
$\|nljK\rangle$	Energy (ħω)		amplitudes	
$\|\nu p^{-1}_{1/2}\rangle$	0	-.600	-.580	0
$\|\nu p^{-1}_{3/2}\rangle$	-.040	.332	.431	.408
$\|\nu f^{-1}_{5/2}\rangle$	0	-.725	-.680	-.872
$\|\nu f^{-1}_{7/2}\rangle$	-.272	.048	.102	.218
$\|\nu h^{-1}_{9/2}\rangle$	-.418	-.046	-.078	-.159
$\|\nu h^{-1}_{11/2}\rangle$	-1.305	.001	.004	.015

APPENDIX 6

THE EFFECT OF A 2 MeV OCTUPOLE PHONON

Since we assume that the extra octupole energy depression of the single particle energies caused by a 2 MeV phonon is "hidden" in the residual interactions the single particle energies are corrected for this.

TABLE A6.1: E(oct) for "single particle states" if the 3^- state is at 2 MeV

Configuration	E(oct) (keV)
$i_{13/2}$	530
$f_{7/2}$	457
$j_{15/2}$	626
$g_{9/2}$	243

It is perhaps significant that the Kuo and Herrling (Kuo71) values for the maximally aligned two-nucleon residual interactions are generally underestimated, especially for particles which couple strongly to the particle-octupole-vibration configurations. For example the $(\pi i\nu j)_{14}+$ residual interaction is underestimated by 400 keV. We note that the extra energy depression which would result from the vibrational phonon having an energy of 2 MeV for the $(\pi i\nu j)_{14}+$ configuration is 320 keV. The matrices used to calculate the $49/2^+$ and $43/2^-$ states in ^{211}Rn are listed below. It should be noted that the diagonal entries remain the same. The wavefunctions and energies are also reproduced. The basis used for these calculations are given in appendix 4.

MATRIX FOR THE 43/2- STATE IN 211RN WITH A 2MEV PHONON

6.320	-0.310	-0.090	-0.910	-0.440	-0.870	0.000	-0.130	0.000	0.000	0.000	-0.050
-0.310	7.160	-0.020	-0.770	0.550	-1.100	0.000	0.000	0.000	0.000	-0.150	-0.010
-0.090	-0.020	7.250	-0.090	0.000	0.000	-1.130	-1.230	-0.490	-0.870	-0.330	-0.100
-0.910	-0.770	-0.090	7.660	0.000	0.000	-0.140	0.000	0.000	0.000	0.000	0.000
-0.440	0.500	0.000	0.000	9.505	0.000	0.000	0.000	0.000	0.000	0.000	0.000
-0.870	-1.100	0.000	0.000	0.000	9.505	0.000	0.000	0.000	0.000	0.000	0.000
0.000	0.000	-1.130	-0.140	0.000	0.000	8.910	0.000	0.000	0.000	-0.770	0.000
-0.130	0.000	-1.230	0.000	0.000	0.000	0.000	9.858	-0.040	-0.270	0.000	0.000
0.000	0.000	-0.490	0.000	0.000	0.000	0.000	-0.040	10.630	0.000	0.890	0.000
0.000	0.000	-0.870	0.000	0.000	0.000	0.000	-0.270	0.000	10.630	-1.580	0.000
0.000	-0.150	-0.330	0.000	0.000	0.000	-0.770	0.000	0.890	-1.580	8.075	0.000
-0.050	-0.010	-0.100	0.000	0.000	0.000	0.000	0.000	0.000	0.000	0.000	7.325

43/2- STATES IN 211RN WITH A 2MEV PHONON

Energies (MeV) are :

5.228	5.806	6.898	7.318	7.463	8.109	9.206	9.661	10.168	10.380	10.905	11.681

Wavefunctions are :

0.706	0.225	-0.544	0.085	0.129	0.235	0.020	-0.193	0.193	0.034	0.003	0.005
0.428	0.121	0.752	-0.094	-0.125	0.238	0.004	0.129	0.373	0.012	0.004	0.020
0.214	-0.707	-0.110	-0.101	-0.449	0.062	-0.129	0.017	-0.019	0.286	0.336	-0.124
0.413	0.100	0.099	0.001	-0.079	-0.871	-0.085	0.040	-0.186	-0.012	-0.004	-0.008
0.023	0.010	-0.236	0.039	0.058	-0.011	0.022	0.956	0.153	-0.010	0.000	0.004
0.254	0.089	0.136	-0.014	-0.012	0.334	0.075	0.169	-0.872	-0.049	-0.005	-0.012
0.106	-0.354	0.010	0.036	0.022	-0.083	0.862	-0.030	0.043	-0.229	-0.158	0.178
0.081	-0.225	-0.067	-0.038	-0.204	0.064	-0.356	-0.007	0.034	-0.826	-0.284	-0.028
0.001	0.001	-0.056	-0.075	-0.273	0.019	0.026	0.011	-0.003	0.360	-0.824	-0.328
0.072	-0.273	0.041	0.076	0.216	0.017	-0.288	0.008	-0.043	0.225	-0.309	0.797
0.116	-0.406	0.169	0.222	0.715	-0.018	-0.128	-0.003	-0.008	0.019	-0.083	-0.457
0.029	-0.038	-0.072	-0.953	0.288	-0.026	0.006	0.003	-0.004	-0.010	-0.009	0.003

MATRIX FOR THE 49/2+ STATE IN 211RN WITH A 2MEV PHONON

7.858	-0.032	-0.150	0.000	0.360	-1.230	0.000	-0.290	0.000	0.000	-0.380	-0.890	-0.260
-0.032	7.506	-0.770	-0.910	0.000	0.000	0.000	-0.100	0.000	0.000	0.050	-0.120	-0.085
-0.150	-0.770	8.320	-0.310	-0.030	-0.090	-1.290	0.000	0.000	0.000	0.000	0.000	0.000
0.000	-0.910	-0.310	9.250	-0.010	-0.020	-1.090	-0.090	-0.150	0.000	0.000	0.000	0.000
0.360	0.000	-0.030	-0.010	9.240	0.000	-0.040	-0.220	-0.080	0.440	0.000	0.000	-0.040
-1.230	0.000	-0.090	-0.020	0.000	9.240	-0.130	-0.740	-0.320	-1.510	0.000	0.000	-0.160
0.000	0.000	-1.290	-1.090	-0.040	-0.130	9.660	0.000	0.000	-0.014	0.000	0.000	0.000
-0.290	-0.100	0.000	-0.090	-0.220	-0.740	0.000	8.625	-1.130	0.000	0.520	-1.130	0.200
0.000	0.000	0.000	-0.150	-0.080	-0.320	0.000	-1.130	10.675	-1.090	0.000	0.000	0.000
0.000	0.000	0.000	0.000	0.440	-1.510	-0.014	0.000	-1.090	10.910	0.000	0.000	0.000
-0.380	0.050	0.000	0.000	0.000	0.000	0.000	0.520	0.000	0.000	10.940	0.000	0.000
-0.890	-0.120	0.000	0.000	0.000	0.000	0.000	-1.130	0.000	0.000	0.000	10.940	0.000
-0.260	-0.085	0.000	0.000	-0.040	-0.160	0.000	0.200	0.000	0.000	0.000	0.000	8.980

ENERGIES AND WAVEFUNCTIONS OF 49/2+ STATES IN 211RN WITH A 2MEV PHONON

Energies (MeV) are :

6.110	6.515	7.893	8.131	8.844	8.985	9.254	9.436	10.737	11.007	11.169	11.495	12.652

Wavefunctions are :

-0.469	0.434	-0.507	-0.188	-0.381	0.081	0.123	0.091	-0.113	0.052	-0.281	0.126	0.120
-0.425	-0.513	0.146	-0.671	0.067	0.058	-0.168	0.066	0.032	-0.194	-0.053	0.048	-0.007
-0.368	-0.391	-0.193	0.481	-0.174	-0.013	-0.522	-0.096	-0.099	0.332	0.090	-0.057	0.012
-0.260	-0.294	0.045	0.067	0.112	0.008	0.754	0.031	-0.068	0.476	0.135	-0.083	0.028
0.041	-0.063	0.230	0.079	-0.301	-0.466	-0.016	0.774	-0.070	-0.002	-0.085	-0.084	0.096
-0.382	0.338	-0.025	0.075	0.477	-0.012	-0.127	0.341	0.396	0.065	0.286	0.057	-0.357
-0.233	-0.243	-0.106	0.470	0.022	-0.027	0.292	-0.016	0.169	-0.701	-0.184	0.114	-0.033
-0.333	0.273	0.661	0.097	-0.256	-0.083	-0.002	-0.286	0.088	-0.001	0.172	0.326	0.264
-0.153	0.123	0.285	0.092	0.210	-0.030	-0.025	-0.048	-0.650	-0.001	-0.386	0.036	-0.501
-0.162	0.142	0.050	0.085	0.503	0.075	-0.098	0.077	-0.213	-0.083	-0.133	-0.361	0.685
0.003	0.011	-0.181	-0.032	-0.007	0.037	0.034	0.123	-0.553	-0.280	0.720	0.208	0.052
-0.176	0.144	0.104	-0.050	-0.301	-0.008	0.053	-0.160	0.015	-0.203	0.231	-0.817	-0.231
-0.053	0.027	-0.231	-0.133	0.190	-0.870	0.010	-0.362	-0.009	-0.004	0.032	0.009	0.020

Energies and wavefunctions for the 49/2+ states in 211Rn if the <fj|Vsh|ig> matrix element is -410keV, the (ig) diagonal interaction is -557keV and the (fJ) diagonal residual interaction is -490keV (sensitivity study).

Energies (MeV) are :

6.081	6.500	7.695	8.416	8.651	9.140	9.778	9.809	10.586	11.279	11.675	11.841	13.122

Wavefunctions are :

0.529	-0.338	-0.554	-0.002	0.318	-0.237	-0.018	0.108	0.209	-0.229	-0.134	-0.056	-0.108
0.405	0.703	0.013	0.522	0.162	0.074	-0.106	-0.082	0.002	0.008	0.009	-0.137	0.002
0.236	0.346	-0.076	-0.628	-0.122	-0.113	-0.236	-0.471	0.071	-0.011	-0.062	0.332	0.000
0.188	0.293	0.030	-0.216	-0.077	0.033	0.458	0.665	-0.039	-0.021	-0.073	0.407	-0.008
-0.033	0.036	0.161	0.001	-0.171	-0.320	-0.754	0.498	0.066	-0.056	0.059	0.018	-0.114
0.370	-0.232	-0.053	-0.064	-0.045	0.518	-0.295	0.100	-0.506	0.133	0.004	0.051	0.399
0.120	0.173	-0.021	-0.450	-0.121	-0.030	0.128	0.157	-0.076	0.041	0.167	-0.813	-0.012
0.449	-0.254	0.611	0.069	-0.137	-0.337	0.153	-0.136	-0.167	0.142	-0.329	-0.054	-0.150
0.210	-0.123	0.310	-0.010	-0.188	0.351	-0.004	0.019	0.742	-0.193	0.074	-0.048	0.299
0.137	-0.091	0.044	-0.032	-0.061	0.466	-0.054	-0.021	0.012	0.024	0.236	0.057	-0.828
-0.010	-0.007	-0.155	-0.023	0.075	0.042	-0.062	0.090	0.324	0.898	-0.208	-0.018	-0.018
0.205	-0.110	0.058	0.052	0.060	-0.298	0.109	-0.052	-0.006	0.241	0.854	0.172	0.131
0.078	-0.022	-0.399	0.267	-0.860	-0.094	0.096	-0.071	-0.014	0.032	-0.007	0.003	-0.011

REFERENCES

Ack83 H. Ackermann, P. Heitjans and J.-J. Stockman in Hyperfine Interactions of Radioactive Nuclei (Springer-Verlag, 1983), ed. J. Christiansen.

And78 C.G. Andersson, G. Hellstrom, G. Leander, I. Ragnarsson, S. Aberg, J. Krumlinde, S.G. Nilsson and Z. Szymanski, Nucl. Phys. A309 (1978) 141.

Bab72 C.V.K. Baba, T. Faestermann, D.B. Fossen and P. Proetel, Phys. Rev. Letts. 29 (1972) 496.

Bas80 R. Bass, Nuclear Reactions with Heavy Ions (Springer-Verlag, Berlin, 1980).

Bau73 R. Bauer, J. Speth, V. Klemt, P. Ring, E. Werner and T. Yamazaki, Nucl. Phys. A209 (1973) 535.

Bee77 J.R. Beene, O. Hausser, A.B. McDonald, T.K. Alexander and A.J. Ferguson, Hyp. Int. 3 (1977) 397.

Ber85 I. Bergstrom and B. Fant, Physica Scripta V31 (1985) 26.

Blo60 J. Blomqvist and S. Wahlborn, Arkiv Fysik 16 (1960) 545.

Blo77 J. Blomqvist, I. Bergstrom, C.J. Herrlander, L.G. Linden and K. Wikstrom, Phys. Rev. Letts. 38 (1977) 534.

Blo79 J. Blomqvist, Proc. Symp. on High-Spin Phenomena in Nuclei, Argonne (1979) ANL/PHY-79-4, p.155.

Boh69 Aage Bohr and Ben R. Mottelson, Nuclear Structure, Volume I (W.A. Benjamin, 1969).

Boh75 Aage Bohr and Ben R. Mottelson, Nuclear Structure, Volume II (W.A. Benjamin, 1975).

Bro70 J.A. Broglia, J.S. Lilley, R. Perazzo and W.R. Phillips, Phys. Rev. C1 (1970) 1508.

Bru77 P.J. Brussaard and P.W.M. Glaudemans, Shell-Model Applications in Nuclear Spectroscopy (North-Holland, 1977).

Byr82 A.P. Byrne and G.D. Dracoulis, Nucl. Phys. A391 (1982) 1.

Byr85 A.P. Byrne, Ph.D thesis, Australian National University (1985) (unpublished); and A.P. Byrne, G.D. Dracoulis, C. Fahlander, H. Hubel, A.R. Poletti, A.E. Stuchbery, J. Gerl, R.F. Davie and S.J. Poletti (to be published in Nucl. Phys.).

Cer79 M. Cerkaski and Z. Szymanski, Acta Phys. Polon. B10 (1979) 163, from Z. Szymanski, Fast Nuclear Rotations (Oxford Univ. Press, Oxford, 1983).

Dae77 W.W. Daehnick, M.J. Spisak, R.M. Delvecchio and W. Oelert, Phys. Rev. C 15 no. 4 (1977) 594.

Daf78 E. Dafni and G.D. Sprouse, Hyp. Int. 4 (1978) 777.

Dia80 R.M. Diamond and F.S. Stephens, Ann. Rev. Nucl. Part. Sci. 30 (1980) 85.

Dra81 G.D. Dracoulis, C. Fahlander and A.R. Poletti, Phys. Rev. C24 (1981) 2386.

Dud80 J. Dudek, Z. Szymanski and T. Werner, Phys. Rev. C23 (1981) 920.

Fan84 B. Fant, T. Weckstrom, T. Lonnroth, C.J. Herrlander, K. Honkanen and A. Kallberg, Nucl. Phys. A429 (1984) 296.

Ham74 I. Hamamoto, Phys. Rep. (section C of Phys. Letts.) 10, no. 2 (1974) 63.

Ham76 I. Hamamoto, Nucl. Phys. A271 (1976) 19.

Ham76b I. Hamamoto, Phys. Letts. 61B (1976) 343.

Ham77 I. Hamamoto, in "Elementary Modes of Excitation in Nuclei, Proc. of Int. School of Physics "Enrico Fermi" Course LXIX", ed. A. Bohr and R.A. Broglia.

Hau76 O. Hausser, T.K. Alexander, J.R. Beene, E.D. Earle, A.B. McDonald, F.C. Khanna and I.S. Towner, Nucl. Phys. A273 (1976) 253; and O. Hausser, J.R. Beene, A.B. McDonald, T.K. Alexander, E.D. Earle, F.C. Khanna, I.S. Towner, G.A. Beer and A. Olin, Phys. Letts. 63B (1976) 279.

Hau78 O. Hausser, J.R. Beene, T. Faestemann, T.K. Alexander, D. Horn, A.B. McDonald and A.J. Ferguson, Hyp. Int. 4 (1978) 219.

Her69 J.N. Hertel, D.G. Flemming, J.P. Schiffer and H.E. Grove, Phys. Rev. Letts. 23 (1969) 488.

Hor77 D. Horn, O. Hausser, T. Faestermann, A.B. McDonald, T.K. Alexander, J.R. Beene and C.J. Herrlander, Phys. Rev. Letts. 39 (1977) 389.

Kal85 A. Kallberg, "Studies of the Origin of the Yrast States in the Lead Region", ISBN 91-8170-963-8, R.S.I., Stockholm (1975).

Kuo68 T.T.S. Kuo, Nucl. Phys. A122 (1968) 325.

Kuo71 T.T.S. Kuo and G.H. Herling, NRL Memorandum Report 2258.

Law80 R.D. Lawson, Theory of the Nuclear Shell Model (Clarendon Press, Oxford, 1980).

Led78 C.M. Lederer and V.S. Shirley (eds.), Table of Isotopes (7th ed.), (Wiley, N.Y., 1978).

Lew85 P. Lewis, A.R. Poletti et al. (to be published); see also A.P. Byrne, Ph.D thesis, Australian National University (unpublished).

Lon80 T. Lonnroth, J. Physique 41 (1980) L-185.

Lon80b T. Lonnroth, "Experimental and Theoretical Two-Nucleon Interaction Energies in the Lead Region", unpublished.

Lon80c T. Lonnroth, Ph.D dissertation, University of Jyvaskyla Research Report 3/1980.

Ma73 C.W. Ma and W.W. True, Phys. Rev. C8 (1973) 2313.

Mai71 K.H. Maier, J.R. Leigh, F. Puhlofer and R.M. Diamond, Phys. Letts. 35B (1971) 401.

Mai81 K.H. Maier, D.J. Decman, H. Grawe, H. Haas and D.-D. Zeitz, Hyp. Int. 9 (1981) 87.

Mar77 M.J. Martin, Nucl. Data Sheets 22 (1977) 545.

Mat78 K. Matsuanagi, T. Dossing and K. Neergaid, Nucl. Phys. A307 (1978) 253.

Mor76 H. Morinaga and T. Yamazaki, In-Beam Gamma-Ray Spectroscopy (North-Holland, 1976), 424.

Mye65 N.D. Myers and W.J. Swiateki, Nucl. Phys. 81 (1966) 1.

New74 J.O. Newton, in Nuclear Spectroscopy and Reactions, Part C, ed. J. Cerny (Academic Press, New York, 1974), 185.

Nor70 R. Nordhagen, G. Goldring, R.M. Diamond, K. Nakai and F.S. Stephens, Nucl. Phys. A142 (1970) 577.

Pel82 D. Pelte and D. Schwalm, in Heavy Ion Collisions, vol. 3, ed. R. Bock (North-Holland, Amsterdam, 1982).

Pol81 A.R. Poletti, G.D. Dracoulis, C. Fahlander and I. Morrison, Nucl. Phys. A359 (1981) 180.

Pol82 A.R. Poletti, G.D. Dracoulis, C. Fahlander and I. Morrison, Nucl. Phys. A380 (1982) 335.

Pol85 A.R. Poletti, G.D. Dracoulis, A.P. Byrne, A.E. Stuchbery, S.J. Poletti and J. Gerl, Phys. Letts. (in press).

Rah77 V. Rahkonen, I. Bergstrom, J. Blomqvist, O. Knuttila, K.-G. Rensfelt, J. Sztarkier and K. Westerberg, Z. Physik A284 (1977) 357.

Rec74 E. Recknagel, in Nuclear Spectroscopy and Reactions, Part C, ed. J. Cerny (Academic Press, New York, 1974), 83.

Rin74 P. Ring and J. Speth, Nucl. Phys. A235 (1974) 315.

Rin80 P. Ring and P. Schuck, The Nuclear Many-Body Problem (Springer-Verlag, New York, 1980).

Sch80 M.R. Schmorak, Nucl. Data Sheets 31 (1970) 283.

Stu85 Private communication from A. Stuchbery.

Stu85b A. Stuchbery, G. Dracoulis, A. Byrne and A.R. Poletti et al. (to be published).

Tow76 I.S. Towner, F.C. Khanna and O. Hausser, Nucl. Phys. A277 (1977) 285.